Evaluation of New Test Methods for Fire Fighting Clothing

by

Brian David Gagnon

A Thesis

Submitted to the Faculty

of the

WORCESTER POLYTECHNIC INSTITUTE

in partial fulfillment of the requirements for the

Degree of Master of Science

in

Fire Protection Engineering

by

May 2000

APPROVED:

Professor Nicholas A. Dembsey, P.E., Major Advisor

Dr. N. R. Keltner, Co-Advisor

Professor David A. Lucht, P.E., Head of Department

ABSTRACT

Despite advancements in the development of synthetic fibers and materials that provide better insulation, fire ground burn injuries remain a significant issue. The current test methods for fire fighting clothing were investigated to determine their adequacy in evaluating the actual performance of clothing materials. This investigation uncovered several potential problems with the current test methods. A series of new, small scale, tests were used to evaluate the shortcomings of the current test methods and develop possible improvements.

A small test apparatus, designed and donated by Ktech Corporation, was used to measure the thermal properties (thermal conductivity and volumetric heat capacity) of a series of fire fighting clothing materials. The thermal properties were estimated for single fabric layers, as well as ensembles, with various levels of moisture added to simulate actual end use conditions.

In addition, a skin simulant sensor was used to assess the time to 2nd degree burn for exposures similar to those required in current standards for fire fighting clothing. A one dimensional heat conduction model was developed to predict the time to 2nd degree burn for the skin simulant sensor protected with outer shell materials that may be used as wildland fire fighting clothing, using the thermal property data obtained from earlier tests. An alternative method was developed to calculate the time to 2nd degree burn for ensembles evaluated with the new skin simulant sensor. The predictions for the time to 2nd degree burn obtained from the new skin simulant sensor were compared against results obtained using the sensor specified in the current test methods. The predictions for the skin simulant sensor were consistently shorter than those from the current test sensor. The current test sensor predictions for the time to 2nd degree burn were nominally 40% to 50% higher than the predictions from the skin simulant sensor during the evaluations of outer shell materials.

ACKNOWLEDGEMENTS

Thanks to Professor Dembsey for his interest and guidance in support of this work, and his unbelievable level of patience with my endless series of questions. His professionalism and vast body of knowledge in the topics covered in this thesis were critical to the completion of this work, and I cannot express my level of gratitude.

Thanks to Dr. Ned Keltner, who provided a tremendous level of support throughout this process, taking time out of his busy schedule to act as Principal Investigator for this project. Dr. Keltner provided guidance on a variety of topics, and was instrumental to the understanding and completion of the work presented in this thesis. Thanks to Ktech Corporation, Albuquerque, NM, for whom Dr. Keltner is employed as a Senior Engineer, for providing funding for this thesis, and incorporating the findings into the Small Business and Innovative Research Project Report, Phase II: "New Methods for Evaluating Thermal Performance of Protective Clothing for Fire Fighters."

Thanks to James R. Lawson, of the Fire Safety Engineering Division, Building and Fire Research Laboratory of the National Institute of Standards and Technology, whose interest in the protection of fire fighters provided the funding for this work. Mr. Lawson served as the Contracting Officer's Technical Representative for this SBIR project, Contract Number 50-DKNB-8-90127.

Thanks to all of the faculty and staff of the Center of Firesafety Studies for providing guidance throughout my thesis and graduate studies. Special thanks to Professor Clougherty, who, along with Professor Dembsey, worked as part of a team on the Phase I and Phase II parts of this SBIR project.

Thanks to everyone who works in the fire lab for their patience and understanding with regard to my frequently inefficient work habits, and occasional less than focused attitude.

Finally, thanks to my girl friend and family, whose encouragement, support, and occasional badgering, was enormously helpful and necessary for the final completion of this work.

TABLE OF CONTENTS

LIST OF TABLES

LIST OF FIGURES

LIST OF EQUATIONS

NOMENCLATURE

a	Absorbtivity
c_p	Specific Heat of Solid [J/kg K]
E_b	Emissive Power [kW/m^2]
Fo	Fourier Number
h	Heat Transfer Coefficient [W/m^2 K]
h_i	Interfacial Conductance [W/m^2 K]
k	Thermal Conductivity [W/m K]
P	Tissue Damage Frequency Factor [1/s]
q_c''	Average Convective Cooling at Material Surface [kW/m^2]
q_i''	Incident Radiant Heat Flux to Material Surface [kW/m^2]
q_n''	$q_i'' - q_c'' - q_r''$ Net Radiant Heat Flux to Material Surface [kW/m^2]
q_r''	Average Radiant Cooling at Material Surface [kW/m^2]
R	Universal Gas Constant [kJ kg/mol-K]
s	Nodal Spacing [m]
t	Time [s]
T	Temperature [^{o}C]
x	Distance [m]
ΔE	Tissue Damage Activation Energy [J/mol]
Ω	Arbitrary Function of Epidermal Injury
α	$k/\rho c_p$ Thermal Diffusivity [m^2/s]
δ	Thickness [m]
ε	Emissivity
λ	Wavelength [μm]
ρ	Density [kg/m^3]

ρc_p	Volumetric Heat Capacity [J/m^3-K]
σ	Stefan-Boltzman Constant [5.67E-8 W/m^2 K^4]
τ	Transmissivity
$\sqrt{k\rho c_p}$	Thermal inertia [W s$^{1/2}$/m^2 K]

1.0 INTRODUCTION

1.1 Impetus for this Research

Fire fighting is an inherently dangerous profession, and much work has been done to provide satisfactory protection for the individuals willing to risk their lives to aid others in need. Historically, protective clothing was designed based upon subjective comments, and not on the physiology of the user or basic physical principles.[1] This practice began to change in the 1940's, when the armed services initiated programs to investigate protective clothing, due to the climatic extremes encountered by servicemen.[1] This initial military work led to the standardized tests, such as the Thermal Protective Performance Test[2] described in this thesis, which have been incorporated into the standards used to design and test fire fighting clothing today. The National Fire Protection Association (NFPA) first released an industry wide standard on fire fighting clothing in 1975, designated NFPA 1971 *Protective Clothing for Structural Fire Fighting.*[2] This document has been revised every three to five years, per the normal NPFA standard developmental process.

Despite advancements in the development of synthetic fibers and materials that provide better insulation, fire ground burn injuries remain a significant issue.[3] Recent data collected by NFPA, Table 1, shows that nearly 10 percent of all fire ground injuries to fire fighters are burns (chemical and fire).[3] The percentage of burns is nearly equivalent to the percentage of injuries caused by smoke and gas inhalation, and ranks behind only two categories of physical injuries such as sprains or cuts.

Table 1 : Fire Fighting Injuries (1997).[3]

Nature of Injury	Number of Injuries	Percentage of Total
Heart attack or stroke	205	0.7
Other respiratory distress	840	1.6
Dislocation, fracture	915	2.4
Thermal Stress (frostbite or heat exhaustion)	2,840	5.9
Eye irritation	2,265	6.0
Other	2,735	6.3
Burns (Fire or chemical)	3,755	9.5
Smoke or gas inhalation	2,980	10.2
Wound cut or bleeding, bruise	8,795	19.2
Strain, sprain, muscular pain	15,590	38.2
Total	40,920	100

By improving the understanding of the thermal properties of fire fighting clothing, as well as the physiology of the user, improvements can be made in the testing procedures of these materials. Improvements could lead to fire fighting clothing designs that can significantly reduce the numbers of burns on the fire ground. In addition to reducing the number of burns experienced on the fire ground, this work could lead to potential cost reductions in the clothing, as manufactures will have a better understanding of the impact of the individual material properties as well as how the different components act together.

The current test methods[2,4] do not utilize thermal property information in the assessment of the clothing performance. These test methods utilize a sensor with properties much different than those of human skin to assess the time until a thermal endpoint is reached. These methods do not determine the heat transfer through the clothing, or evaluate the heat flux imposing on the sensor directly, and do not factor into the burn calculations the effect of the clothing layer on skin cooling. By ignoring these effects, the burn time estimates produced by the current test methods may be higher than the actual exposure time required to produce a 2nd degree burn.

The new test methods proposed in this thesis outline a procedure to determine the thermal properties of the individual clothing layers, as well as clothing ensembles used as fire fighting clothing. In addition to the property determination, a procedure for the use of a skin simulant sensor to predict the time to 2nd degree burn is presented. The skin simulant sensor is used to

determine the heat flux at the skin simulant surface. This heat flux exposure level is then used as input into a heat conduction model of human skin to predict the time to 2nd degree burn. Two separate methods to predict the time to 2nd degree burn for the skin simulant sensor are presented. One utilizes the thermal properties of the clothing in a heat conduction model of the clothing and skin simulant, or clothing and skin, system. The other method determines the heat flux at the skin simulant surface from the temperature rise of the skin simulant sensor. This heat flux data is then applied to a model of the skin, and the time to 2nd Degree Burned determine using Henriques Burn Damage Integral. These test methods yield consistently shorter, more conservative, results for the time to 2nd degree burn than those determined by the current test methods.[2,4]

1.2 Research Outline

One of the primary goal of this research is to incorporate the determination of the thermal properties (thermal conductivity, k, and volumetric heat capacity, ρc_p) of fire fighting clothing into the design and evaluation of that clothing's performance, including the effects of moisture and compression. Several materials were evaluated, ranging from outer shells (Nomex, PBI), a representative moisture barrier, and a representative thermal liner. Ensembles composed of these materials were also evaluated. The material property determination was based upon a small-scale test performed in a Plexiglas test fixture, hereafter referred to as the Thermal Properties Test Fixture (TPTF). This test fixture was used to expose the materials to low heat flux levels (approximately 4 kW/m^2), and assess the temperature rise of the clothing and a skin simulant sensor located behind the clothing. The skin simulant sensor was constructed of Macor, a glass ceramic material with a thermal inertia similar to that of skin.[5] The exposure heat flux and temperature rise information of the clothing material and the skin simulant from the TPTF was then used in a property estimation code[6] to assess the materials' thermal properties. This test apparatus is described in greater detail in Section 3.1.1 of this thesis.

In addition to developing a test procedure which allows quick and easy determination of the material thermal properties, an alternative test method and evaluation technique, utilizing the skin simulant sensor, is proposed for the Radiant Protective Performance Test (RPP) currently used to evaluate wildland fire firefighting clothing.[4] A series of RPP tests were conducted with a copper calorimeter[16] and the skin simulant. These tests were used to assess the ability of the skin simulant to accurately predict the time to 2nd degree burn when exposed to time varying heat flux levels behind the layer of clothing, and to compare these values against those predicted by the copper calorimeter. The core similarity in the current test procedures for wildland and structural firefighting clothing should allow the techniques used in assessment of the time to 2nd degree burn in the alternative proposed RPP test to be applied to the Thermal Protective Performance Test (TPP)[2], used to evaluate structural firefighting clothing ensembles.

A final series of tests were run using the Thermal Properties Compression Fixture (TPCF). This test is instrumented in a manner similar to that of the TPTF, however it incorporates the capability to apply pressure to the system, assessing the clothing's material thermal properties under various compression loads. This capability can be used to assess the heat flux through, and the thermal properties of, fire fighting clothing ensembles in situations other than the non-compressed case evaluated by the TPTF. Although not used in this work, the TPCF also provides a capability for evaluating clothing performance during sudden contact with a hot surface. In addition, the TPCF allows one to conduct non-destructive, compressed and non-compressed, evaluations of new and used turnout gear. The results of such evaluations can be used to assess and track the material properties over the life of the clothing. The description of the TPCF is included in Appendix D: Compression Test Fixture, along with a sample of test results collected with the apparatus.

2.0 LITERATURE REVIEW

2.1 Skin Burns

One of the primary objectives in the design of fire-fighting clothing is the prevention of thermal damage to the skin. To properly develop new test methods for the evaluation of fire-fighting clothing, one must have a sound understanding of the affects of thermal exposure on the skin. One of the areas of focus in this thesis is the determination of the affects of radiant heat on fire fighting clothing, and the determination of when damage to the underlying skin will occur. The assessment of the damage to the skin throughout this thesis is the onset of superficial 2nd degree burn. This level of damage is used in the assessment methods in the current standards.[2,4]

The skin is composed of three layers: the epidermis, dermis, and the hypodermis. A superficial 2nd degree burn, referred to as a 2nd degree burn throughout the remainder of this thesis, is indicative of complete necrosis of the epidermis, and is equivalent to the time to blister of the skin.[7] This level of damage provides a relatively severe, yet survivable, performance criterion level.[7] The skin will not naturally regenerate if damaged beyond this point.[7] The normal human skin temperature at the surface is 32.5^{o}C, and thermal damage will begin when the temperature at the base of the epidermis, approximately 80-μm below the surface, is increased above 44^{o}C.[8] Damage to the skin is a function of the skin temperature, and the period of time when this temperature is greater than 44^{o}C. The rate of damage to the skin increases logarithmically, such that the rate of damage at 50^{o}C is 100 times greater than the rate of damage at 45^{o}C.[9] Extrapolation of the rate of damage due to thermal radiation versus temperature curve indicates the a 2nd degree burn will occur virtually instantaneously when the basal temperature is 72^{o}C.[8] Regardless of the mode of application of the heat flux, the temperature rise, and therefore the 2nd degree burn tolerance time, are related to the amount of heat absorbed by the skin.[10] Thermal damage to skin protected with fire fighting clothing is via conduction when the clothing is placed in contact with the skin.

Damage to the skin can be represented as a chemical rate process, governed by an activation energy, ΔE, and pre-exponential constant, P.[11] The rate at which epidermal injury will occur is represented by Equation 1.

$$\frac{d\Omega}{dt} = Pe^{\left(-\frac{\Delta E}{R(T+273)}\right)} \qquad \text{Equation 1}$$

The level of damage is based upon the amount of time, t, where the temperature, T (^{o}C), of the basal layer, 80 μm below the skin surface, is greater than 44^{o}C. The rate process equation can be integrated to obtain a function for the total amount of damage, presented in Equation 2.

$$\Omega = \int_0^t Pe^{(-\Delta E/R(T+273))}dt \qquad \text{Equation 2}$$

The severity of a burn is determined based upon the values obtained for the injury parameter, Ω, over a given temperature-time history. A value for Ω greater than or equal to1.0 is equivalent to a 2nd degree burn. The values for the Activation Energy, ΔE, and the Tissue Damage Frequency Factor, P, were originally set to 6.28x10^{8} J/kmol and 3.1x10^{98} 1/sec respectively.[11] These values did not include the damage to the skin that occurs while it is cooling. To provide more accurate burn damage assessments, application of the burn damage integral to include this cooling period lead to new values for the Activation Energy and the Tissue Damage Frequency Factor.[7] The revised values for the Activation Energy and the Tissue Damage Frequency Factor developed by Weaver and Stoll provided the best estimation for the time to 2nd degree burn compared to test data.[7] Table 2 presents the values for the Activation Energy and the Tissue Damage Frequency Factor developed by Weaver and Stoll.[12]

Table 2: Henriques Burn Integral Constants[12]

Basal Layer Temperature Range (^{o}C)	Activation Energy DE (J/kmol)	Tissue Damage Frequency Factor, P (1/sec)
44≤T≤50	7.82 x 10^{8}	2.185 x 10^{124}
50>T	3.27 x 10^{8}	1.823 x 10^{51}

Equation 2 cannot be solved analytically, so numerical techniques are employed to calculate the value for the damage function, Ω. The temperature history must first be divided into equivalent

time steps. Equation 2 can be solved for a given time step, and the trapezoidal rule can be used to integrate this function over time. This calculation method can be used for each time step where the temperature of the basal layer is greater than 44^{o}C. The trapezoidal rule for the solution of Equation 2 is presented in Equation 3.

$$I_i = \sum_i \frac{\left(\left(\frac{d\Omega}{dt}\right)_i + \left(\frac{d\Omega}{dt}\right)_{i+1}\right)}{2}\left(t_{i+1} - t_i\right) \qquad \text{Equation 3}$$

When using this method to determine the level of damage to the skin, it is often helpful to consider the sequence of events that will lead to the formation of a 2nd degree burn. When the skin is exposed to a heat source, its temperature will begin to rise. When the basal layer temperature increases above 44^{o}C, thermal damage will begin to occur, with the rate of damage dependent upon the temperature. When the heat source is removed, the skin will begin to cool, however, damage will continue as long as the basal layer temperature is greater than 44^{o}C. The amount of damage occurring while the skin is cooling must be considered in the analysis, particularly when a protective clothing layer lies between the skin and the heat source, as this layer will initially be at a higher temperature than the skin and will prevent the skin from cooling rapidly.

The thermal properties of human skin are critical to the determination of the time to 2nd degree burns. The values for the thermal properties of human skin vary from literature source to literature source, and are dependent on the individual involved and the body location.[7,13] As the determination of the time to 2nd degree burn is to be calculated using the Weaver and Stoll burn integral parameters, the thermal properties for human skin presented in their report were also used in order to obtain accurate prediction results.[12] Weaver and Stoll experimentally determined the thermal properties of the skin. The thermal conductivity was found to be dependent on the heat flux exposure level. Different values were determined for the thermal conductivity when the skin was being heated or cooled. Table 3 presents a linear approximation of the thermal

properties of the skin, developed from the Stoll and Weaver Data, used in the prediction of the time to 2nd degree burn in this thesis.[12]

Table 3: Skin Thermal Properties

Property	Symbol	Heat Flux Range (kW/m^2)	Value
Thermal Conductivity (heating)	k_h	q"<5.9 5.9<q"<11.8 11.8<q"<16 q">16	0.0487*q"+0.1604 0.01804*q"+0.3412 0.0075*q"+0.4664 0.5878
Thermal Conductivity (cooling)	k_c	q"<5.9 5.9<q"<11.8 q">11.8	0.0436*q"+0.1683 0.0043*q"+0.4007 0.4518
Volumetric Heat Capacity	ρc_p	All Heat Flux Values	4,186,800 J/m^3-K

These values for the thermal properties of human skin were used during the development of a one dimensional, finite difference model to calculate the time to 2nd degree burn. This model of human skin was originally developed to calculate these times when exposed to steady heat pulse levels, and compared to test data presented by Stoll et al.[9,12] The 1-D finite difference model, which is presented in greater detail in Section 3.2.2, utilized the thermal property values listed in Table 3 when exposed to constant heat flux levels. When the model was adapted to calculate the time to 2nd degree burn when exposed to a time varying heat flux, the values for the thermal conductivity during heating were determined at each time step using the values from Table 3. However, the thermal conductivity during cooling was assumed to be 0.4518 W/m-K throughout. The thermal conductivity values listed in Table 3 are based upon steady heat pulse exposures. During a time varying exposure, such as the heat flux at the surface of the skin when protected by a layer of protective clothing, there is no constant heat pulse level that can be used to determine the thermal conductivity of the skin during the cooling stage.

Much of the work in the development of models and correlations relating to skin burns relates to data collected by Stoll and Greene.[9] These data measured the time to second degree burn under a variety of heat flux levels. Table 4 presents a summary of the time to 2nd degree burn when exposed to various heat flux levels.

Table 4: Heat Flux versus Burn Time - Measured Data Summary[9]

Absorbed Heat Flux (cal/cm^2 sec)	Absorbed Heat Flux (kW/m^2)	Exposure Time to 2^{nd} Degree Burn (s)
1.128	47.2	1.1
0.94	39.4	1.4
0.752	31.5	2.0
0.564	23.6	3.0
0.376	15.7	5.6
0.282	11.8	7.8
0.188	7.9	13.4
0.141	5.9	20.8
0.094	3.9	33.8

These data provide a reference point to models and calculation methods exposed to steady heat flux levels. However, the application of these data requires with absolute certainty that the heat pulse levels imposing on the skin be rectangular in shape, as any variation in shape invalidates the application of these results.[12] This stipulation invalidates the use of the test data in the formation of a simple temperature endpoint curve to determine the time to 2^{nd} degree burn under a fabric specimen using the information from Table 4, as the heat flux reaching the skin is no longer rectangular in shape. Figure 1 provides a sample heat flux curve for a sensor placed behind a layer of protective clothing exposed to 21 kW/m^2. The heat flux level at the surface of the sensor is not a steady pulse, such as the values in the Stoll and Greene Tests,[9] and this calls into question the applicability of these data to tests of this nature.

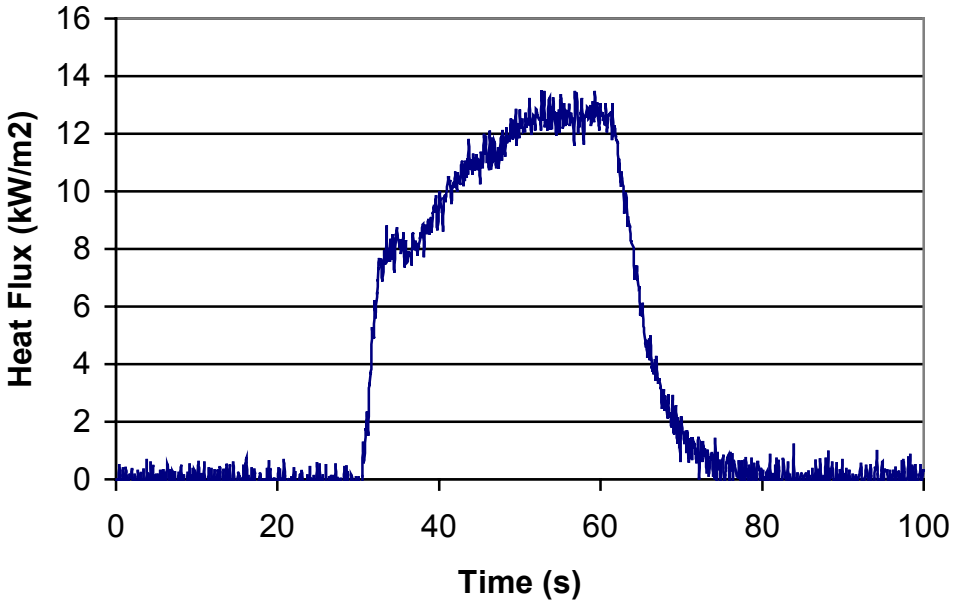

Figure 1: Sample Heat Flux Curve - Skin Simulant Sensor Placed Behind 1 Layer of Clothing Exposed to 21 kW/m^2.

2.2 Fire Fighting Clothing Design

In order to develop new and improved test methods, one must have an understanding of the desired performance characteristics of fire fighting clothing, as well as the current test methods and design criteria used to asses clothing designs. There are several different types of protective clothing used by fire fighters, and consequently several different standards outlining the performance requirements of each type.

2.2.1 PERFORMANCE CHARACTERISTICS

Due to the hazardous environment in which firefighters work, the protective clothing worn must provide protection over a wide range of heat flux levels and temperatures. Much of the research done regarding protective clothing concentrates on heat flux exposures simulating situations where the fire fighter is enveloped in flames.[14] This research focuses on the ability of the clothing to provide limited protection under direct flame exposure for a short duration. However, fire

fighter clothing should be designed to provide protection over wide ranges of heat flux levels over various time durations. Veghte reported that the typical structural fire radiant level is approximately 8 – 25 kW/m^2, as opposed to that heat flux levels of 84 – 125 kW/m^2 that would be expected in the cases with direct flame contact.[15]

Structural fire fighting clothing is typically constructed of a flame resistant outer shell, and an insulating thermal liner consisting of a moisture barrier and a thermal barrier.[14] The outer shell material resists ignition when being exposed to thermal radiation or direct flame contact. The moisture barrier prevents the passage of moisture between the thermal barrier exposed to the skin and the outer shell, exposed to the fire environment. This barrier will prevent water, as well as chemicals, from passing through the garment to the wearer. A moisture barrier may prevent only liquid movement or liquid and vapor movement. The thermal barrier is a thicker, air filled, material that resists heat flow to the skin. In addition to preventing excessive heat from reaching the wearer, the clothing ensemble prevents the flow of heat and moisture from the body, reducing the ability of the body to give off excess heat.

Wildland fire fighting clothing is not designed to provide the same level of protection as that provided by structural fire fighting clothing, due to the differences in the anticipated work environment. Wildland fire fighting clothing is designed to provide protection from radiant environments, the primary thermal hazard encountered.[4] The anticipated proximity of the fire fighter to the fire in these situations can range from a few feet to several miles. Additional equipment, such as a fire shelter, is included in the standard for wildland fire fighting equipment to protect the fire fighters from serious injury or death in the event of a more severe exposure.[4]

NFPA has test standards for both types of fire fighting clothing discussed above, designated NFPA 1971, *Protective Clothing Ensemble for Structural Fire Fighting*[2] and NFPA 1977, *Protective Clothing and Equipment of Wildland Fire Fighting*.[4] The protective performance in each of these standards is based upon the ability of the clothing to delay the time to 2nd degree

burn. The previous section of this thesis presents information on skin burns, and test data on the time to 2nd degree burns resulting from constant, uniform heat flux levels. This information was coupled with desired performance levels of the fire fighting clothing to produce test standards that provide a means to compare the performance of different types of protective clothing.

2.2.2 CURRENT TEST METHODS

There are different standards applicable to each of the various types of clothing used by fire fighters, ranging from station uniforms to proximity clothing. The information presented in this thesis focuses on three standards,[2,4,16] and the accompanying test methods, when developing and verifying the performance of the new test methods and sensor assemblies.

ASTM D 4108, Standard Test Method for Thermal Protective Performance of Materials for Clothing; Open Flame Method

ASTM D 4108, *Standard Test Method for Thermal Protective Performance of Materials for Clothing; Open Flame Method*, was removed from publication in 1996.[16] However, the NFPA standards referenced in this thesis cite this document in the explanation of their flame resistance testing. ASTM D 4108 rates textile materials for thermal resistance and insulation when exposed to short duration convective flux levels of approximately 83 kW/m^2.[16] This heat flux is meant to simulate direct flame exposure. This test method could be used to assess either individual fabric layers, or protective ensembles. When individual layers were evaluated, ASTM D 4108 required that a 6.4 cm spacer be placed between the sensor and the fabric layer to prevent the fabric from acting as a heat sink during the exposure. This spacer was not required when evaluating ensembles, due to the greater overall thickness of the sample.

Each of the fabric standards presented in this thesis is based upon the measurement of the temperature rise of a sensor placed behind a fabric specimen. A copper calorimeter, which acts as an adiabatic slug calorimeter, is used to measure this temperature rise. Two copper calorimeters, similar to those described in ASTM D 4108,[16] were constructed for this evaluation,

and used to provide an assessment of the current test methods, against which the results from the new test methods could be compared.

The copper calorimeter temperature rise could be used to assess the time to second degree burn using the human tissue tolerance information included in Table 1 of ASTM D 4108.[16] This information, Table 5, presents an elaboration on the test data[8,9] (Table 4) on the time to 2nd degree burn for rectangular heat pulse levels ranging from approximately 4 kW/m^2 to 50 kW/m^2. Stoll and Chianta stressed the importance of the heat pulse being rectangular when using this data for any purpose, for a variation from this shape invalidates the data.[9] In addition to the heat flux information, this table presents the calorimeter equivalent temperature rise to produce a 2nd degree burn at each time value, which can be determined using Equation 4. The temperature rise can be determined by dividing the exposure flux-time product by the density, specific heat, and thickness of the copper calorimeter. The numerical values for the density, specific heat, and thickness of the copper calorimeter are presented in Section 3.2.1.

$$q_r'' = \rho c_p \delta \left(\frac{\Delta T}{\Delta t} \right) = 5.685 \left(\frac{\Delta T}{\Delta t} \right) \qquad \text{Equation 4}$$

Table 5: Stoll and Chianta – Human Tissue Tolerance to 2nd Degree Burn[16]

Exposure Time (s)	Heat Flux (cal/cm^2 sec)	Heat Flux (kW/m^2)	Calorimeter Equivalent Temperature Rise (^oC)
1	1.2	50.0	8.9
2	0.93	38.8	10.8
3	0.55	22.9	12.2
4	0.45	18.8	13.3
5	0.38	15.8	14.1
6	0.34	14.2	15.1
7	0.3	12.5	15.5
8	0.274	11.4	16.2
9	0.252	10.5	16.8
10	0.233	9.7	17.3
11	0.219	9.1	17.8
12	0.205	8.5	18.2
13	0.194	8.1	18.7
14	0.184	7.7	19.1
15	0.177	7.4	19.7
16	0.168	7.0	19.8
17	0.16	6.7	20.2
18	0.154	6.4	20.6
19	0.148	6.2	20.8
20	0.143	6.0	21.2
25	0.122	5.1	22.6
30	0.107	4.5	23.8

The calorimeter equivalent temperature rise from Table 5, determined using the exposure time required to produce a 2nd degree burn under constant heat flux, can be used to produce a temperature curve that signifies the point at which a 2nd degree burn will occur. This curve is referred to as the Stoll and Chianta Curve throughout this thesis. The use of this curve assumes that the constant heat flux information can be used to assess the time to 2nd degree burn under time varying heat flux conditions, despite the specific warnings against this by Weaver and Stoll.[12] When the copper calorimeter temperature rise during a test is graphed on the same axis as the Stoll and Chianta Curve, Figure 2, a 2nd degree burn is said to occur at the time when the measured curve crosses the Stoll and Chianta Curve.[16] The Stoll and Chianta Curve is approximated by Equation 5, which is the best fit curve of the time and calorimeter equivalent temperature rise information from Table 5. The value t in this equation is the time after the exposure begins. After the time to 2nd degree burn is determined using this method, this information is summarized in a Thermal Protective Performance Rating, which can be determined

by multiplying the exposure time to cause a 2nd degree burn by the heat flux applied to the clothing (83 kW/m^2).[16]

$$T = 8.87(t)^{0.29} \qquad \text{Equation 5}$$

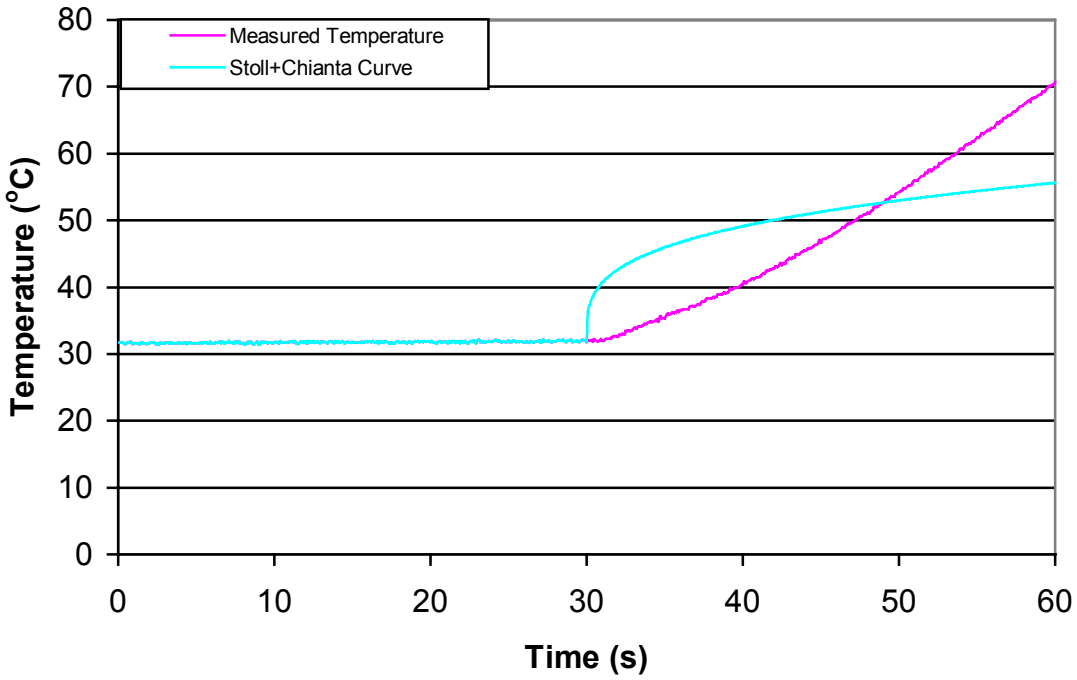

Figure 2: Copper Calorimeter Burn Determination – Second Degree Burn is Said to Occur when Measured Temperature Increases Above Stoll and Chianta Curve. Heat Flux Exposure Begins 30 Seconds into Data Collection Procedure. Before Heat Flux Exposure Begins, Stoll and Chianta Curve Values Set Equal to Measured Temperature Values. Application of Equation 5 Begins when the Exposure Begins.

This method for the prediction of 2nd degree burns is based upon test data on rectangular heat pulse exposures. These data are used to set the copper calorimeter temperature endpoint levels that will produce 2nd degree burns. Therefore, this method provides very accurate predictions when the copper disc is exposed directly to a constant heat flux. However, when placed behind a layer of clothing, the heat flux that reaches the copper calorimeter is no longer rectangular in shape, and this may invalidate the methodology used to produce the calorimeter equivalent temperature rise curve.

NFPA 1971, *Protective Ensemble for Structural Fire Fighting*

Two NFPA test standards; NFPA 1971, *Protective Ensemble for Structural Fire Fighting*[2] and NFPA 1977, *Protective Clothing and Equipment for Wildland Fire Fighting*[4] reference ASTM D 4108 in their thermal protective performance sections.[16] This thesis was concerned only with the material flammability and thermal protection aspects of these two standards, and the standards' descriptions will focus on these elements only.

NFPA 1971 provides design information on clothing ensembles to be used by structural fire fighters. These ensembles are typically constructed of three layers, an outer shell, a moisture barrier, and an inner liner. This standard includes several thermal protection related tests for the overall protection of the fire fighter, including boots, gloves, helmets, etc. The section related to the current work is based upon ASTM D 4108.[16] This section is titled the Thermal Protective Performance Test (TPP). The NFPA TPP Test requires that a sample of the ensemble, mounted in front of the copper calorimeter, be exposed to a combined radiative (quartz lamps) and convective (Meker burners) heat flux of 83 kW/m^2 $\pm$ 4 kW/m^2 (2.0 cal/cm^2s $\pm$ 0.1 cal/cm^2s), simulating a direct flame contact exposure.[2] After the ensemble has been prepared and mounted as outlined in NFPA 1971, it is exposed for at least 30 seconds. The ensemble specimen, cut into 15.2 cm x 15.2 cm (6" x 6") squares, is mounted in contact with the copper calorimeter. The specimen is oriented above the heat sources, with the outer shell material facing downward, with the calorimeter placed above the thermal liner of ensemble. The specimen can be mounted by placing the material to be used as the outer shell on a mounting plate with a 10.2 x 10.2 cm (4" x 4") hole cut out of its center. The side to be used as the exposed surface faces downward to the heat sources below. The subsequent layers in the ensemble are then placed on top in the order used in the garment, such that the surface to be worn towards the skin is facing up. Once all of the layers have been added, the copper calorimeter can be placed in direct contact with the thermal liner material, facing downward. This mounting plate then is placed 12.7 cm (5") from the quartz lamp array.

Using the Stoll and Chianta Curve[16] approach described in the previous section of this thesis, the time to 2nd degree burn is measured by determining the thermal end point where the measured temperature curve and the Stoll and Chianta Curve cross. This information is used to calculate the Thermal Protective Performance (TPP) of the ensemble by multiplying the exposure heat flux (83 kW/m^2) and the time to burn values. NFPA 1971 requires that ensembles consisting of an outer shell, moisture barrier, and thermal barrier inner liner, to be used in structural fire fighting, have a TPP rating of not less than 1450 kJ/m^2 (35.0 cal/cm^2).[2]

NFPA 1977, *Protective Clothing and Equipment for Wildland Fire Fighting*

NFPA 1977, *Protective Clothing and Equipment for Wildland Fire Fighting*, provides fit and testing requirements for garments intended to be used during wildland fire fighting operations.[4] This standards includes specifications on protective clothing, helmets, gloves, footwear, and fire shelters to be used during wildland fire fighting operations. The portions of this standard relevant to the current work are incorporated into the sections on the Radiant Protective Performance (RPP) Test. This test, like the TPP test, requires the use of the copper calorimeter described in ASTM D 4108[16] for the evaluation temperature rise behind the clothing material. Unlike the TPP test, only a radiant exposure, produced by a quartz lamp assembly, is required in the RPP test.

The RPP test requires that textile fabrics used for wildland protective clothing be exposed to 21 kW/m^2 $\pm$ 4 kW/m^2 (0.5 cal/cm^2s $\pm$ 0.1 cal/cm^2s) from a bank of five quartz lamps. This heat flux level is determined by the temperature response of the copper calorimeter using Equation 4.[4] The quartz lamps are arranged in a vertical array, centered behind transite board with a 5.7 cm x 14 cm (2.25” x 5.5”) cutout. The fabric specimens, measuring 7.6 cm x 25.4 cm (3” x 10”), are held in place on the same assembly as the quartz lamps with a holder plate, such that the front surface is 2.5 cm (1”) from the surface of the quartz lamps. The front face of the fabric holder plate has a 6.5 cm x 15.2 cm (2.5” x 6”) cutout, through which the fabric sample is actually exposed to the radiation from the quartz lamp. The fabric is placed within this front holder plate,

and then held in place with a rear holder plate, which has a 7.6 cm x 12.7 cm (3" x 5") center cutout for the copper calorimeter. The copper calorimeter is held in place behind the fabric sample using brackets on the back surface of the rear holder plate. There is no spacer required in this test method, although a small gap will exist between the fabric and the copper calorimeter due to the thickness of the rear holder plate.

After the test apparatus has been set up, a shutter is placed between the fabric and the lamp array, and the lamps allowed to heat up for 60 seconds. During the test, the shutter is removed, and the clothing exposed to the 21 kW/m^2 heat flux for at least 25 seconds. The performance of the protective clothing is evaluated using the thermal endpoint criteria described in the discussion of ASTM D 4108.[16] The temperature rise of the copper calorimeter is plotted against the Stoll and Chianta Curve to obtain a value for the time to 2nd degree burn. This time is then multiplied by the fabric exposure heat flux to determine an RPP value. NFPA 1977 requires that textile fabrics to be used for wildland protective clothing have an average RPP value of not less than 290 kJ/m^2 (7.0 cal/cm^2).

2.3 Current Test Limitations and Proposed Improvements

The current test methods for fire fighting clothing provide a means to compare the materials and ensembles. Unfortunately, the basis for the determination of the time to 2nd degree burn specified in these tests is based upon rectangular heat pulse exposures to bare skin, and cannot be accurately applied to the time varying heat flux exposures experienced while wearing fire fighting clothing.[12] The assumption regarding the applicability of the Stoll and Green data[9] to the evaluation of fire fighting clothing is based upon the equivalency of the heat flux-time product imposed on the copper calorimeter. The use of these data assumes that the burn times predicted using the Stoll and Chianta Curve,[8] which is based upon constant heat flux levels, should be accurate regardless of the shape of the heat flux curve.

One simple case where this method for predicting the time to 2nd degree burn appears to be erroneous is introduced below. This example exposes the copper calorimeter to two rectangular heat flux levels, one at 4 kW/m^2, which is nominally the lowest heat flux level presented in ASTM D 4108, and one at 50 kW/m^2, which is nominally the highest heat presented in ASTM D 4108.[16] This example exposes the copper calorimeter to the low heat flux throughout the exposure, with the exception of a 1 second interval when it is exposed to the high heat pulse level. The copper calorimeter temperature response is determined using Equation 4. This temperature information is compared against the Stoll and Chianta Curve to determine whether or not a 2nd degree burn will occur.

When the high heat flux limit is introduced at the beginning of the exposure, the copper calorimeter will increase above the Stoll and Chianta Curve, and a 2nd degree burn is said to occur 1 second after the beginning of the 50 kW/m^2 exposure (Exposure A, Figure 4). However, when the copper calorimeter is exposed to 4 kW/m^2 for 10 seconds, then exposed to the 50 kw/m^2 heat pulse level for 1 second, the curves do not cross, and this high flux limit will not produce a 2nd degree burn (Exposure B, Figure 4). If the application of the 4 kW/m^2 heat pulse continues after the one second high heat level stops, it will eventually lead to a 2nd degree burn (Exposure B, Figure 4). However, the 1 second exposure to 50 kW/m^2 no longer produces a 2nd degree burn. If a third case is evaluated, with the copper calorimeter exposed to 4 kW/m^2 for 20 seconds, before being exposed to the 50 kW/m^2 for 1 second, then the curves cross, and a 2nd degree burn is said to occur (Exposure C, Figure 4). Therefore, the determination of the whether a 2nd degree burn will occur or not is dependent upon not just the heat flux exposure, but when this exposure occurs. In the second case of the previously outlined example, the copper calorimeter was exposed to more total heat than in the first case. However, when the high level heat flux was applied, no 2nd degree burn was said to occur.

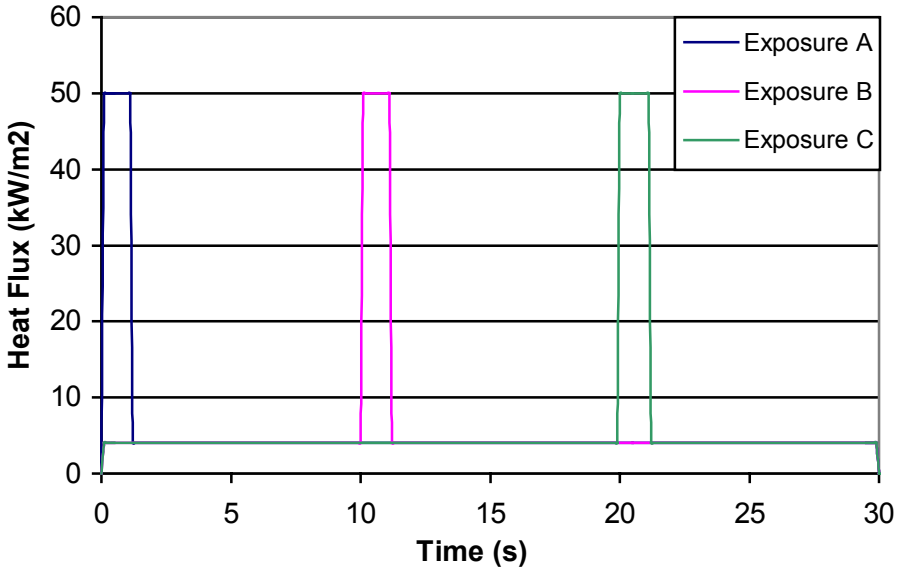

Figure 3: Copper Calorimeter Temperature Response Example - Heat Flux Exposure Cases. Exposure A, 4 kW/m^2 Exposure for 30 Seconds, with 50 kW/m^2 Pulse for 1 Second Starting at Beginning. Exposure B, 4 kW/m^2 Exposure for 30 Seconds, with 50 kW/m^2 Pulse for 1 Second Starting at 10 Seconds. Exposure C, 4 kW/m^2 Exposure for 30 Seconds, with 50 kW/m^2 Pulse for 1 Second Starting at 20 Seconds.

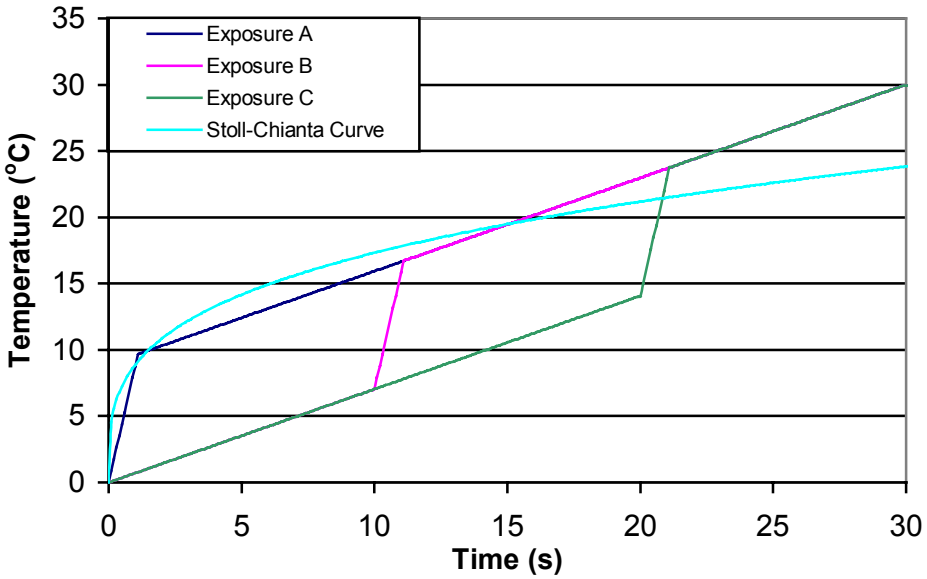

Figure 4: Copper Calorimeter Temperature Response Example – Comparison of 2nd Degree Burn Predictions for Exposures A, B, C (Figure 3). 50 kW/m^2 Heat Flux for 1 Second in Exposures A and C Will Produce a 2nd Degree Burn, while 50 kW/m^2 Heat Flux for 1 Second in Exposure B Will Not Produce a 2nd Degree Burn. If 4 kW/m^2 Flux Continues After Removal of 50 kW/m^2 Flux in Case B, 2nd Degree Burn will Result.

If the temperature response of actual skin is modeled, as outlined in Section 3.2.2 of this thesis, then exposure to a high flux level of 50 kW/m^2 for 1 second will always produce a 2nd degree burn, regardless of when it is applied. The new test methods proposed in this thesis utilize a skin simulant sensor to measure the temperature rise behind a layer of clothing (Section 3.2.1). These temperature measurements are then used in conjunction with heat conduction models of the skin simulant sensor and the skin to predict the time to 2nd degree burn using the Henriques Burn Integral.[11] This calculation procedure for the skin simulant sensor is outlined in Section 3.2.2

The method for the prediction of the time to 2nd degree burn using the copper calorimeter is based upon the time for the copper calorimeter to reach a thermal endpoint, at which a 2nd degree burn is said to occur. This information is based upon tests conducted on bare skin. The application of these results to cases where the skin is covered by protective clothing does not consider the effects of the clothing on the cooling of the skin. During the exposure, the clothing layer between the skin and the heat source will rise to temperatures higher than those of the skin. When the heat source is removed, the clothing will begin to cool, while the skin is still being heated by conduction from the hot clothing. After a period of time, the skin will also begin to cool, but not as rapidly as bare skin due to the hot clothing layer. This hot clothing layer will restrict the flow of heat away from the skin. As the thermal endpoint information is based upon the heating and cooling of bare skin, this information cannot be directly applied to the cases with a clothing layer over the skin, because the cooling no longer takes place at the same rate as bare skin.

The burn assessment methods for the skin simulant sensor do not use a thermal endpoint method based upon data for burns to bare skin to predict the time to 2nd degree burn. The methods presented in this thesis use the heat flux to the skin during the heating and cooling stages of the test to determine the exposure time that will produce a 2nd degree burn. These methods calculate or estimate the delay time between the removal of the heat source and the onset of skin cooling, while also accounting for the slower cooling rate of the skin due to the hot

clothing layer. There are two methods used to predict the time to 2nd degree burn for the skin simulant tests. The first models the heat transfer through the clothing into the skin simulant sensor or the skin, and is presented in the Skin Simulant Sensor portion of Section 3.2.2. The second method calculates the heat flux at the skin simulant surface from the measured surface temperature of the skin simulant, and then inputs this information into a model of the skin to predict the time to 2nd degree burn. This method is presented in Section 4.2.2.

The current test methods provide a means to compare the clothing materials against each other, without accurately predicting the time to 2nd degree burn. These test methods do not calculate or evaluate the thermal properties of the materials. This information is indirectly related to the RPP and the TPP rating, as materials with more appropriate thermal properties will increase the time to 2nd degree burn, and increase the RPP or TPP ratings. However, this effect cannot be quantified in the current test method, as the thermal properties do not play an active role in the clothing evaluation. If the thermal properties of the clothing can be determined and the clothing system modeled accurately, this information could be used by designers to select the best materials for different clothing applications. This information would allow the designers to determine the actual affects of the different thermal properties, while also allowing them to predict the clothing performance without having to run a series of destructive tests. A method to predict the thermal properties of individual clothing samples, or ensembles, is presented in Section 3.1. This information is then used in a heat conduction model (Section 3.2.2) of the clothing and the skin simulant sensor, and the clothing and the skin, to predict the time to 2nd degree burn.

The current test standards do not consider the effects of moisture on the performance of the clothing. This information may be important, as the clothing may become wet due to water spray, or perspiration from the fire fighter. Additionally, the current test methods do not evaluate the affects of compression on the clothing performance. This information may be important, as burns can results when the clothing is compressed by contact with a hot object. Additionally, the material properties of a clothing ensemble may be different when compressed due to the loss of

the air gaps that form between the layers and in the thermal liner material. While most of the clothing remains uncompressed while in use, certain parts, such as the area around the straps of the SCBA, or around the shoulders of the coats, may become compressed, diminishing the protective performance.

The sensor specified in the current test methods, while easy to construct and instrument, has thermal properties vastly different from those of skin. These differences lead to different temperature responses of the copper calorimeter, as opposed to a sensor with properties similar to those of human skin. These temperature differences may not only lead to different calculated values for the heat flux reaching the skin, but may also impact the amount of heat transmitted through the clothing. This effect may be exaggerated in tests in which moisture is added to the clothing, as the temperature differences of the sensor behind the clothing may in turn lead to differences in the water transmission through the clothing during the test. In addition, if the damage caused during skin cooling is to be assessed, then the sensor used to measure the temperature rise and fall throughout the test must be able to accurately track the temperature during heating and cooling. The copper calorimeter has vastly different cooling properties than that of human skin, and this does not allow one to assess the impact of the clothing on skin cooling.

In addition to problem with the copper calorimeter, and it's use in the prediction of the time to 2nd degree burn, the current test methods utilize a heat flux source with spectral characteristics very different from those of actual fires. The quartz lamps provide a relatively easy means to produce the required heat flux levels in a short period of time; however, they operate at much higher temperatures than typical fires, and therefore have different wavelength distributions for the radiant energy. This temperature difference may produce different results for the burn time predictions if the clothing materials evaluated have wavelength dependent emissivity and reflectivity values. While determining the emissivity of the clothing materials was outside the scope of this project, the RPP results for the quartz lamp are compared against RPP results

obtained through tests conducted using a cone heater. The cone heater operates at much lower temperatures than the quartz lamp, and may provide a more accurate representation of a fire. A more in depth discussion of the differences between the quartz lamp and the cone heater is presented in Section 4.2.2 of this thesis.

3.0 PROPOSED NEW TEST METHODS

3.1 Thermal Properties Test Fixture

The Thermal Properties Test Fixture (TPTF) was designed to allow small samples of clothing to be tested for the purpose of determining their thermal properties when either dry or damp.[5] The test fixture was constructed such that individual materials could be evaluated separately, or combined into ensembles. The heat flux levels used to evaluate the clothing properties were generally much lower of than those experienced by firefighters during firefighting operations, typically on the order of 4 kW/m^2. These low heat flux levels did not damage the clothing samples, and the effects of material charring or other related damage were not assessed.

3.1.1 TEST CONFIGURATION

The Thermal Property Test Fixture was designed by Ktech Corporation to evaluate dry and damp fabric materials. The test apparatus consists of a four-sided, 10 cm x 10 cm Plexiglas box, providing low thermal conductivity walls that also prevent moisture loss from the edges of the clothing. The test is set up in a sandwich like format, with two skin simulant sensors centered about an etched foil heater. The clothing samples are placed between the etched foil heater and the skin simulant sensors, allowing the heat transferred through the clothing to be determined. Figure 5 presents a picture of the TPTF.

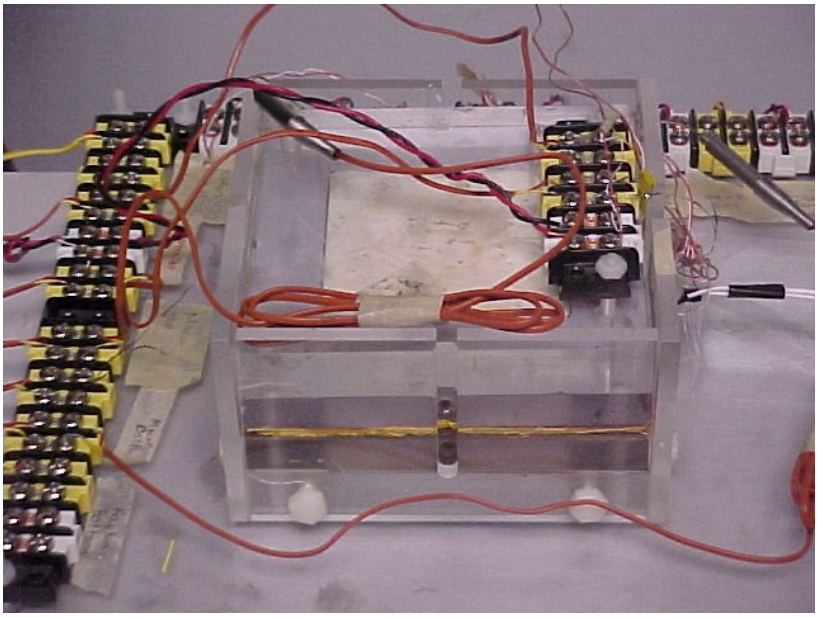

Figure 5: Thermal Properties Test Fixture – Heater Located Between Nomex Layers (Yellow Material Inside Test Fixture). White Material Visible Through Plexiglas on Top of Test Fixture is the Unexposed Face of the Macor Skin Simulant. Skin Simulant Sensors Located on Top and Bottom of Assembly.

Figure 6 provides a depiction of the test fixture cross section, while Table 6 provides a description of the thermocouple or thermopile heat flux sensor locations. Each of the thermocouples in the system were of the Type K variety. Depending upon the type of material being evaluated, between one and three layers of clothing were tested at one time.

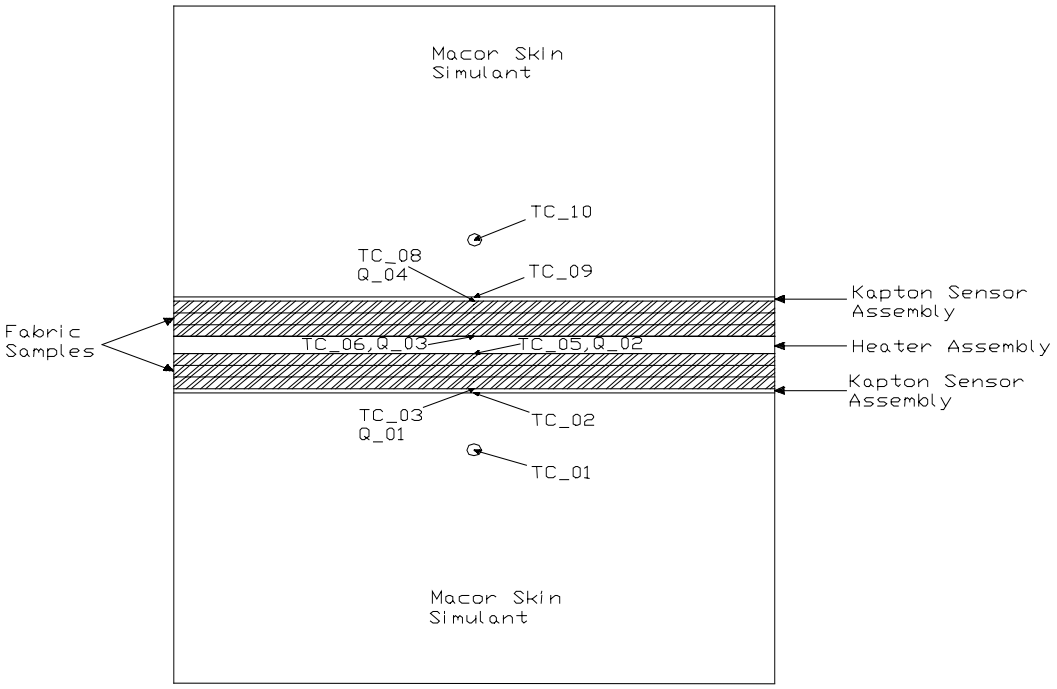

Figure 6: Thermal Properties Test Fixture Cross Section – Drawn to Scale. Sensor Description Presented in Table 6. Thermocouples TC_04 and TC_07 Not Included. Macor Skin Simulant Sensor Held with Plexiglas Holding Assembly within Plexiglas Box.

Table 6: Thermal Properties Test Fixture Sensor Description

Sensor	Description
TC_10	Upper Skin Simulant Sensor Subsurface Thermocouple – Nominally 2.5 mm below exposed Macor surface
TC_09	Upper Skin Simulant Sensor Foil Thermocouple – Mounted on Macor surface
TC_08	Thermocouple mounted on downward facing surface (towards heater) of upper Kapton assembly
TC_07	Optional 30 gage thermocouple placed between fabric layers
TC_06	Thermocouple mounted on upward facing surface of heater assembly
TC_05	Thermocouple mounted on downward facing surface of heater assembly
TC_04	Optional 30 gage thermocouple placed between fabric layers
TC_03	Thermocouple mounted on upward facing surface (towards heater) of lower Kapton assembly
TC_02	Lower Skin Simulant Sensor Foil Thermocouple – Mounted on Macor surface
TC_01	Lower Skin Simulant Sensor Subsurface Thermocouple – Nominally 2.5 mm below exposed Macor surface
Q_04	Thermopile heat flux sensor mounted on downward facing surface (towards heater) of upper Kapton assembly
Q_03	Thermopile heat flux sensor mounted on upward facing surface of heater assembly
Q_02	Thermopile heat flux sensor mounted on downward facing surface of heater assembly
Q_01	Thermopile heat flux sensor mounted on upward facing surface (towards heater) of lower Kapton assembly

The heating assembly used in this phase of the testing consisted of a 10 cm x 10 cm etched foil heater laminated with a Kapton film on each side, and powered by a DC voltage supply. This heater was capable of producing heat fluxes up to 15 kW/m^2, although the adhesive used in the construction had a temperature limit of 125^{o}C. The typical TPTF test was run with 40 VDC supplied to the heater, producing heat fluxes ranging from approximately 3.0 to 4.5 kW/m^2, depending upon the material being evaluated, and the condition of this material. As shown and described in Figure 6 and Table 6, the heater had thermocouples and thermopile heat flux sensor mounted on each side. Additional thermocouple and thermopile heat flux sensors, mounted on a Kapton film, were used in the TPTF to provide additional measurements of the heat transmission through the clothing. The test apparatus was set up such that additional thermocouples could be added between the clothing layers, providing additional temperature data that could be used to assess the thermal properties of the material evaluated.

The top and bottom of the TPTF consisted of skin simulant sensors, enclosed in Plexiglas holding assemblies. The skin simulants were constructed of Macor, a ceramic material with a thermal conductivity of approximately 1.5 W/m-K and a thermal inertia parameter of approximately 1750 W-s$^{1/2}$/m^2-K.[17] The thermal properties of the Macor ceramic materials were assumed to be independent of temperature throughout this thesis. The thermal inertia parameter is approximately 18% higher than that of skin exposed to 10 kW/m^2. The surface temperature rise during the heating of a semi-infinite solid is inversely proportional to the thermal inertia parameter, meaning that the surface temperature rise of the Macor will be lower than that of actual skin under a given heat flux. The Macor skin simulant sensor blocks used in this phase were 12.7 mm thick. A Macor block this thick will exhibit semi-infinite behavior for approximately 55 seconds.[18] The Macor skin simulant was instrumented with 2 thermocouples. A foil thermocouple was bonded to the exposed surface so that it was flush with the surface of the Macor, while an additional sheathed thermocouple was inserted into a hole, nominally 2.5 mm below the exposed surface.

The power to the heater was supplied by a DC voltage supply. A simple circuit was set up to connect the heater to the power supply. This circuit allowed the power to the heater to be determined, by monitoring the voltage and current throughout the test. The temperature and voltage data from the TPTF was collected with an IOTech Daqbook 200, data acquisition system.

The TPTF tests began by placing the clothing layers to be evaluated into the test fixture, and waiting for the temperature to balance out throughout the apparatus. Typically, the test began when the temperature of the heater was within 1^{o}C of the temperature of the Macor blocks. Data from the TPTF tests were collected for total of three minutes. Twenty seconds after the initiation of the data acquisition system, a constant voltage was applied across the heater, until the temperature reached approximately 120^{o}C – 125^{o}C. The twenty second period allowed an average, pre-heat temperature to be determined, while also ensuring consistency amongst the thermocouples or thermopile heat flux sensor measurements throughout the test fixture. The heating period typically lasted between forty and eighty seconds, depending on the material being evaluated. When the temperature of the heater reached nominally 120^{o}C, the power supply was shut off, and the system was allowed to cool. Figure 7 presents a graph of the temperature and heat flux levels attained in a typical test in the TPTF.

The heat flux levels attained during this testing were not high enough to damage the clothing materials or the test apparatus. This level was selected because it was easily attainable using a DC power supply, and allowed the properties to be determined over a heating and cooling period in a relatively short period of time. After each test, the fabric samples were removed from the test fixture and allowed the cool. The skin simulant sensors were allowed to cool for approximately 10 to 15 minutes, allowing the Macor to return to isothermal conditions throughout. The next fabric samples to be evaluated were then placed into the test fixture, the apparatus was allowed to thermally balance out, and the next test was set to begin.

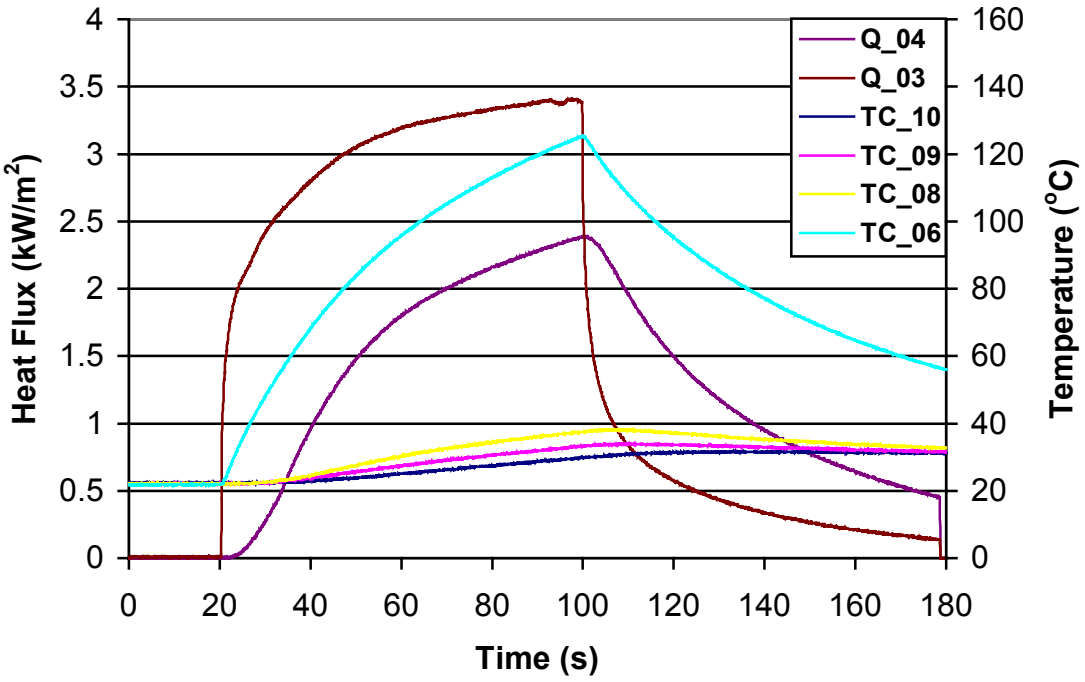

Figure 7: Thermal Property Test Fixture – Sample Temperature and Heat Flux Versus Time from Top Half of Thermal Properties Test Fixture. Q_04 – Kapton Heat Flux, Q_03 – Heater Heat Flux, TC_10 – Macor Subsurface Temperature, TC_09 – Macor Surface Temperature, TC_08 – Kapton Assembly Temperature, TC_06 – Heat Temperature

Early in the testing process, one side of the heater developed an air bubble between the Kapton film and the thermopile heat flux sensor. This air bubble prevented a uniform heat flux over the entire area of the heater on that side, and invalidated the results for that half of the test fixture. However, the other half continued to produce consistent results. Near the end of this thesis, a new heater was obtained, allowing results to be determined from both halves of the test fixture.

Initially, the TPTF evaluations were conducted with the Daqbook 200 data acquisition rate set at one-second. Due to the inherent uncertainty in the measurement abilities of the thermocouples and the data acquisition system, 2°C and 1°C respectively, the initial temperature measurements had an uncertainty of approximately 1°C to 2°C at ambient conditions. This temperature uncertainty band is presented in Figure 8 for one of the thermocouples in the TPTF.

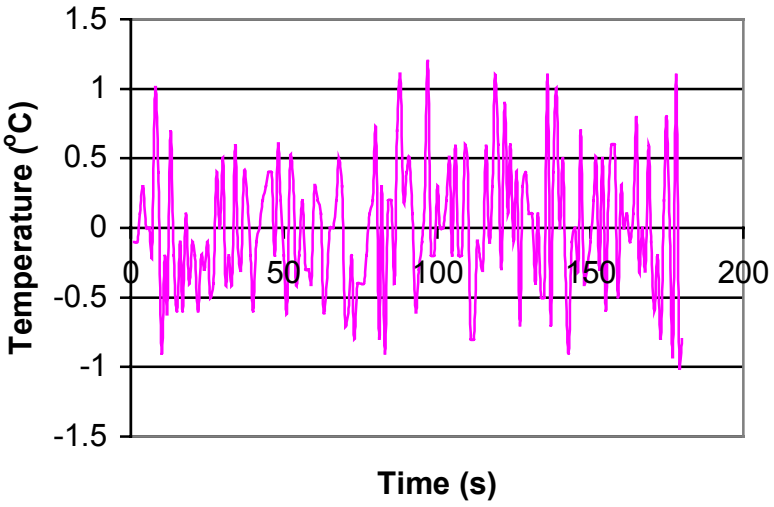

Figure 8: Temperature Precision TC_09 – Macor Surface Thermocouple Difference Between Measured Temperature and Average Temperature over Three Minute Time Span at Ambient Conditions. 1 Second Data Acquisition Rate, and No Averaging of Measurements. Average Standard Deviation of 0.5°C.

The temperature measurement uncertainty was compounded in the calculation of heat flux levels from the Macor temperature response, which is discussed later in this section. In addition, this measurement uncertainty could later lead to problems in the calculation of the time to 2nd degree burn from the skin simulant. Damage only occurs when the temperature of the skin is greater than 44°C, and the uncertainty could lead to temperature measurements which increased to temperatures greater than 44°C at one time step and less than 44°C at the next. In order to decrease the uncertainty of the temperature measurements, the measurement acquisition rate was increased (faster acquisition rate) and the measurement data were smoothed using a running average function in the data acquisition program Daqview, the interface program for the IOTech Daqbook. The data was smoothed using an averaging function in Daqview.

Table 7 presents the different measurement procedures, along with the uncertainty of each. The uncertainty is presented as the Standard Deviation of the difference between the individual temperature measurements from the average temperature over a three minutes time span at ambient conditions. This value was determined for each thermocouple in the TPTF, and an

average value calculated for the entire apparatus. This information is presented in graphical form in Figure 9.

Table 7: Data Acquisition Measurement Uncertainty. Standard Deviation of the Difference Between the Temperature Measurements from the Average Temperature Over a Three Minute Time Span at Ambient Conditions.

Time Step	Running Average	Average Standard Deviation for Apparatus (^{o}C)
1 Second	No Average	0.50
1 Second	3 Point	0.30
0.1 Second	5 Point	0.23
0.1 Second	10 Point	0.17
0.1 Second	20 Point	0.13
0.1 Second	30 Point	0.10

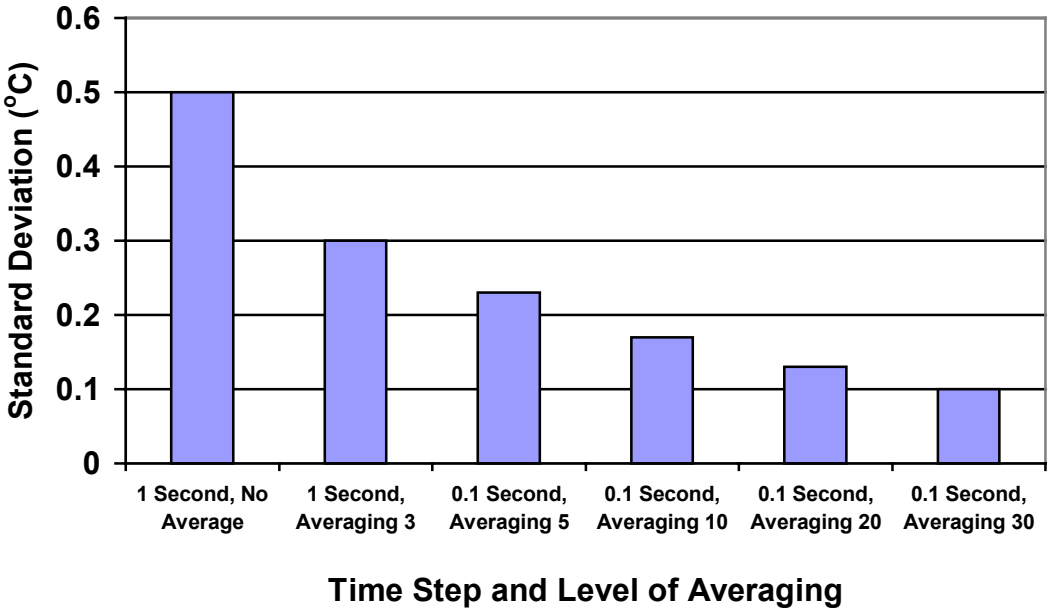

Figure 9: Thermocouple Measurement Uncertainty at Ambient Conditions – Comparison of Different Time Step and Averaging Levels. Values Presented are the Average of the Standard Deviation of the Difference Between the Measured Temperature at Each Time Step and the Average Value at Ambient Conditions for Each Thermocouple in the Apparatus. The Level of Averaging Set in Daqview.

A 0.1-second time step, with Daview set to average 30 readings, was selected for the remainder of testing. This provided measurements with an uncertainty of 0.10^{o}C. The revised temperature

uncertainty band for this measurement and averaging level is presented in Figure 10 for one of the thermocouples in the TPTF.

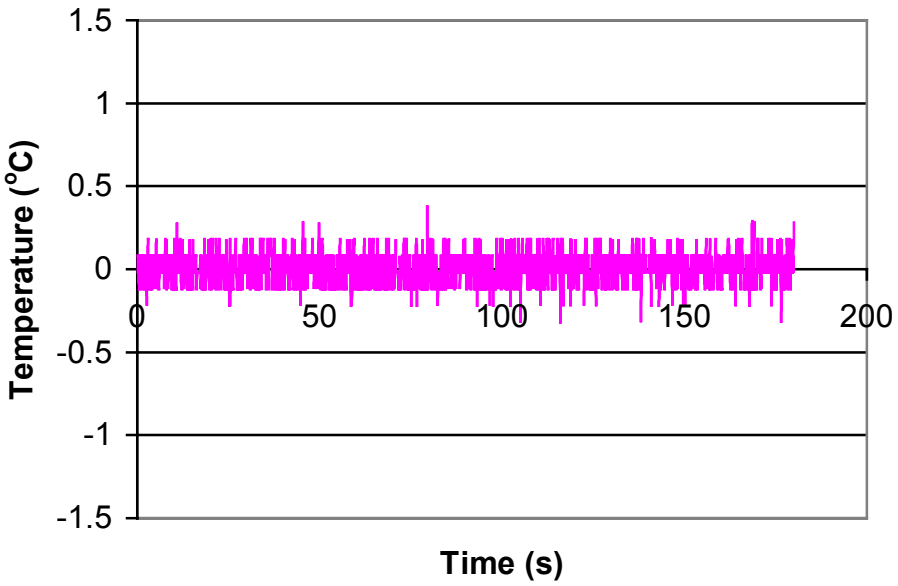

Figure 10: Temperature Precision TC_09 – Macor Surface Thermocouple Difference Between Measured Temperature and Average Temperature over Three Minute Time Span at Ambient Conditions. 0.1 Second Data Acquisition Rate, with 30 Point Moving Averaging of Measurements. Average Standard Deviation of 0.1°C.

The Daqview computer program saved the measured temperature data as a text file (.txt) which could be viewed using a spreadsheet program. The capabilities of the data acquisition system as currently configured did not allow for direct heat flux measurements. The thermocouple card for the Daqbook automatically converted the voltage measurements for the thermocouples into a temperature reading, based upon the thermocouple type. The voltage readings for the thermopile heat flux sensors were collected as Type K thermocouple data. These values were then converted to voltage readings, which were then used to calculate heat flux.

A macro was written Microsoft Excel to calculate the voltage from the thermopile heat flux sensor readings using the Newton-Raphson method. The temperature readings from the data acquisition system for each thermopile heat flux sensor were copied into a separate sheet in

Excel, and the difference between these temperature readings and the cold junction temperature were determined. The macro then determined voltage readings that would produce equivalent temperatures. The macro used an initial voltage estimate of 0.01 V for the heat flux reading, and calculated the temperatures using the Type K temperature conversion equation in the Omega Temperature Handbook.[19] The calculation method then determined the difference between the calculated temperatures and the measured temperatures minus the cold junction temperature. These values were then divided by the respective derivatives of the Type K temperature conversion equation. These values were then subtracted from the original voltage estimate to calculate revised voltage estimates. This calculation technique was then repeated, until there were no changes in the voltage estimates from one iteration to the next. The voltages calculated via this method could be converted back to temperature data using the Type K conversion equation.[19] After four iterations, the temperatures calculated from the voltages were equivalent to those measured with the thermopile heat flux sensors. The heat flux voltage estimates were multiplied by temperature correction factors, and then converted to heat flux readings using conversion factors obtained from the manufacturer for each thermopile heat flux sensor. In addition to converting the temperature measurements for the thermopile sensors to heat flux values, the Macro also added headings to the temperature and voltage data, and produced graphs of the temperature and heat flux values throughout the three minute test.

The Kapton thermopile sensors provided a measurement of the heat flux to the skin simulant surface. This heat flux level could be calculated using the temperature response of the Macor as well. One aspect of this project was the use of an Inverse Heat Conduction Code to calculate the heat flux through the clothing.[20] This program can calculate the heat flux level at the location of the thermocouples throughout the TPTF. This program uses the temperature data from the TPTF, as well as the thermal properties of the materials involved, as input to predict the heat flux.

In order to calculate the heat flux to the skin surface without having to run a separate program, a calculation procedure was incorporated into the Microsoft Excel data collection macro for the

TPTF. The estimates produced by this algorithm provided an accurate track to the values measured by the thermopile heat flux sensors. However, there was more fluctuation in the estimates from the algorithm than those produced by the Inverse Heat Conduction Code. The heat flux algorithm, Equation 6, is referred to as the Diller's Algorithm throughout this thesis, and is based upon the change in temperature at the surface of a semi-infinite solid.[25] The determination of the net heat flux at a sample time step, t_n, is based upon the temperature change (T_j-T_{j-1}) at all previous time steps, including the one at t_n.

$$q''_n(t_n) = \frac{\sqrt{k\,\rho c_p}}{\sqrt{\pi \Delta t}} \sum_{j=1}^{n} \frac{T_j - T_{j-1}}{\sqrt{n+1-j}} \qquad \text{Equation 6}$$

This equation was incorporated into the Microsoft Excel macro. Figure 11 presents a comparison of the heat flux calculated using Diller's Algorithm and that measured by the Kapton sensor located next to the Macor skin simulant. While the Heat Flux calculated using Diller's Algorithm fluctuates throughout, it does match the shape of the heat flux exposure measured by the Kapton sensor.

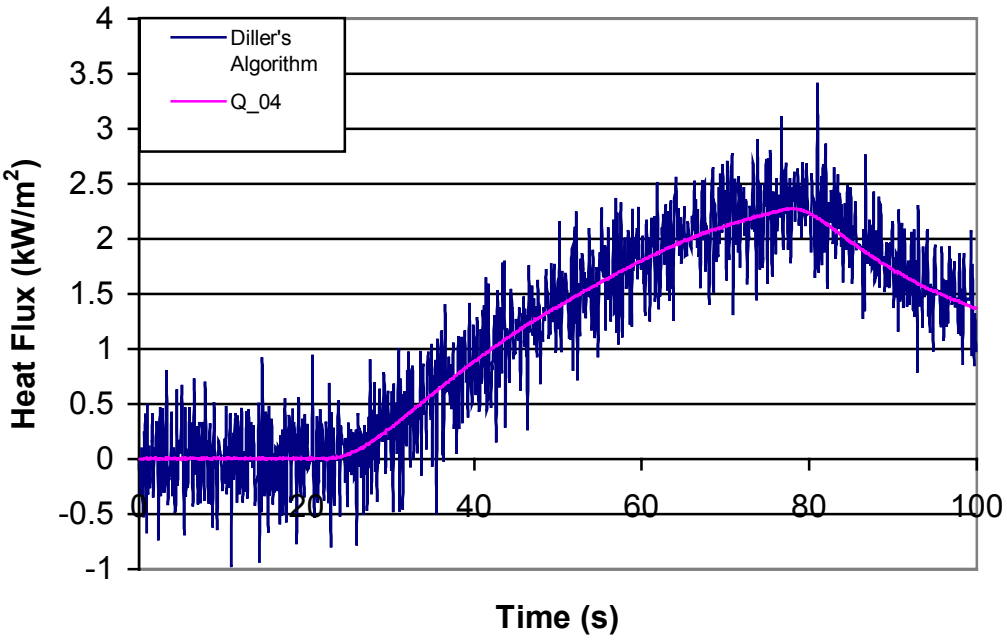

Figure 11: Heat Flux at Macor Skin Simulant Surface – Comparison of Measurement Q_04 (Upper Kapton Thermopile Heat Flux Sensor) and Values Calculated Using Diller's Algorithm, Based upon Temperature Measurement from TC_09 (Upper Macor Skin Simulant Surface Thermocouple).

3.1.2 TEST CASES

Several characterization tests were run using the TPTF in order to ensure consistent performance. These tests were also used to determine the most efficient means to run the test and collect the data. Following the determination of a set testing procedure and calculation process, a full test plan was compiled. This test plan involved the evaluation of turnout gear material obtained from Lion Apparel, as well as sample materials used in various tests at WPI in the past. The materials tested can be separated into three primary types; outer shell and stand alone fabrics, moisture barrier, and thermal liner. Only one type of moisture barrier and thermal liner were obtained for this testing, while several different types of outer shell or stand alone fabrics were evaluated. Table 8 below includes a summary of the fabrics involved in the testing.

Table 8: Test Materials Evaluated in Thermal Properties Test Fixture.

Fabric Types	Anticipated Use
Nomex IIIA 7.5 ounce/square yd (oz/sq yd)	Outer Shell/Stand-Alone
Nomex 6.0 oz/sq yd	Outer Shell/Stand-Alone
Nomex 5.5 oz/sq yd	Outer Shell/Stand-Alone
PBI 7.5 oz/sq yd	Outer Shell/Stand-Alone
PBI 6.0 oz/sq yd	Outer Shell/Stand-Alone
Navy Blue Mat. 6.8 oz/sq yd	Outer Shell/Stand-Alone
Southern Mills Green Mat. 8.5 oz/sq yd	Outer Shell/Stand-Alone
Aralite (Southern Mills)	Thermal Liner
Crosstech E-89	Moisture Barrier

To prevent damage to the sensor and heater assemblies within the TPTF by compressing the thermocouples and heat flux sensors, the outer shell and moisture barrier materials were tested with three layers of each on both sides of the heater, while the thermal liner was tested with one layer on each side of the heater. With the exception of the Crosstech E-89 Moisture Barrier, each of these materials were tested at various moisture contents. The materials were evaluated wet to determine the effect of the added moisture on the thermal properties of the clothing. The materials may become wet during actual use, from either water spray or perspiration, and this added moisture may adversely affect the performance of the clothing materials. To evaluate the materials wet, distilled water was added on a gram of water per gram of fabric basis.

In addition to the individual material tests, several ensembles were evaluated. Each of the ensemble tests included the use of the Aralite thermal liner, the Crosstech moisture barrier, and one of the outer shell materials. Ensemble tests were completed using Nomex IIIA 7.5 oz/sq yd, Nomex 6.0 oz/sq yd, and PBI 7.5 oz/sq yd as the outer shell materials. The ensembles utilizing the Nomex IIIA 7.5 oz/sq yd outer shell were also tested with 1.0 and 1.5 grams of water per gram of Aralite added. The moisture was added to the Aralite Thermal Liner to simulate perspiration, and to determine the effect of this moisture on the thermal properties. Table 9 presents a summation of the material tests completed in the TPTF for this project. A complete set of test results for the TPTF is presented in Appendix A: Thermal Property Test Fixture Data.

Table 9: Moisture Contents Evaluated.

Material Type	Moisture Contents (grams water/grams fabric)
Outer Shell/Stand Alone	Dry, 0.25, 0.5, 1.0
Moisture Barrier	Dry
Aralite Thermal Liner	Dry, 1.0, 1.5
Ensemble	Dry, 1.0 (Aralite), 1.5 (Aralite)

3.1.3 MATERIAL PROPERTY DETERMINATION - PROP1D

The primary intention of the Thermal Property Test Fixture was to produce test data that can be used to assess the thermal properties of the materials tested. A parameter estimation code, provided by Beck Engineering Consultants Company, was used for this purpose.[6] The parameter estimation code uses the temperature and heat flux measurements for the Thermal Property Test Fixture as input. The parameter estimation technique involves minimizing a weighted sum of squares criterion, S, that involves the measured temperatures in the TPTF, Equation 7.[6]

$$S = \sum_{j=1}^{J_T} \sum_{i=1}^{n} (Y_{ji} - T(\boldsymbol{b})_{ji})^2 \qquad \text{Equation 7}$$

J_T is the number of thermocouples, Y_{ji} represents the measured temperature at location x_j and time t_i, and $T(\beta)_{ji}$ is the corresponding calculated temperature determined using the finite control volume method in PROP1D. The calculated temperature $T(\beta)_{ji}$ is a function of the estimated thermal parameters, the thermal conductivity (k) and the volumetric heat capacity (ρc_p). The vector β contains the "true" parameter values, and the estimated values of the parameters are found by minimizing S through the use of a modified Gauss method.[5] The parameter estimates, calculated in vector b, are determined through the use of an iterative scheme using Equation 8.[21]

$$b^{i+1} = b^i + (X^{T^i} X^i)^{-1} (X^{T^i} (Y - T^i)) \qquad \text{Equation 8}$$

Where i is the iteration number, Y is the measured temperature, and T^i is the temperature vector calculated knowing b^i, which is the vector containing the estimated parameters at the i^{th} iteration. The quantity X is a temperature dependent sensitivity coefficient matrix. The vector temperature, T^i, is calculated at each iteration using a numerical solution of the one dimensional energy equation using the parameter estimates, b^i. At each iteration, T^i is determined using the numerical solution of the one-dimensional heat transfer governing equation, Equation 9.[21]

$$\frac{\partial}{\partial x}\left(k_l \frac{\partial T_l}{\partial x} \right) = \left(\rho c_p \right)_l \frac{\partial T_l}{\partial t} \text{ ,where } l \text{ is the index of materials} \qquad \text{Equation 9}$$

PROP1D uses finite difference approximations of the governing equations with the Crank-Nicolson method to determine the calculated vector temperature.[6] The PROP1D program updates the parameter estimates as new experimental information is added at each time step.

The PROP1D estimation input files were typically 150 seconds long, with 0.1-second time steps, producing a total of 1500 data points for each sensor. The typical test had the Kapton layer located against the Macor skin simulant. The program was set up with 10 calculated time steps per measured time steps, as recommended in the user's manual.[6] The heat flux measurement from the heater assembly was used as the heat flux boundary condition on the front face of the fabric, while the back face of the Macor block (back face of TPTF Apparatus) was assumed to be held at the initial temperature. In order to decrease the computation time, there is an option in the program allowing one to set a skip interval, which instructs the program to read from the experimental data at that interval. Due to the large input data file size, this interval was set at five, which did not impact the property estimates, while greatly increasing the computational speed. The properties of the Macor (k=1.5 W/m-K, ρc_p=2,042,000 J/m^3-K) and the Kapton (k=0.98 W/m-K, ρc_p =1,871,000 J/m^3-K)[6] were assumed to be constant, non-temperature sensitive values.

One step in the file setup process for the PROP1D program is the selection of what thermal properties are to be estimated. This setup option allows one to select whether 1, 2, 3, or 4 thermal conductivity or volumetric heat capacity estimates are to be made. A maximum total of four properties can be estimated (2 thermal conductivities and 2 volumetric heat capacities for example). If one selects 2 for the number of thermal conductivity estimates or the volumetric heat capacity values, then PROP1D will either determine the properties as linear functions of temperature for one material, or determine the thermal conductivity or volumetric heat capacity of two different materials. The properties of the clothing materials were determined on a non-

temperature sensitive, or temperature sensitive, basis depending on whether the clothing was evaluated dry or with moisture added. The thermal properties of the dry materials were assumed to be non-temperature sensitive, whereas the thermal properties of the wet materials were assumed to be temperature sensitive. The thermal properties of the wet materials were determined on a temperature sensitive basis because it was felt that the moisture transfer through the clothing away from the heater, may change as the temperature on the heated side increased.

Initially, the heat transfer across the interface of the Kapton sensor assembly and the Macor block was assumed to take place without any temperature discontinuity caused by a contact resistance between the two materials. However, during the development of the one dimensional heat conduction model for the determination of the time to 2nd degree burn from the skin simulant sensor, it was found that the incorporation of a contact resistance was necessary to obtain accurate estimates of the temperatures. This one dimensional heat conduction code is presented in latter sections of this thesis. The temperature drop across the interface is a function of the local linear temperature profiles in each material, just away from the contact disturbance.[22] Figure 12 presents a depiction of a temperature discontinuity at an interface between two materials, such as the one between the Kapton and the Macor skin simulant.

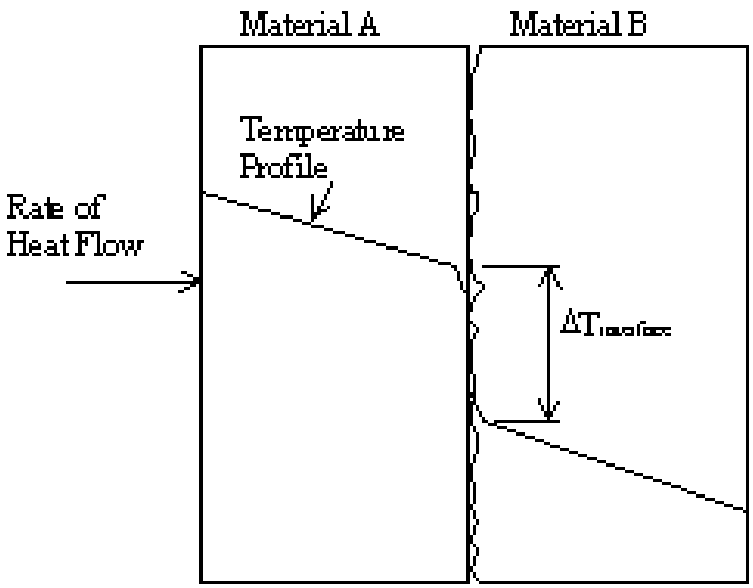

Figure 12: Interface Between Two Materials and the Effect on the Temperature Profile. Temperature Drop at the Interface Caused by a Discontinuity between the Two Materials.

The drop in temperature at the interface of the two materials can be determined by dividing the heat flux at the interface by the interfacial conductance, h_i, as shown in Equation 10.

$$\Delta T = \frac{q''}{h_i} \qquad \text{Equation 10}$$

In a perfect interface between two materials, such as a welded surface, the interfacial conductance approaches infinity, and the temperature drop at the interface will decrease to zero. The border between the Kapton sensor and the Macor skin simulant did not form a perfect interface, and the level of resistance varied from test to test. This variation of the contact resistance between one test to the next necessitated the calculation of the interfacial conductance for each individual test. The incorporation of the contact resistance into the material property input files was accomplished by adding an additional, fictitious layer into the analysis with a thickness of 1 m between the Kapton sensor and the Macor skin simulant. The volumetric heat capacity of this fictitious layer was made very small. The input file for the Prop1D computer program was configured to calculate the thermal conductivity of the 1 m thick fictitious layer.

Equation 11 presents the method for the determination of the interfacial conductance from the calculated thermal conductivity for this setup.

$$h_i = \frac{k}{L_h} \qquad \text{Equation 11}$$

By setting the thickness of the fictitious layer, L_h, equal to 1 m, the calculated value for the thermal conductivity, k, divided by the thickness of the fictitious layer would be numerically equivalent to the value for the interfacial conductance. The addition of this fictitious layer into the property analysis files improved the property estimation results, leading to lower temperature residuals in the property output files.

The calculated value for the interfacial conductance in the TPTF property evaluation provides an estimation of the proper order of magnitude for the interfacial conductance that should be used in the one dimensional heat conduction analysis used in the RPP testing analysis. This heat conduction analysis is presented in more detail in Section 3.2.2. Typical values for the interfacial conductance vary over a wide range for different materials, with values reported for ceramic-ceramic interfaces ranging from 500 W/m^2-K to 3000 W/m^2-K.[23] Typical values for the interfacial conductance during the TPTF evaluations of dry materials ranged from nominally 200 W/m^2-K to 400 W/m^2-K.

3.2 Modified Radiant Protective Performance Test

The Radiant Protective Performance (RPP) test, presented in NFPA 1977, *Protective Clothing and Equipment for Wildland Fire Fighting*[4], was selected as a means to evaluate the use of the Macor skin simulant blocks to assess fire fighting clothing for it's ability to prevent 2nd degree burns. This test was selected due to its reproducibility, as it requires only the use of a quartz lamp in a relatively simple setup. The TPP test[2], used to evaluate protective ensembles for structural fire fighting, requires that both radiant and convective heat sources be employed in a more difficult configuration than the RPP test. The evaluation criteria, through the use of the copper calorimeter and the Stoll and Chianta Curve as outlined in ASTM D 4108[16], is similar for

both standardized tests. If the skin simulant can be used to accurately predict the results in the RPP test, it should be sufficient for use in the TPP test as well.

Several potential problems with the copper calorimeter, and it's applicability to the determination of the time to 2nd degree burn for skin protected by clothing, are outlined in Section 2.3. For these reasons, the Macor sensor was used to assess the ability of this skin simulant to predict the time to 2nd degree burn when the sensor, protected by a layer of clothing, is exposed to 21 kW/m^2. Two different methods are proposed to determine the time to 2nd degree burn from the Macor skin simulant sensor, and the results appear to be a more accurate representation of the actual performance of the protective clothing. These calculation methods are presented in Sections 3.2.2 and 4.2.2. In addition to the use of the skin simulant in the evaluation of the clothing materials, a different heat source is evaluated. The quartz lamp has a much different radiant wavelength band than a fire, as it operates at much higher temperature than most fires. To assess the potential impact of the different radiant wavelength band, alternative RPP type tests were run using a cone heater, which operated at temperatures of approximately 800 – 900 K, as opposed to temperatures of approximately 1600 K for the quartz lamp.

3.2.1 TEST CONFIGURATION

The initial Radiant Protective Performance tests were run using a quartz lamp, built and donated by Ktech Corporation. The quartz lamp supplied by Ktech was built to mimic the performance of the quartz lamp assembly required by NFPA 1977.[4] It consisted of five, 500 watt, tubular, translucent quartz lamps having a 12.7 cm (5") lighted length. These lamps were mounted in a vertical array utilizing a Unistrut frame, centered behind a 5.7 cm x 14.0 cm (2¼" x 5½") insulating fiberboard window. The lamp assembly is shown in Figure 13.

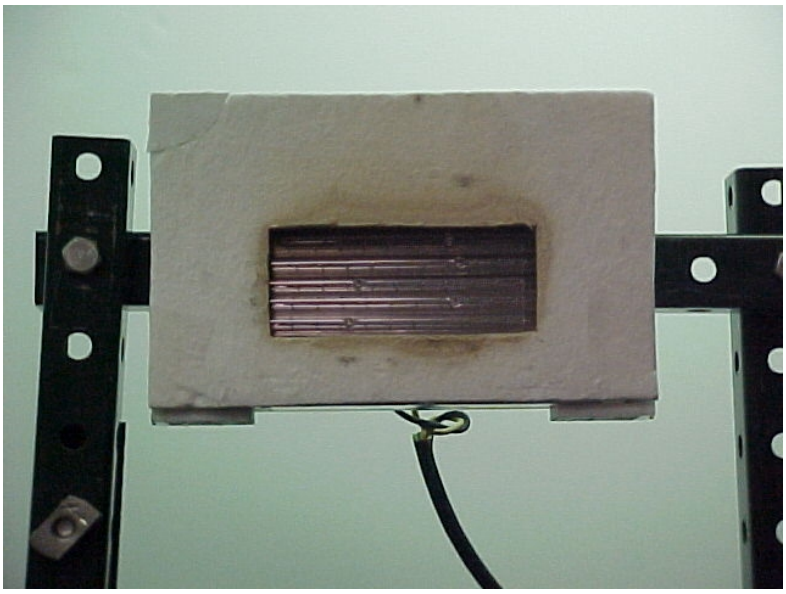

Figure 13: Quartz Lamp Assembly- Five, 500-Watt Quartz Lamps, Centered behind Insulating Fiberboard Window. Lamp Assembly Supported on Unistrut Frame. Sensor and Clothing Samples Were Placed Upon a Flat Surface So that the Front Face of the Clothing Sample was 2.5 cm (1") from Closest Face of Quartz Lamp.

The quartz lamp assembly used in this testing did not have the sample holder specified in NFPA 1977[4] incorporated into it. Instead, the RPP testing relied upon manually placing the sample and sensor on a flat surface so that the front face of the sample was 2.5 cm (1") from the nearest edge of the lamp surface and the sensor was centered in the cutout of the fiberboard window.

NFPA 1977, *Protective Clothing and Equipment for Wildland Fire Fighting*[4], requires that the fabric specimens be exposed to a thermal flux of 21 kW/m^2 $\pm$ 4 kW/m^2 (0.5 cal/cm^2 sec $\pm$ 0.1 cal/cm^2 sec).[4] The heat flux from the quartz lamps was controlled with a 120 VAC, 15 amp Variac, which controlled the voltage supply to the lamp array. As required by NFPA 1977, the copper calorimeter was used to set the heat flux from the quartz lamps.[4] At a Variac setting of 40 (out of 120), the heat flux, determined by the copper calorimeter using Equation 4, was nominally 21 kW/m^2. This heat flux level was verified using the heat flux sensor from the WPI cone calorimeter.[24]

An alternative series of RPP tests was run using the cone calorimeter heater assembly,[24] to assess the impact of the difference in the spectral distribution between the quartz lamps and the cone heater on the RPP results. The load cell of the cone calorimeter was set at a height where the fabric surface was 2.5 cm (1") from the cone heater. The heat flux from the cone was measured using the heat flux sensor, and verified by the copper calorimeter, and set at a level of 21 kW/m^2. Figure 14 below presents a photograph of the Macor skin simulant sensor during a typical RPP test conducted with the cone heater.

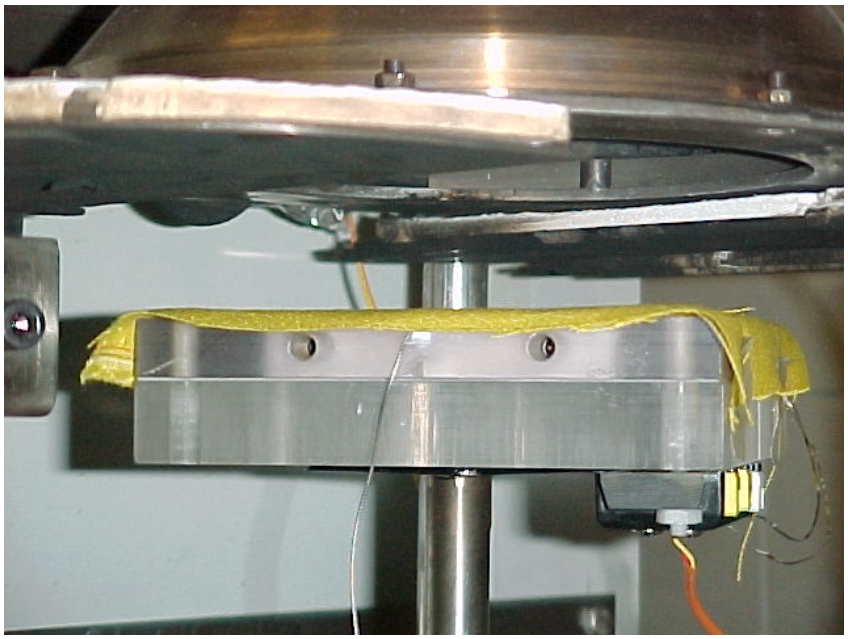

Figure 14: Macor RPP Cone Exposure – Typical Test Setup with Front Face of Fabric 2.5 cm (1") from Cone Heater. No Gap Between Skin Simulant Sensor and Clothing Materials. Enlarged Fabric Sample Used to Protect Plexiglas Frame Housing the Macor Skin Simulant.

Two copper calorimeters were constructed for use in this thesis. These sensors consist of a copper disc mounted in a ceramic support board. Each calorimeter, constructed using the information included in ASTM D 4108,[16] consisted of 0.0016 m thick, electrical grade, copper (ρ = 8666 kg/m^2, c_p = 0.410 kJ/kg-C) disc with four, 30 gauge, Type K thermocouples peened into holes drilled into the back face of the copper. The thermocouples were connected in parallel, and wired to the data acquisition system, providing an average reading from the four points on the calorimeter. The front face of the copper was covered with a thin layer of Krylon 1602 flat black

paint (ε = 0.97) to improve the radiant absobtivity.[25] The copper disc was then mounted into a 0.1 m by 0.1 m, 0.0635 m thick, Marinite ceramic support board, such that the copper surface was flush with the marinate support board. The copper calorimeters, acting as slug calorimeters as described in ASTM E 457 – 96,[26] could be used to assess the heat flux exposure on the copper surface using Equation 4. An additional thermocouple was peened into the back face of the copper disc offset slightly from the center thermocouple required by ASTM D 4108[16], providing an alternative temperature measurement to the thermocouples required by ASTM D 4108.[16] The data from the offset thermocouple could be compared against the data from the thermocouples required by ASTM D 4108[16] to ensure that both were producing similar temperature measurements. The temperature rise and heat flux calculation from the two copper calorimeters were compared against each other, and the heat flux sensor from the WPI cone calorimeter,[24] to ensure proper construction and performance levels.

A complete set, consisting of 3 RPP tests, were run using the copper calorimeter and the Macor skin simulant sensor with each heat source on each fabric sample. The insulating block housing the copper calorimeter was modified such that is would fit in the standard cone calorimeter sample holder. A 3 mm (1/8”) spacer was placed between the copper sensor and test fabric for the initial set of tests. Alternative sets of tests were run using the cone calorimeter with the test fabric directly against the copper calorimeter. The Macor skin simulant tests were completed with the fabric placed such that there was no gap between the fabric and the sensor.

The fabric samples used in each test were nominally 12.7 cm x 12.7 cm, with the exception of the tests conducted with the Macor skin simulant sensor exposed with the cone heater. In the tests conducted with the copper calorimeter, the fabric was placed over the sensor and the 3 mm spacer, and taped to the sides of the insulating Marinite support board. Enough tension was applied so that the fabric was pulled flat, although not enough tension was applied to distort the fabric specimens. Once the fabric was mounted over the copper calorimeter, the sensor was placed within the cone calorimeter sample holder and was set for testing. The fabric samples for

the Macor skin simulant tests were simply placed over the skin simulant and taped down, such that the fabric lay flat over the sensor with no wrinkles or air gaps between the sample and the sensor. The 12.7 cm x 12.7 cm samples were nominally the same size as the Plexiglas housing for the skin simulant sensor. In the quartz lamp tests, only the middle portion of the fabric/sensor was exposed to the heat source due to the dimensions of the fiberboard window, and the tape could be applied to the upper and lower portions of the sample without it being exposed to the incident flux. Figure 15 shows a 12.7 cm x 12.7 cm sample placed over the Macor skin simulant and Plexiglas holding assembly.

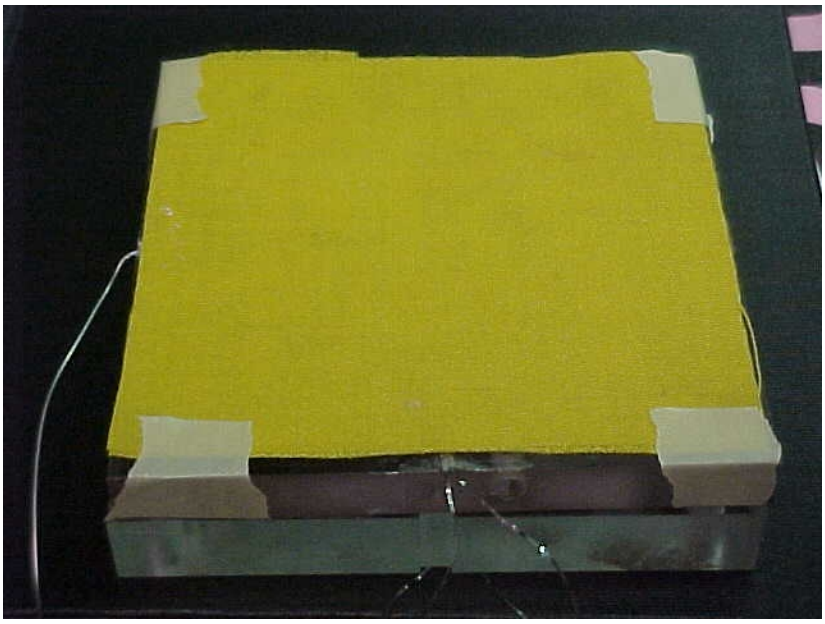

Figure 15: Macor Skin Simulant Sensor with 12.7 cm x 12.7 cm Nomex 7.5 oz/sq yd Sample. Sample Prepared for Quartz Lamp Exposure. Only Middle Portion of Clothing and Skin Simulant Sensor Exposed.

In the cone heater tests, the entire top portion of the sample was exposed. To prevent exposure of the tape used to attach the samples to the Plexiglas holding assembly for the skin simulant sensor, larger samples were used. The samples were taped down on the sides of the Plexiglas housing assembly, as shown in Figure 14. This prevented the tape from being exposed, while also ensuring that the entire Plexiglas frame was protected from direct radiant exposure.

Before each test, the copper calorimeter and the skin simulant sensor were adjusted to approximate skin temperatures by placing them against the palm of the hand. The standard test for the quartz lamp began by placing the fabric/sensor assembly 2.5 cm (1") from the nearest edge of the lamp surface. A reflective, insulated shutter was then placed between the quartz lamps and the fabric/sensor. The Variac was then set to 40, and the lamp allowed to heat up for approximately 30 seconds. The data acquisition system was then activated. After an additional 30 seconds, the shutter was removed, and the fabric was exposed to nominally 21 kW/m^2 (0.5 cal/cm^2 sec) for 30 or 40 seconds. To prevent damage to the Plexiglas housing assembly for the Macor skin simulant, the tests were terminated before the surface temperature of the Macor increased above 80^oC. At this time, the power to the lamp was removed and the system was allowed to cool. The data acquisition files for both the copper calorimeter and the Macor skin simulant were set to collect 120 seconds of data. The copper calorimeter data acquisition files recorded the temperature information from the four thermocouples wired in parallel with each other, as well as the additional offset thermocouple. The temperature readings from both the Macor surface and subsurface thermocouples were collected during the skin simulant RPP tests.

The RPP tests were completed on each of the outer shell materials listed in Table 8 using each sensor type. Additionally, a number of tests were completed on ensembles with Nomex IIIA 7.5 oz/sq yd and PBI 7.5 oz/sq yd as the outer shell materials. These tests were run using both the copper calorimeter and the Macor skin simulant exposed with the cone heater. Additional tests were conducted with the cone heater using the Macor skin simulant and an ensemble with Nomex IIIA 7.5 oz/sq yd as the outer shell material, with 1.0 grams of water/grams of Aralite added to the thermal liner material. RPP tests were also run with the cone calorimeter set at 21 kW/m^2 with the Green Southern Mills material with 0.5 and 1.0 grams of water per gram of material added. Water was added to the outer shell material and to the thermal liner of the ensemble to evaluate the effects of moisture on the time to 2^{nd} degree burn during an RPP type exposure. The final series of tests were conducted on the PBI 6.0 oz/sq yd and the Navy Blue 6.8 oz/sq yd materials, with the cone heater set at 10 kW/m^2. These tests were completed to

ensure the predictive capabilities of the Macor skin simulant at heat flux levels other than those used during the typical RPP test. A complete summary of these additional RPP type tests is presented in Table 10.

Table 10: Additional RPP Tests Completed Using Cone Heater.

Additional RPP Tests	Measurement Device
Ensemble with Nomex 7.5 oz/sq yd Outer Shell	Copper Calorimeter
Ensemble with PBI 7.5 oz/sq yd Outer Shell	Copper Calorimeter
Ensemble with Nomex 7.5 oz/sq yd Outer Shell	Macor Skin Simulant
Ensemble with PBI 7.5 oz/sq yd Outer Shell	Macor Skin Simulant
Ensemble with Nomex 7.5 oz/sq yd Outer Shell with 1.0 grams of water/gram of Aralite	Macor Skin Simulant
Southern Mills 8.5 oz/sq yd with 1.0 grams of water per gram of fabric added	Macor Skin Simulant
Southern Mills 8.5 oz/sq yd with 0.5 grams of water per gram of fabric added	Macor Skin Simulant
PBI 6.0 oz/sq yd Exposed to 10 kW/m2	Macor Skin Simulant
Navy 6.8 oz/sq yd Exposed to 10 kW/m2	Macor Skin Simulant

3.2.2 2ND DEGREE BURN DETERMINATION

The performance criterion for the RPP test is the time to 2nd degree burn, determined by the copper calorimeter using the Stoll and Chianta Curve developed from Table 1 in ASTM D 4108.[16] While this table was developed using test data for bare skin, the results are applied to the clothing tests specified in NFPA 1971[2] and 1977[4]. One goal of this project was to develop a method to determine the time to 2nd degree burn, taking into account the heat transfer through the clothing, and between the clothing and the skin using a test sensor with properties similar to those of human skin.

Copper Calorimeter

The time to 2nd degree burn for the copper calorimeter tests is determined through the use of the Stoll and Chianta Curve.[16] The development of this curve is presented earlier in this thesis. To determine the time after which a 2nd degree burn will occur, the measured temperature data from the copper calorimeter is compared to the Stoll and Chianta Curve. A burn is said to occur when the measured temperatures are greater than the Stoll and Chianta values. To evaluate the copper calorimeter test data, an Excel Macro was written which opened the temperature

measurement file, and imported the Stoll and Chianta Curve. For the first 30 seconds of the test, or the time before the heat flux exposure begins, the Stoll and Chianta Curve values are set equal to the temperature of the copper calorimeter. When the heat flux exposure begins, the values determined using Equation 5 were added to the temperature at the last time step before the heat flux exposure began to plot the Stoll and Chianta Curve

Skin Simulant Sensor

There are several problems associated with the method used by the copper calorimeter to predict the time to 2nd degree burn (See Section 2.3). These problems suggest that a skin simulant such as the Macor material would provide a better evaluation of the time to 2nd degree burn. Initially the hope was to develop a test method that would provide a temperature cutoff, similar to the Stoll and Chianta Curve for the copper calorimeter. This could be accomplished utilizing Equation 12, where the surface temperature, ΔT, of the Macor skin simulant can be determined for the various heat flux, q", and exposure times, t, which cause 2nd degree burns as listed in Table 5.[5]

$$\Delta T = \frac{2q''}{\sqrt{k\rho c_p}}\left(\sqrt{\frac{t}{\pi}}\right) \qquad \text{Equation 12}$$

This approach provides a simple, easy to calculate determination of the time to 2nd degree burn. However, this approach is based upon data for bare skin exposed to rectangular heat flux levels, and would have many of the same problems as those associated with the use of the copper calorimeter. These problems led to the exploration of a more accurate means to determine the time to 2nd degree burn from the skin simulant data.

A different approach for determining the time to 2nd degree burn for the Macor skin simulant utilized the heat flux levels reaching the skin to determine its temperature response. Second-degree burns are dependent on the temperature rise of the skin at 80 μm, and damage occurs for the total amount of time when the skin is above 44°C. Any determination of the time to 2nd degree burn for the skin simulant material must accurately predict the temperature of the material

80 μm below the surface before and after the heat flux application. The RPP tests were run for at least 30 seconds, however, skin burns were anticipated to occur after approximately 10 – 15 seconds. A method to predict the time to a 2nd degree burn must then be able to simulate the temperature rise and fall of the skin under a given imposed heat flux for durations shorter than the 30 seconds used.

There are several algorithms to predict the temperature history of the skin through heating and cooling presented in the SFPE Task Group guide "Predicting 1st and 2nd Degree Skin Burns from Thermal Radiation".[7] Equation 13 presents one algorithm that can be used to predict the temperature history of the skin when exposed to a square-wave heat pulse.

$$T = T_o + \frac{q}{k}\left[\frac{2\sqrt{\alpha t}}{\sqrt{\pi}}\exp\left(\frac{x^2}{4\alpha t}\right) - x\left(1 - erfc\left(\frac{x}{2\sqrt{\alpha t}}\right)\right)\right] - \frac{q}{k}\left[\frac{2\sqrt{\alpha (t-\tau)}}{\sqrt{\pi}}\exp\left(\frac{x^2}{4\alpha (t-\tau)}\right) - x\left(1 - erfc\left(\frac{x}{2\sqrt{\alpha (t-\tau)}}\right)\right)\right] \quad \text{Equation 13}$$

This equation is presented in three basic terms. During the heating stage, when the time t is less than the exposure time τ, the first two terms are real, and the third term is imaginary. During the cooling stage, when the time t is greater than the exposure time τ, all three terms are real. The first term, T_o, is simply the initial temperature of the skin (32.5°C). The second term is a determination of the skin temperature rise, assuming it acts as a single layer, opaque, semi-infinite solid. The third term is a Laplace solution for a negative heat flux input equivalent to the initial heat pulse level. This Laplace solution is applicable for the interval $\tau < t \leq$ infinity, so that the effective heat input into the skin is zero.[7] Unfortunately this equation cannot be used with a time varying heat flux as would be expected to reach the skin through the clothing in an RPP test.

Equations that can calculate the temperature response of semi-infinite solids exposed to time varying heat flux levels were investigated for use in determining the time to 2nd degree burn for the Macor RPP tests.[27] These equations required accurate heat flux levels at the surface of the

skin simulant. Two methods that were employed to predict this heat flux level are Diller's Algorithm (Equation 6) and the Inverse Heat Conduction Code.[20] The Inverse Heat Conduction Code uses the temperature measurements for the Macor skin simulant, in addition to the material's thermal properties, to predict the net heat flux to the surface. The net heat flux exposure is determined, such that the temperatures calculated at the thermocouple locations in the Macor skin simulant agree in a least squares sense with the temperatures measured by the thermocouples.[20] Diller's Algorithm (Equation 6) uses the temperature rise of the foil thermocouple bonded to the Macor surface to calculate the net heat flux at this location.

Both of these methods can be used to determine the heat flux levels at the skin surface for the entire duration of the RPP test. The fabric/Macor system was exposed for a total of approximately 30 seconds in these tests. If, however, one wanted to know the level of damage that would be produced if the heating stage lasted for only 10 seconds, then these calculation methods would not produce meaningful results for the cooling stages because there is no temperature measurement information available for a 10 second exposure. In order to obtain this information directly, several tests of each fabric with various heat flux exposure durations would have to be conducted to determine the heat flux to the skin for each case.

An alternative approach would be to use the heat flux information from the cooling stage of the 30 second RPP test to develop an assumption regarding the heat flux during the cooling of the Macor block, regardless of the time when the system begins to cool. Figure 16 presents a typical temperature and heat flux curve for the Macor RPP tests. The heat flux at the Macor surface initially decreases at nearly a linear rate during the cooling stage of the test. To apply this information to the calculation of the time to 2nd degree burn during the skin simulant RPP tests; the assumption was made that this linear decrease in the heat flux during the cooling stage is unchanged, regardless of when the system begins to cool. This would mean that if the heat source was removed ten seconds into the test, then the heat flux would decrease at the same rate is if the heat source was removed 30 seconds into the test.

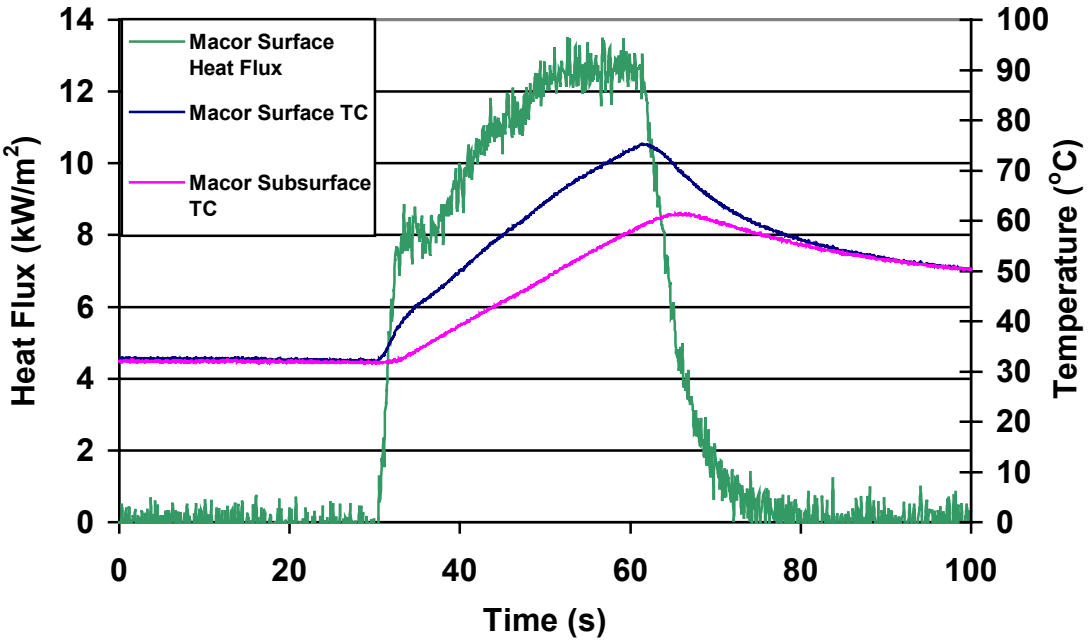

Figure 16: Typical Macor Temperature Measurements and Heat Flux Calculation for RPP Exposure (21 kW/m^2). During Cooling Stages of Test, Macor Surface Heat Flux Decreases at Linear Rate.

This method introduces a certain level of uncertainty regarding the actual heat flux levels during the cooling portion. The uncertainty regarding the accuracy of this method, along with the uncertainty regarding the time duration between the removal of the heat source and the beginning of the actual cooling of the Macor, led to the exploration of other methods to determine the time to 2nd degree burn for the Macor skin simulant evaluations.

The next method investigated for use in simulating the temperature response of a skin simulant under a given imposed heat flux was based upon work completed by Griffith and Horton to calculate the heat flow through a two layer wall.[28] This procedure was later revised and applied to the problem of a layer of fabric covering a skin simulant.[10] The equations below could be used to determine temperature rise at various locations within the clothing/skin simulant system, assuming constant temperatures throughout the system at the beginning of the exposure. Equation 14 can be used to calculate the temperature rise at depth in layer 2 (skin simulant),

Equation 15 can be used to calculate the temperature rise at the surface of the clothing, and Equation 16 can be used to calculate the temperature rise at the interface of the clothing and the skin simulant. Subscript 0 in these equations refers to the exposed surface, subscript 1 to top layer (fabric), and subscript 2 to the base layer (Macor).

$$T_2 = \frac{2q_n'' f\sqrt{a_1}}{g}\sum_{n=0}^{n=\infty}\left(-\frac{1}{g}\right)^n \left\{ \begin{array}{l} 2\sqrt{\left(\frac{a_2 t}{p}\right)}\frac{e^{-\left\{x-d\left\{1-\sqrt{(a_2/a_1)}(2n+1)\right\}\right\}^2}}{4a_2 t} - \left[x-d\left\{1-\sqrt{(a_2/a_1)}(2n+1)\right\}\right] \\ \left(1-erf\left(\frac{x-d\left\{1-\sqrt{(a_2/a_1)}(2n+1)\right\}}{2\sqrt{a_2 t}}\right)\right) \end{array} \right\}$$

Equation 14

$$T_0 = \frac{q_n''}{k_1}\left[2\frac{\sqrt{a_1 t}}{p} - \frac{4}{g}\sum_{n=0}^{n=\infty}\left(-\frac{1}{g}\right)^n \left\{\sqrt{\left(\frac{a_1 t}{p}\right)}e^{-d^2\frac{(n+1)^2}{t a_1}} - d(n+1)\left(1-erf\left(\frac{d(n+1)}{\sqrt{a_1 t}}\right)\right)\right\}\right]$$

Equation 15

$$T_s = \frac{q_n''}{k_1}\sum_{n=0}^{n=\infty}\left(-\frac{1}{g}\right)^n\left(1-\frac{1}{g}\right)\left[2\frac{\sqrt{a_1 t}}{p}e^{-\left(\frac{d(2n+1)}{2\sqrt{a_1 t}}\right)^2} - d(n+1)\left(1-erf\left(\frac{d(n+1)}{\sqrt{a_1 t}}\right)\right)\right]$$

Equation 16

Where:
x = Total thickness from surface to point of temperature rise
δ = Thickness of layer 1

$$g = \frac{k\rho c_{p_2} + \sqrt{(k\rho c_p)_1 (k\rho c_p)_2}}{k\rho c_{p_2} - \sqrt{(k\rho c_p)_1 (k\rho c_p)_2}}$$

$$f = \left(k_2\sqrt{a_1} - k_1\sqrt{a_2}\right)^{-1}$$

Equation 14 and Equation 16 slightly under-predicted the temperature of the Macor skin simulant, and had a delayed response at the Macor surface and subsurface thermocouple locations. Additionally, these equations did not calculate the temperature after the incident heat flux returns

to zero, and the net heat flux at the surface of the fabric becomes negative as the system begins to cool. The temperature rise calculated with these equations following the removal of the heat source suddenly dropped to a negative value. The temperatures predicted using this method are presented in Figure 17 below. Following this setback, this modeling technique was no longer used.

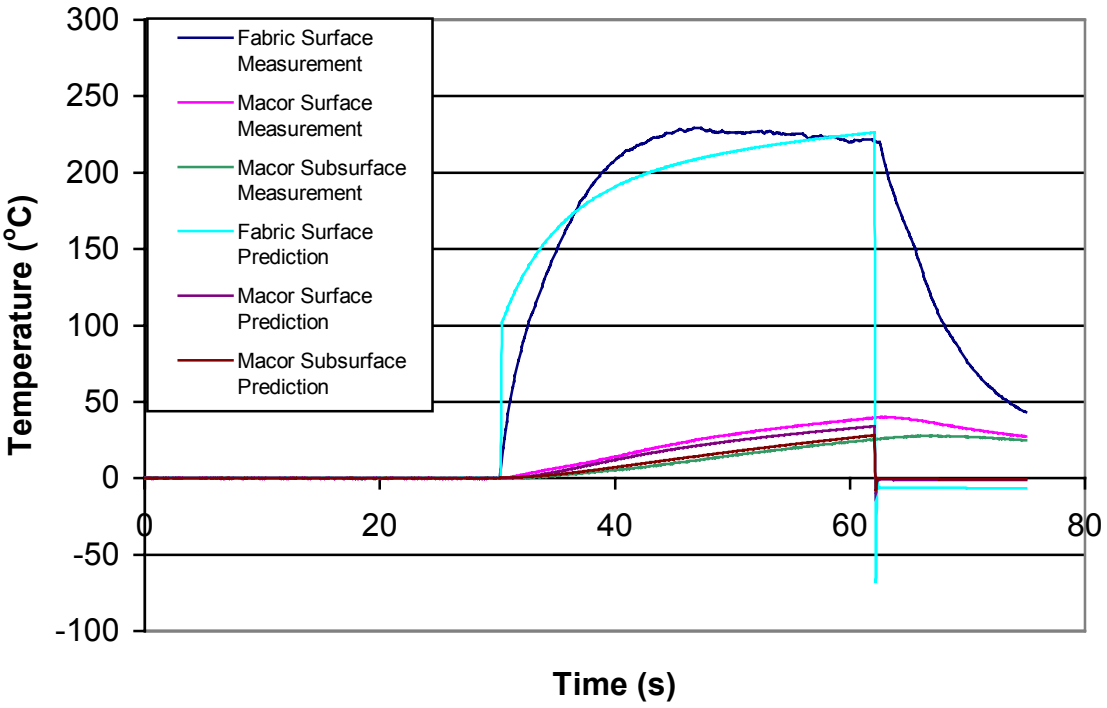

Figure 17: Modified Griffith and Horton Calculation[28] of Temperature Response During Macor RPP Test. Method Under-Predicts Temperatures at Macor Surface During Heating, and Does Not Calculate Temperatures Accurately During Cooling.

The final technique investigated to determine the temperature rise of the skin under a fabric sample when exposed to a given incident heat flux was a one dimensional (1-D) heat conduction model of the clothing/skin simulant system. This heat conduction model utilized the thermal properties of the clothing, as determined from the TPTF, as well as the properties of the Macor skin simulant block (k=1.5 W/m-K, ρc_p=2042000 J/m^3-K, δ=12.7 mm). The initial step in the development of the 1-D heat conduction model of the fabric/skin system was to develop a model that could accurately predict the time to 2nd degree burn for steady exposures where the skin

simulant was not covered by clothing. This model was developed and compared to the skin tolerance and 2nd degree burn information presented in Table 4 and Table 5.

Equation 17 presents the governing equation for the one dimensional heat conduction model developed in this thesis.

$$\rho c_p \frac{\partial T}{\partial t} = k \frac{\partial^2 T}{\partial x^2} \qquad \text{Equation 17}$$

The following initial and boundary conditions were applied to evaluate the skin simulant sensor.

$$T(x, t = o) \; = \; T_{initial} \qquad \text{Equation 18}$$

$$T_{\text{Plexiglas Backing}} = T_{\text{initial}} \quad (t>0,\ X \to \infty) \qquad \text{Equation 19}$$

$$k(\partial T/\partial x) + q_n''(t) = 0 \quad (x=0,t) \qquad \text{Equation 20}$$

$$q_n'' = q_i'' - q_c'' - q_r'' \qquad \text{Equation 21}$$

These equations were used as the basis for the development of a 1-D heat conduction model under unsteady heat flux conditions, using finite difference equations. The heat flux in Equation 20 is the net heat flux, and is determined by subtracting the radiative and convective losses from the surface of the exposed material from the incident heat flux, Equation 21. After the heat source is removed and the incident flux drops to zero, the radiative and convective losses continue until the surface temperature returns to ambient conditions. The convective heat transfer coefficient, used to determine the convective losses from the exposed surface, was assumed to be 5 W/m^2-K throughout.

The finite difference method was used to model the temperature response of the Macor skin simulant and the skin. To simplify the analysis, the Macor thickness was rounded down to 12.5 mm. The Macor block was divided into 20 nodes with equal nodal spacing, Δx, equivalent to 0.625 mm. The time step used for the 1-D heat conduction analysis is 0.1 seconds, which is equivalent to the time step used throughout the data collection. The following finite difference equations were used to model the temperature response of the Macor skin simulant.[23]

$$Internal\ Nodes\ -\ T_o^{i+1} = Fo(T_1^i + T_2^i) + (1\text{-}2Fo)T_o^i \qquad \text{Equation 22}$$

$$Back\ Interface\ (Against\ Adiabatic\ Material)\text{-}T_o^{i+1} = 2Fo(T_1^i) + (1\text{-}2Fo)T_o^i \qquad \text{Equation 23}$$

$$Exposed\ Surface\text{-}T_o^{i+1} = 2Fo\left(T_1^i + \left(\frac{q_n^i \Delta x}{k}\right)\right) + (1\text{-}2Fo)T_o^i \qquad \text{Equation 24}$$

$$Fo = \frac{\alpha \Delta t}{\Delta x^2} \leq \frac{1}{2} \qquad \text{Equation 25}$$

The superscript i in these equations refers to the time, such that the solutions for time i+1 are based upon the temperature and heat flux values at time i. The subscripts refer to the node location. Subscript 0 refers to the Node whose temperature is being calculated, while subscripts 1 and 2 refer to Nodes located on either side of Node 0. The Fourier number, Fo, for the Macor skin simulant, with a nodal spacing of 0.625 mm, and a 0.1 second time step, is 0.19. To avoid divergent oscillations in the finite difference temperature determinations, the Fourier number must be less that 0.5. The 1-D finite difference model of the Macor skin simulant was compared to measured temperatures from the surface and subsurface thermocouples on the Macor block. Figure 18 presents a comparison of the temperatures predicted by the 1-D finite difference model to those measured by the Macor thermocouples. The heat flux at the Macor surface and measured temperatures were those presented in Figure 16.

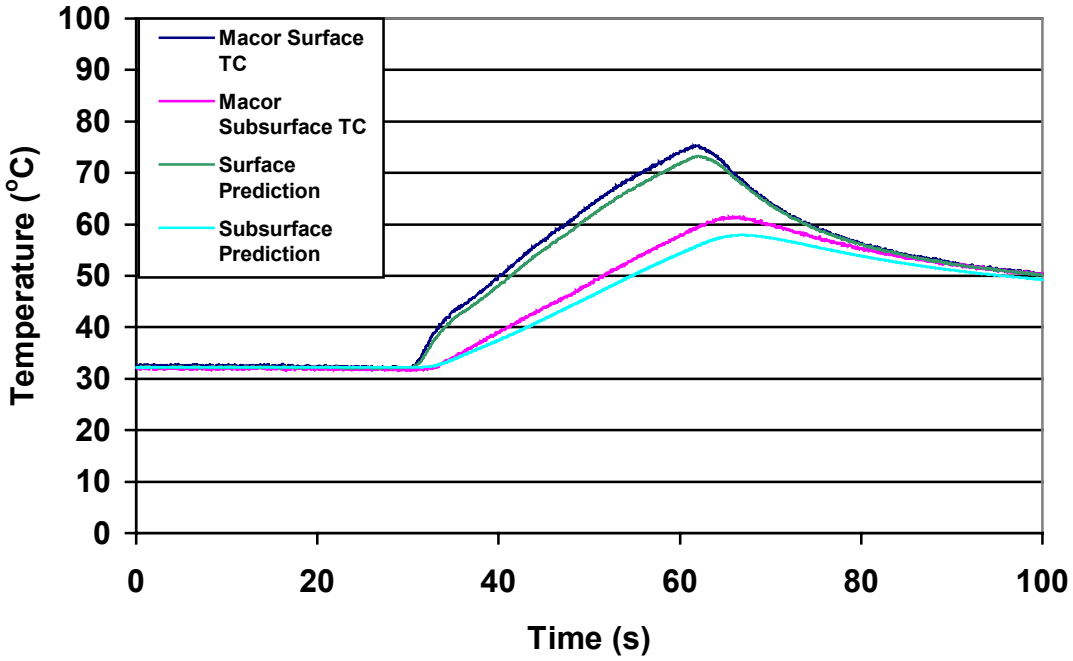

Figure 18: Macor Temperature Comparison – Measured Values at Macor Surface and Subsurface Thermocouple Locations vs. 1-D Finite Difference Model Predictions for Surface and Subsurface Thermocouple Locations. Diller's Algorithm Used to Calculate Heat Flux Used in 1-D Model.

The 1-D finite difference model provides an accurate temperature simulation at the two Macor thermocouple locations. The average difference between the measured temperature and the surface temperature prediction is 0.7°C for the entire 120-second test period. The average difference between the measured temperature and the subsurface prediction is 1.4°C. The larger difference between the measured and predicted temperatures for the subsurface thermocouple is due to the uncertainty regarding the exact depth of the thermocouple, as well as uncertainty regarding the exact properties of the Macor skin simulant and the effect of the thermally conductive silicone grease that was used to fill in the hole drilled for the subsurface thermocouple.

The 1-D finite difference model provided accurate temperature predictions for the Macor skin simulant, particularly at the surface. The temperature at the basal layer, 80 μm below the surface, was calculated by linearly interpolating the temperatures at the surface and 0.625 mm

below the surface. To assess the ability of the Macor skin simulant to predict the time to 2nd degree burn, incident heat flux values ranging from 3 kW/m^2 to 20 kW/m^2 were input into the 1-D finite difference model. The time to 2nd degree burn was determined using the Henriques Burn Integral. The exposure time was varied until the damage function, Ω, (Equation 2), increased above 1.0, at which time a 2nd degree burn will have occurred. The time to 2nd degree burn predictions for the Macor skin simulant were greater than the values developed from a best fit curve of the time to 2nd degree burn formation of human skin when exposed to various heat flux levels. This equation for the best fit curve, Equation 26, was developed using the human skin tolerance information from Table 5. The comparison of the Macor 1-D finite difference model predicted values and this curve are presented in Figure 19. The minimum heat flux values presented in Table 5 are 4.5 kW/m^2. However, the best fit curve was extrapolated to calculate a theoretical time to 2nd degree burn for lower heat flux levels. These low heat flux values may be less accurate than the curve prediction for higher heat flux levels, as blood perfusion affects will become more significant as the time to 2nd degree burn increases.

$$\text{Time to 2nd Degree Burn} = 221(q''_n)^{-1.35} \qquad \text{Equation 26}$$

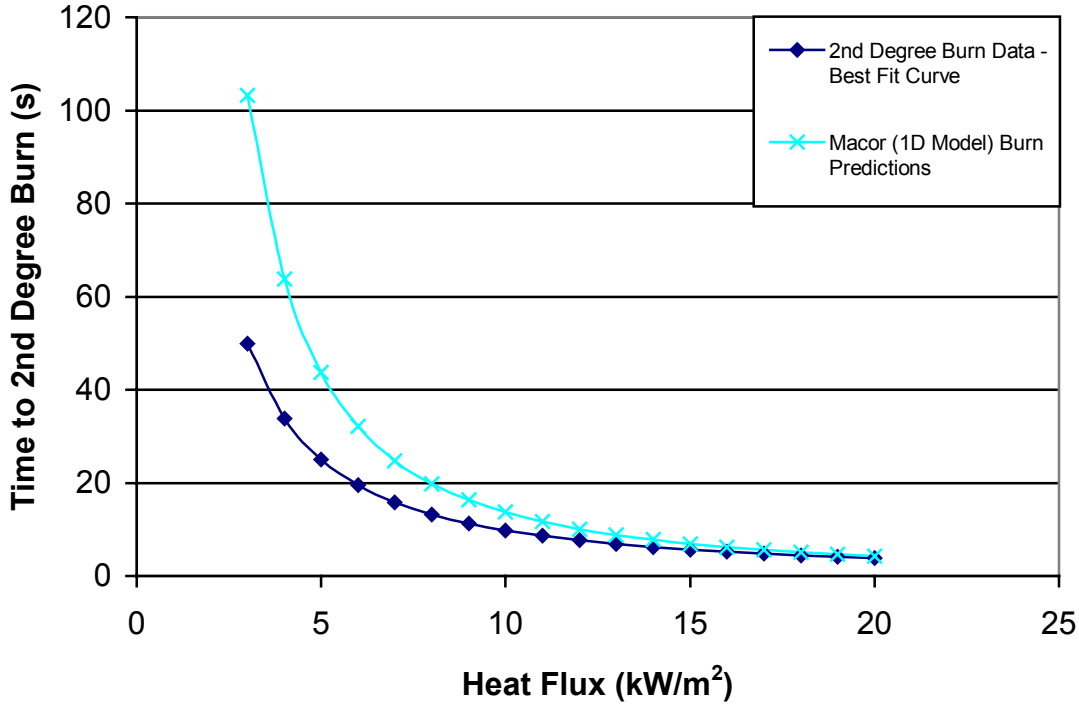

Figure 19: Time to 2nd Degree Burn - Comparison of Macor 1-D Finite Difference Model Predictions with Henriques Burn Integral with Best Fit Curve Developed Using Data Presented in Table 5. Table 5 Information Based upon 2nd Degree Burn Test Data.[9] Best Fit Curve to Test Data Extrapolated to Obtain Burn Predictions at Heat Flux Levels Below 4.5 kW/m^2.

The 1-D finite difference predictions from the Macor skin simulant were close to the measured values at high heat flux levels, within 0.5-seconds at 20 kW/m^2. However, this difference increased as the heat flux was decreased. The difference between the Macor skin simulant prediction and the extrapolated best fit curve at 3 kW/m^2 was greater than 50 seconds.

Due to the Macor skin simulant's inability to predict the time to 2nd degree burn, a modified 1-D finite difference model was set up using the properties of human skin. This model utilized the varying thermal properties discussed earlier in this thesis, summarized in Table 3. The skin thickness was estimated from the literature to be 12.08 mm.[13] Table 11 below presents a breakdown of the skin thickness. Each of these thickness values varies depending upon the location on the body. The SFPE task group report "Predicting 1st and 2nd Degree Skin Burns from

Thermal Radiation"[7] lists the thickness of each layer as 75 to 150 μm for the epidermis, 1 to 4 mm for the dermis, and 0 to 2 cm for the sub-cutaneous layer.

Table 11: Skin Thickness.[7]

Layer	Thickness
Epidermis	0.08 mm
Dermis	2.0 mm
Sub-Cutaneous Layer	10 mm

The thermal properties of the skin layers were assumed to be the same throughout the 12.08 mm thickness. The temperature of the outer surface of the skin was set to 32.5°C, while the back face temperature of the skin was set to 37°C, which is the core body temperature.[13] A linear temperature gradient was assumed between the front and back surfaces. The skin was assumed to be an opaque black body, which produces slightly different temperatures than would result if the emissivity of the skin[9] (0.94) were used. The skin was separated into 50 nodes, with a nodal thickness of 0.2416 mm, and the time step for the analysis was set at 0.1-seconds. Because the thermal conductivity changed depending on whether the skin was being heated or cooled, and depending upon the incident heat flux, there is not a constant value for the Fourier number. This setup ensured that the Fourier number would be less than 0.5, which is the cutoff value to prevent the finite difference equations from diverging at all of the incident heat flux levels investigated. Equation 22 and Equation 24 were used to solve for the surface and internal node temperatures, while the back face of the skin layer was held at 37.5°C throughout the analysis.

The temperature predictions of this 1-D finite difference model of the skin were compared to the temperatures calculated using Equation 13 at a net heat flux exposure of 15.7 kW/m^2. Equation 13 was shown to provide an accurate prediction of the temperature response of the skin at this heat flux exposure level.[7] Figure 20 presents the comparison of the temperature response of the skin calculated by Equation 13 and the 1-D finite difference model of the skin. The results are nearly identical through the heating stage, where the average difference between the two is less than 0.2°C. There is a slight increase in the difference in the temperature predictions during the cooling stages, where the average difference increases to 0.4°C. The jump in temperature at the

transition from heating to cooling in the temperature results for Equation 13 is due to the use of the 0.1 second time step. If this time step is increased then this temperature jump is removed. This comparison demonstrates the ability of the 1-D finite difference model to accurately predict the temperature response of the skin.

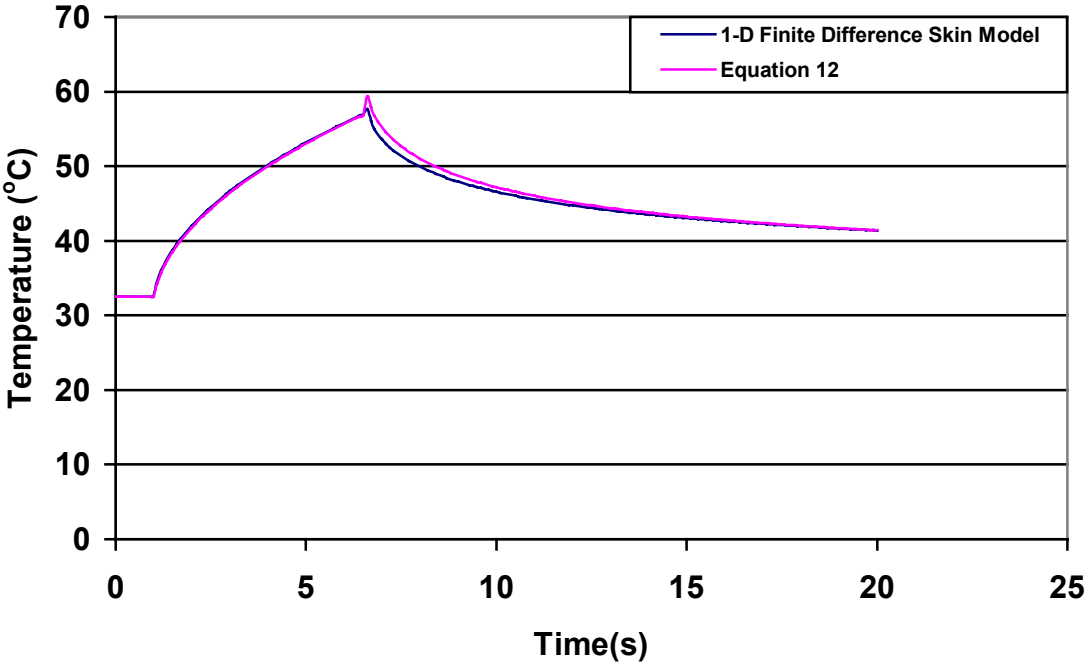

Figure 20: 1-D Finite Difference Skin Model Basal Layer Temperature Comparison to Equation 13 – 15.7 kW/m^2 Exposure for 5.55 Seconds. Equation 13 Verified in SFPE Task Group Guide, "Predicting 1st and 2nd Degree Skin Burns from Thermal Radiation"[7] for this Exposure.

The finite difference skin model was used to calculate the time to 2nd degree burn from steady incident heat flux levels ranging from 2 kW/m^2 to 20 kW/m^2 in a manner similar to that used for the Macor skin simulant finite difference model. The minimum flux level to produce a 2nd degree burn was reported to be 1.7 kW/m^2.[7] The results obtained for the skin finite difference model were much closer to those measured by Stoll et al[8,9] than the Macor model predictions. Table 12 presents a comparison of the capabilities of each 1-D finite difference model with regards to the ability to accurately predict the time to 2nd degree burn. The times to 2nd degree burn predicted using the methods from the current test standards are also included.[2,4] The predictions are

compared to the best-fit curve approximation of the time to 2nd degree burn, Equation 26, which was developed using the skin tolerance information presented in Table 5.

Table 12: 2nd Degree Burn Times.

Heat Flux	Data	Current Test Methods	Macor (1-D Model)	Skin (1-D Model)
(kW/m^2)	(s)	(s)	(s)	(s)
2	86.4	94.5		87.1
3	49.9	53.4	103.2	49.4
4	33.8	35.5	63.8	34.2
5	25.0	25.9	43.7	26.2
6	19.5	20.0	32.1	21
7	15.8	16.1	24.8	17
8	13.2	13.3	19.8	14.1
9	11.3	11.3	16.3	12
10	9.8	9.7	13.7	10.4
11	8.6	8.5	11.7	9.2
12	7.6	7.5	10.1	8.2
13	6.9	6.7	8.8	7.3
14	6.2	6.0	7.8	6.6
15	5.6	5.5	6.9	5.9
16	5.2	5.0	6.2	5.4
17	4.8	4.6	5.6	4.9
18	4.4	4.2	5.1	4.5
19	4.1	3.9	4.7	4.1
20	3.8	3.6	4.3	3.8

The times predicted by the 1-D finite difference model for the skin are similar to the copper calorimeter time predictions in terms of the difference between the time predictions and the test data. The time residuals, calculated using Equation 27, were determined to be 0.15 seconds for the 1-D finite difference skin model, and 0.46 seconds for the copper calorimeter between the heat flux levels ranging from 2 kW/m^2 to 20 kW/m^2. Much of reason for the larger residual for the copper calorimeter is due to the 9-second difference between the predicted time for the copper calorimeter at 2 kW/m^2 and the measured time. If this time is ignored, the copper calorimeter residuals drop to 0.19 seconds. Overall, the time predictions for the 1-D finite difference model of the skin differed by no more than 7.4% from the measured values, and on average differed from the measured time by 4.1%.

$$Residuals = \frac{\left(\sqrt{\sum \left(t_{predicted} - t_{measured}\right)^2}\right)}{\#of\ points} \qquad \text{Equation 27}$$

The 1-D finite difference models for the Macor and the skin were able to accurately predict the temperatures of the respective materials when exposed to time varying heat flux levels. In addition, the 1-D model of the skin provided an accurate means to predict the time to 2nd degree burn when exposed to heat flux levels between 2 kW/m^2 and 20 kW/m^2. These models were constructed to allow the user to vary the heat flux level and the exposure time, such that the temperature at the surface, or more importantly at the basal layer, could be determined under a variety of conditions. In addition, the skin model, which was developed in a Microsoft Excel Spreadsheet, was linked to a separate Excel sheet that calculated the values for Henriques Burn Integral, Equation 2, based upon the basal layer temperatures. This setup allowed the user to vary the exposure time to determine the exposure duration that would produce a 2nd degree burn. A 2nd degree burn is produced when the damage function, Ω, increased above 1.0.

This 1-D finite difference model of the skin was used to calculate the time to 2nd degree burn for the three cases in the example presented in Section 2.3. This example exposed the copper calorimeter to two constant heat flux levels at different points in the exposure to present a flaw in the current burn calculation method. If the copper calorimeter is exposed to a high heat flux level of 50 kW/m^2 for one second, its temperature curve will cross the Stoll and Chianta Curve,[8] and a 2nd degree burn is said to occur. However, if the copper calorimeter is exposed to a heat flux of 4 kW/m^2 for ten seconds, and then exposed to a heat flux level of 50 kW/m^2 for one second, the temperature curves will not cross. If the 4 kW/m^2 flux continues after the removal of the 50 kW/m^2 flux, then the curves will eventually cross and a 2nd degree burn is said to occur. The 50 kW/m^2 exposure in this case will not produce a 2nd degree burn if evaluated with the copper calorimeter, despite the fact that the flux exposure is equivalent to that of the first case with an additional 4 kW/m^2 for ten seconds. This 4 kW/m^2 exposure would heat the skin up to a point where, when exposed to the 50 kW/m^2 pulse for one second, the damage should be more severe than in case 1. Case 3 exposed the copper calorimeter to 4 kW/m^2 for 20 seconds, and then introduced the 50 kW/m^2 flux for 1 second. This high flux exposure produced a 2nd degree burn. The three cases were evaluated with the 1-D finite difference model of the skin. The 50 kW/m^2

exposure for one second always produced a second degree burn. Table 13 presents a summary of the burn time predictions of the 1-D finite difference skin model for the three cases.

Table 13: Skin Time to 2nd Degree Burn Predictions when Exposed to Combinations of 4 kW/m^2 and 50 kW/m^2.

Heat Flux Exposure (kW/m^2)	Time to Second Degree Burn	Time Between Beginning of 50 kW/m2 Exposure and Onset of 2nd Degree Burn
50 kW/m^2 at Beginning	1.1 Seconds	1 Second
4 kW/m^2 for 10 Seconds, then 50 kW/m^2 for 1 Second	10.7 Seconds	0.7 Seconds
4 kW/m^2 for 20 Seconds, then 50 kW/m^2 for 1 Second	20.5 Seconds	0.5 Seconds

As expected, the time for the 50 kW/m^2 pulse to produce a 2nd degree burn is decreased when the skin is exposed to more heat prior to this exposure. The 4 kW/m^2 exposure for 10 and 20 seconds (Cases 2 and 3), before the skin is exposed to the high level pulse of 50 kW/m^2, increases the basal layer temperature to 42.3^{o}C and 46.5^{o}C respectively. These elevated temperatures at the beginning of the 50 kW/m^2 exposure lead to shorter times to 2nd degree burn.

After verifying the ability of both the Macor and the skin finite difference models to predict temperatures accurately, as well as the ability of the skin model to accurately predict the times to 2nd degree burn under various heat flux exposures, the models were adapted to incorporate a fabric layer. The use of each model is required to predict the time to 2nd degree burn for the various fabrics and ensembles evaluated. Using the properties of the clothing materials determined from literature review, physical measurements, and the TPTF, the Macor finite difference model was set up to predict the temperature response during the 120-second RPP test.

The fabric/Macor 1-D finite difference model was based upon the same governing, initial, and boundary conditions as the bare Macor model. The initial temperature of the fabric and the Macor in the model was assumed constant, and was determined from the average of the Macor surface and subsurface thermocouples over the first thirty seconds of the RPP test, before the heat flux exposure began. The incident heat flux was set at 21 kW/m^2 for each test, although

some variation could be expected for each individual test. The convective heat transfer coefficient, used to determine the convective losses from the fabric surface, was assumed to be 5 W/m^2-K throughout. The emissivity of each fabric evaluated could not be located in the literature, although a value of 0.9 was listed for some representative fabrics.[29] The transmissivity of the fabrics was ignored in this analysis, as it was listed as being on the order of approximately 0.01.[29] In order to provide a comparison with the test data, a 0.1-second time step was used for the analysis. The thickness of each fabric was measured before each test.

The fabric/Macor system was originally thought of as a two-layer wall system with no discontinuity in the temperature flow caused by a contact resistance between the fabric and the Macor skin simulant. The fabric was divided into 5 nodes, with the fifth node located at the back face of the material. The nodal spacing of the Macor was then selected to obtain a Fourier number equivalent to the Fourier number for the fabric layer. This model setup is similar to the setup information presented in Figure 22.

The results of this model setup were compared to RPP tests conducted with the cone heater, with a 40-gage thermocouple wired into the exposed surface of the fabric materials. These characterization tests were run using samples of Nomex 7.5 oz/sq yd, Nomex 6.0 oz/sq yd, PBI 7.5 oz/sq yd, and PBI 6.0 oz/sq yd. In each case, the temperatures predicted by the 1-D finite difference model were much greater than those measured, Figure 21. This large temperature difference was caused primarily by the contact resistance between the fabric and the skin simulant.

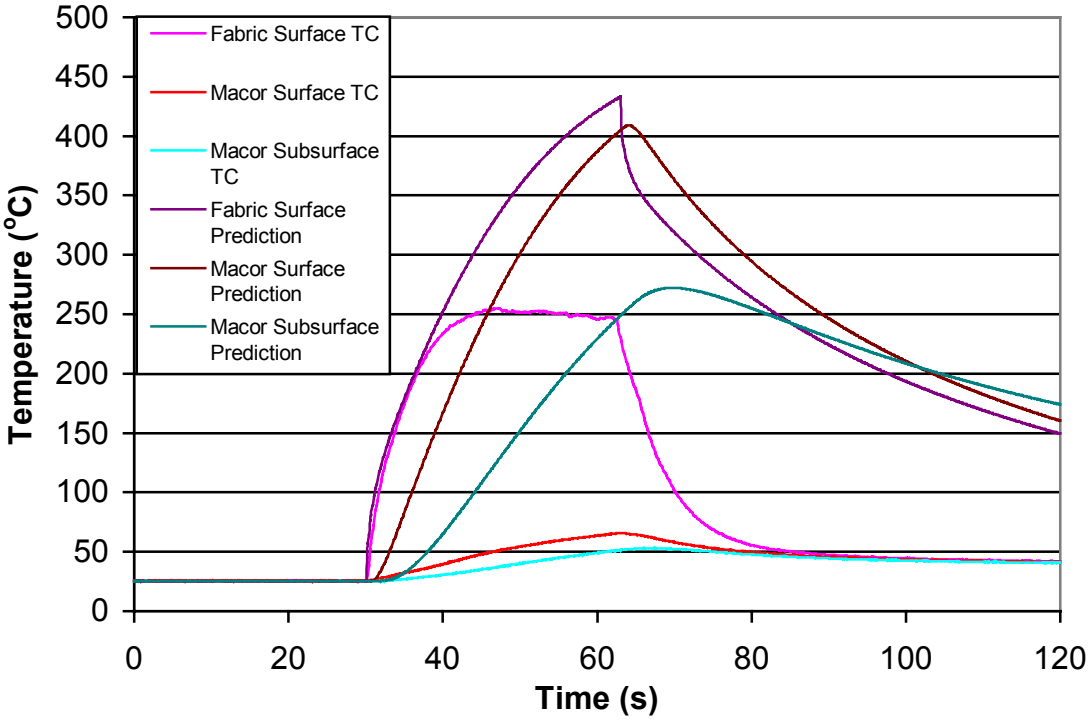

Figure 21: Macor RPP Exposure (21 kW/m^2), Nomex 7.5 oz/sq yd – Measured Temperature Comparison with Macor 1-D Finite Difference Model Predicted Values. No Contact Resistance in 1-D Model.

To improve the temperature predictions, the temperature drop at the interface of the fabric and the skin simulant, caused by the contact resistance between the fabric and the Macor, was incorporated into the finite difference model. The temperature drop is a function of the heat flux at the interface and the interfacial conductance, h_i. Equation 10 was used to calculate the temperature drop between the back face of the fabric and the surface of the Macor skin simulant.

By incorporating the contact resistance into the finite difference model, the clothing/Macor system essentially became two separate finite difference problems, "centered" around the interface between the fabric and the Macor. Because of this, the Fourier number no longer had to be equivalent throughout the clothing/Macor system. The practice of setting the nodal spacing in the Macor block to obtain a Fourier number equivalent to the Fourier number for the fabric layer was

terminated. A constant nodal spacing of 0.625 mm was used, producing 20 nodes for the 12.5 mm thick block.

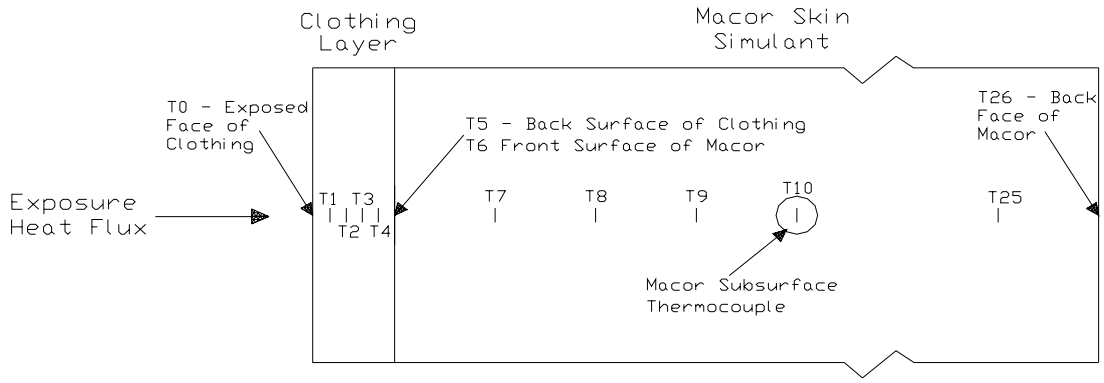

Figure 22: Fabric/Macor 1-D Finite Difference Model with Contact Resistance. – Drawn to Scale. Complete Macor Skin Simulant Not Shown in Figure. Nodes Marked with T and a Number Refer to the Node Designation. Node T_0 is the Front (Exposed) Face of the Clothing. Node T_5 is the Back (Unexposed) Face of the Clothing. Node T_6 is the Surface of the Macor Skin Simulant. Temperature Difference Between Nodes T_5 and T_6 Due to Contact Resistance Between Clothing and Macor. Node T_{26} is the Back Face of Macor. Plexiglas Holder for Macor Skin Simulant Assumed to be Adiabatic Surface.

The nodes in the system are marked in Figure 22 with a T_i. Subscript i refers to the node number. The temperature drop caused by the contact resistance was assessed at the interface of the fabric and the Macor, between nodes T_5 and T_6. The determination of the contact resistance required an estimation of the heat flux at the surface of the Macor. This heat flux was estimated by taking an average of the heat flux in the last element of the clothing (between nodes T_4 and T_5) and the second element of the Macor (between nodes T_7 and T_8). The first element in the Macor (between nodes T_6 and T_7) was not used in this calculation as this caused the model to produce divergent results. This method of estimating the heat flux produced results similar to those obtained through the use of Diller's Algorithm, and was less computationally intensive.

Figure 23 provides a comparison of the values calculated by Diller's Algorithm with those predicted by the 1-D Macor finite difference model for one of the Nomex 7.5 oz/sq yd characterization tests with an interfacial conductance value of 410 W/m^2-K.

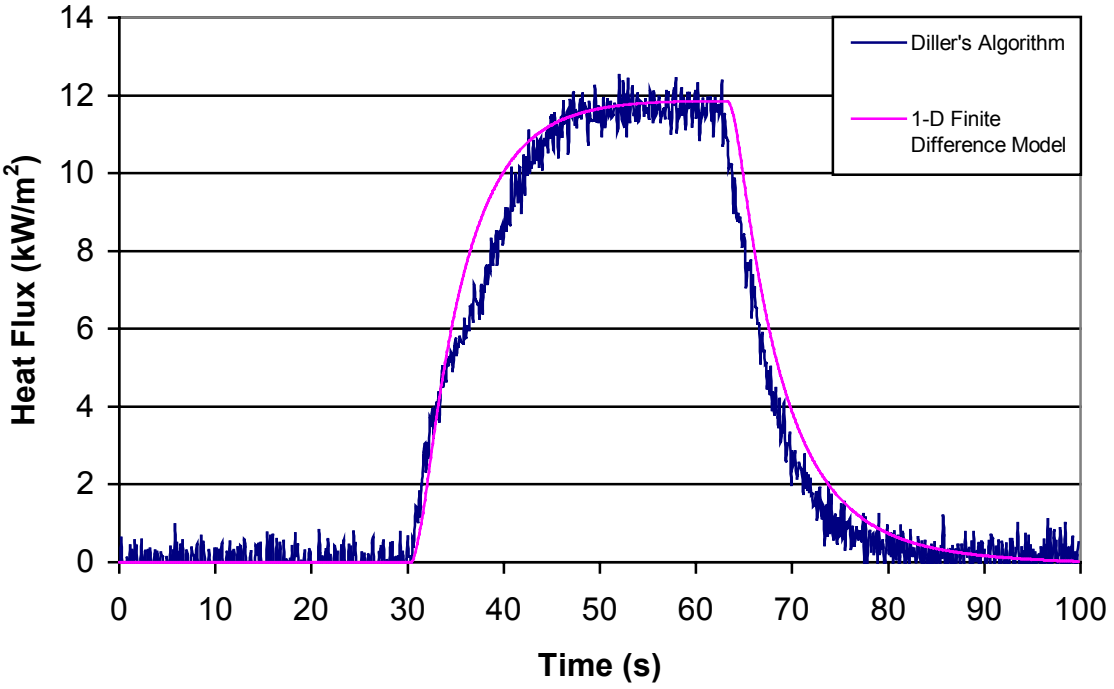

Figure 23: Macor RPP Exposure (21 kW/m^2), Nomex 7.5 oz/sq yd – Diller's Algorithm Compared with 1-D Macor Finite Difference Model of the Heat Flux at Macor Skin Simulant Surface using an Interfacial Conductance Value of 410 W/m^2-K.

A value for the interfacial conductance, h_i, had to chosen to determine the temperature drop at the interface. This temperature drop was then used to calculate the Macor surface temperature (node T_6) by subtracting the temperature drop from the temperature of the back face of the clothing (node T_5) at each time step. The model was constructed such that the value for the interfacial conductance could be varied until accurate temperature values were obtained for the Macor surface and subsurface temperatures, although the Macor surface temperatures were given more priority when the setting the interfacial conductance values. Figure 24 provides a depiction of the revised temperature prediction, which is based upon the same test information shown in Figure 21.

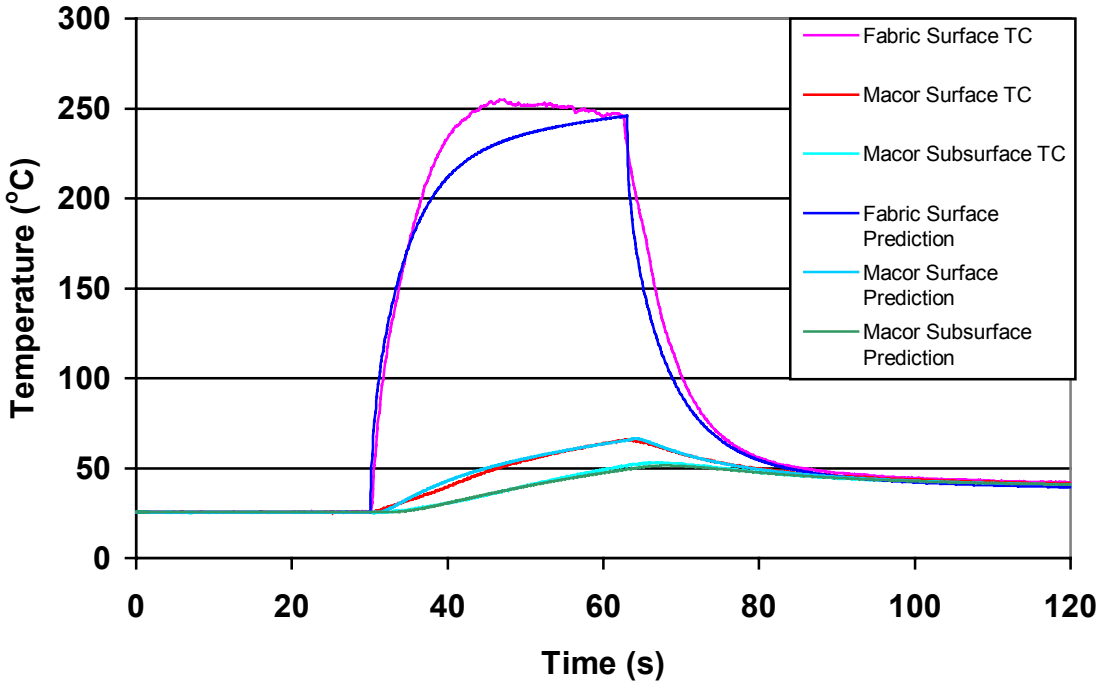

Figure 24: Macor RPP Exposure (21 kW/m^2), Nomex 7.5 oz/sq yd – Measured Temperature Compared with 1-D Macor Finite Difference Model Predicted Values. Interfacial Conductance Value of 410 W/m^2-K used in Model.

Table 14 below provides a depiction of the model setup information for the various fabric/Macor 1-D finite difference model characterization tests. Each of the fabric/Macor 1-D model evaluations required similar interfacial conductance values to accurately predict the temperatures of the Macor thermocouples. The standard deviation of the interfacial conductance values is 8.7 W/m^2-K, which is approximately 2% of the average interfacial conductance value. The interfacial conductance values in the 1-D fabric/Macor model, presented in Table 14, were similar to those calculated by the Prop1D computer program for the Kapton/Macor interface in the TPTF, presented in Table 17. The characterization tests for the 1-D Macor finite difference model proved that accurate predictions of the Macor temperatures could be made through the use of the fabric properties determined using the TPTF.

Table 14: Characterization Tests – Macor Model Setup Information

Fabric	Test Number	Interfacial Conductance	Macor Surface Temp
		h_i (W/m^2 K)	Residuals (^{o}C)
Nomex 7.5 oz/sq yd	1	400	0.026
Nomex 7.5 oz/sq yd	2	410	0.037
Nomex 6.0 oz/sq yd	1	410	0.027
Nomex 6.0 oz/sq yd	2	415	0.036
PBI 7.5 oz/sq yd	1	425	0.037
PBI 7.5 oz/sq yd	2	420	0.036
PBI 6.0 oz/sq yd	1	405	0.024
PBI 6.0 oz/sq yd	2	402	0.024

The calculation sheet for the 1-D fabric/Macor finite difference model was linked in Microsoft Excel to the calculation sheet for the 1-D fabric/skin finite difference model. The input values for the fabric material properties, heat flux exposure level, time at which exposure begins, and the interfacial conductance used in the Macor model were also used in the skin model. In addition, the 1-D fabric/skin model sheet was linked to a sheet that calculated the value for the Henriques Damage Factor, Ω (Equation 2).[11] This Henriques burn time calculation sheet interpolated the temperatures between the skin surface and the first node at depth in the skin to determine the temperatures at 80 μm. The exposure time for the 1-D fabric/skin finite difference model was specified in the Henriques burn calculation sheet in Excel. This time could be varied until the Damage Factor, Ω, increase above 1.0.

To ensure that the 1-D model could predict the Macor temperature response when exposed to different heat flux levels, an alternative series of tests were conducted in which the fabric/Macor system was exposed to 10 kW/m^2 from the cone heater. The measured and predicted temperatures were compared to ensure that the model could accurately predict the temperatures at these heat flux levels, with values for the interfacial conductance, h_i, similar to those presented in Table 14. Three tests were run at this heat flux level using the PBI 6.0 oz/sq yd and the Navy 6.8 oz/sq yd materials. The predicted temperatures at the Macor surface and subsurface thermocouple locations were close approximations of those measured during the 10 kW/m^2

exposure. The results of this evaluation are presented with the Macor RPP results in Section 4.2.2.

4.0 PROTECTIVE CLOTHING PERFORMANCE

4.1 Thermal Properties

One of the primary goals of this project was to determine the thermal properties of fire fighting clothing materials. Several different materials were evaluated. Additional tests were run at various moisture contents to determine the effects of the added moisture on the thermal properties. The temperature and heat flux data from these tests were input in the Prop1D[6] program to determine values for the thermal conductivity, k, and the volumetric heat capacity, ρc_p. The results of these evaluations are presented in a detailed summary in Appendix B: Thermal Property Estimations.

4.1.1 DRY MATERIAL COMPARISON

Table 8 provides a summary of the materials evaluated in this thesis. In addition, three ensembles were tested, utilizing Nomex 7.5 oz/sq yd, Nomex 6.0 oz/sq yd, and PBI 7.5 oz/sq yd as the outer shell materials. Each fabric or ensemble investigated was tested several times, providing information for a database of fabric properties.

The largest sampling of data collected was on the fabrics with no moisture added. Initially, nine tests were run on each outer layer fabric, while three and five tests were completed on the Crosstech Moisture Barrier and the Aralite Thermal Liner respectively. The property estimates for each test on an individual fabric are expected to vary slightly, as in many cases different samples of the same fabric type were tested, and the fabrics were always removed from the test fixture after each test, and then reinserted into the test fixture before the next test. When the test data were analyzed with the computer program Prop1D[6] certain isolated tests produced non-converging results, or produced results that were unusually dissimilar than the average values. Most of these problems were due to the TPTF not having returned to steady temperatures

throughout. This effect was quantified for one of the fabrics tested, where the results for the tests with steady initial conditions were compared to the results of tests with unsteady initial conditions. Additional variation in the test results was produced by moving the Kapton sensor from against the Macor skin simulant to between the clothing layers in the outer shell material evaluations. When the Kapton sensor was moved between the clothing layers, the program was unable to calculate an accurate value for the contact resistance between the last clothing layer from the heater and the Macor skin simulant, and different results were returned for the material properties. To provide consistency in the property estimations, the material properties provided in this summary are for the tests with the Kapton sensor located against the Macor, as shown in Figure 6.

Figure 7 presents a typical temperature and heat flux graph for the TPTF evaluation of a dry fabric material. The power to the heater was turned on approximately 20 seconds into each test, and turned off when the temperature of the heater increased to between 120^{o}C and 125^{o}C. The heating stages for the dry fabrics varied from approximately 40 seconds for the Aralite Thermal Liner material to approximately 80 seconds for the Nomex 7.5 oz/sq yd material. This time is dependent on the thermal properties of the material involved, as it is a function of the amount of heat transferred away from the heater to the Macor skin simulants. The heat flux levels attained in these dry material tests ranged from approximately 2.5 kW/m^2 for the Aralite Thermal Liner material to approximately 3.5 kW/m^2 for the Nomex 7.5 oz/sq yd. The set of figures below (Figure 25 - Figure 27) presents the differences between the heat flux and temperatures attained in the testing of a heavier outer shell material (Nomex 7.5 oz/sq yd), a lighter outer shell material (Nomex 5.5 oz/sq yd), and the Aralite Thermal Liner.

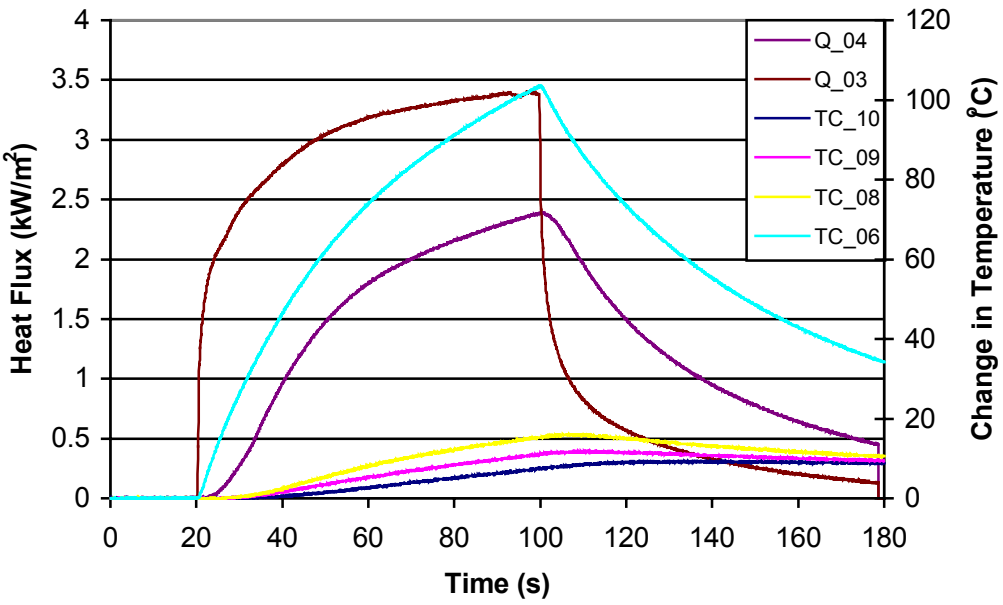

Figure 25: Thermal Properties Test Fixture – Temperature Rise and Heat Flux from Top Half of TPTF with Nomex 7.5 oz/sq yd, 40 VDC Applied to Heater. Q_04 – Kapton Heat Flux, Q_03 – Heater Heat Flux, TC_10 – Macor Subsurface Temperature, TC_09 – Macor Surface Temperature, TC_08 – Kapton Assembly Temperature, TC_06 – Heater Temperature.

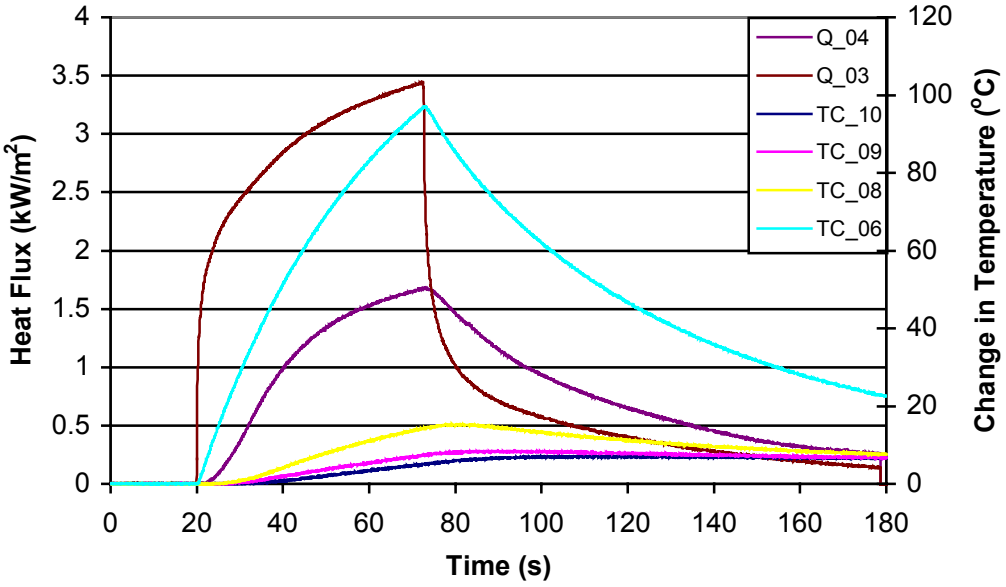

Figure 26: Thermal Properties Test Fixture – Temperature Rise and Heat Flux from Top Half of TPTF with Nomex 5.5 oz/sq yd, 40 VDC Applied to Heater. Q_04 – Kapton Heat Flux, Q_03 – Heater Heat Flux, TC_10 – Macor Subsurface Temperature, TC_09 – Macor Surface Temperature, TC_08 – Kapton Assembly Temperature, TC_06 – Heater Temperature.

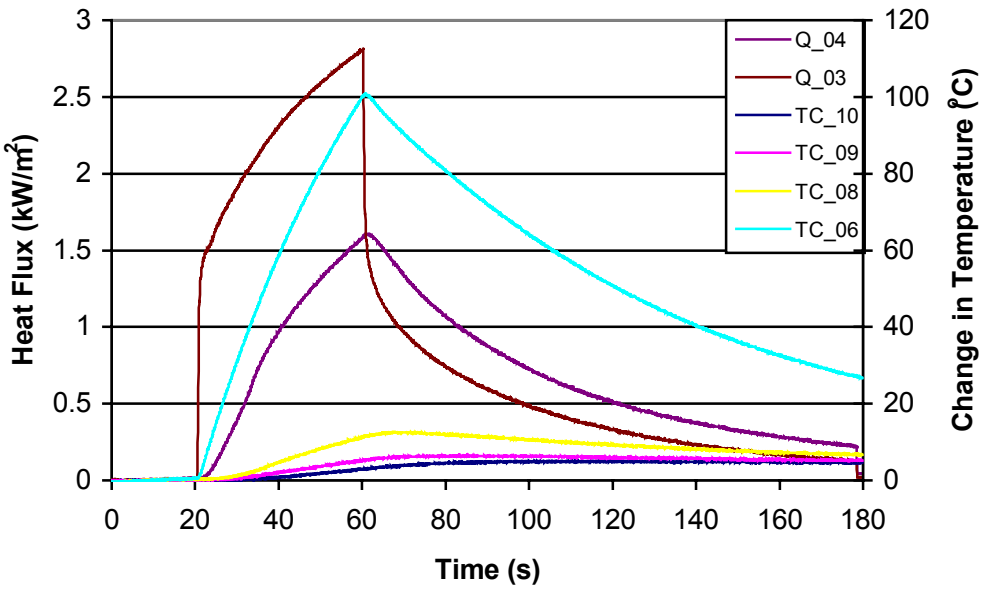

Figure 27: Thermal Properties Test Fixture – Temperature Rise and Heat Flux from Top Half of TPTF with Aralite Thermal Liner, 40 VDC Applied to Heater. Q_04 – Kapton Heat Flux, Q_03 – Heater Heat Flux, TC_10 – Macor Subsurface Temperature, TC_09 – Macor Surface Temperature, TC_08 – Kapton Assembly Temperature, TC_06 – Heater Temperature.

The thermal property estimates were influenced by the initial conditions of the test fixture. If the temperatures at the different thermocouple locations in the TPTF were not allowed to return to relatively equivalent (less than 1°C difference throughout) conditions before the data acquisition system was activated, the property estimates became less accurate and exhibited more variation on a test to test basis. Table 15 provides an example of the differences in the thermal property estimates between cases with steady balanced initial temperature conditions and unsteady initial temperature conditions in the test fixture.

Table 15: Steady Versus Unsteady Conditions for Thermal Property Determination.

PBI 6.0 oz/sq yd	Values	Residuals (K)	K (W/m-K)	ρc_p(J/m^3-K)	h_i (W/m^2-K)
Steady Initial Temperatures	Average	1.77	0.045	1.58×10^6	380
	Standard Deviation		0.0015	2.06×10^4	
Unsteady Initial Temperatures	Average	2.73	0.054	1.55×10^6	235
	Standard Deviation		0.0025	3.92×10^4	

Initially, the Prop1D[6] files did not incorporate the effects of the contact resistance. The output files in which the contact resistance was incorporated into the analysis typically had lower residual (RMS) values, higher thermal conductivities, and lower volumetric heat capacities. Table 16 presents the difference in the property estimates for three sample fabrics when the contact resistance was incorporated into the Prop1D files. The thermal property results presented in this section are based upon the property estimation files incorporating the contact resistance.

Table 16: Contact Resistance Effects on the Fabric Thermal Properties.

Nomex 7.5 oz/sq yd (Dry)	**Residuals (K)**	**k (W/m-K)**	**ρc (J/m^3-K)**	**h_i (W/m^2-K)**
No Contact Resistance	3.08	0.049	1.60E+06	--
Contact Resistance	2.36	0.053	1.56E+06	333
Fraction Change	0.23	0.06	0.03	
PBI 7.5 oz/sq yd (Dry)	**Residuals (K)**	**k (W/m-K)**	**ρc (J/m^3-K)**	**h_i (W/m^2-K)**
No Contact Resistance	4.40	0.046	1.67E+06	--
Contact Resistance	2.93	0.051	1.57E+06	183
Fraction Change	0.33	0.11	0.06	
Southern Mills Green 8.5 oz/sq yd (Dry)	**Residuals (K)**	**k (W/m-K)**	**ρc (J/m^3-K)**	**h_i (W/m^2-K)**
No Contact Resistance	3.06	0.042	1.73E+06	--
Contact Resistance	2.45	0.044	1.63E+06	255
Fraction Change	0.20	0.05	0.06	

A summary of the thermal property information for the dry fabric materials evaluated in the TPTF is presented in Table 17. The average thermal properties are presented for each material, as well as the interfacial conductance value, determined by adding a fictitious layer into the system in the Prop1D[6] program. The dry thermal property values presented in Table 17 were determined on a non-temperature dependent basis. The final column in Table 17 is the number of test cases used to determine the average thermal property values for each fabric. Although nine tests were completed on each of the outer shell materials initially, the tests which did not have steady initial conditions and those where the Kapton sensor was moved between the layers are not considered in this summary.

Table 17: Dry Material Thermal Property Estimates.

Material (Weight oz/sq yd)	Value	Thermal Conductivity (W/m-K)	Volumetric Heat Capacity (J/m^3-K)	Interfacial Conductance (W/m^2-K)	Number of Test Cases
Nomex (7.5)	Average	0.053	1.56×10^6	333	8
	Standard Deviation	0.0043	2.98×10^4		
Nomex (6.0)	Average	0.043	1.56×10^6	347	4
	Standard Deviation	0.0028	7.71×10^4		
Nomex (5.5)	Average	0.043	1.53×10^6	306	5
	Standard Deviation	0.0011	8.07×10^4		
PBI (7.5)	Average	0.051	1.57×10^6	183	13
	Standard Deviation	0.0038	3.88×10^4		
PBI (6.0)	Average	0.045	1.58×10^6	381	3
	Standard Deviation	0.0015	2.06×10^4		
Southern Mills Green (8.5)	Average	0.044	1.63×10^6	255	4
	Standard Deviation	0.0015	6.70×10^4		
Navy (6.8)	Average	0.043	1.62×10^6	413	3
	Standard Deviation	0.00007	1.54×10^4		
Aralite Thermal Liner	Average	0.034	7.46×10^5	334	3
	Standard Deviation	0.0007	6.80×10^3		
Crosstech Moisture Barrier	Average	0.041	9.72×10^5	199	5
	Standard Deviation	0.0026	1.23×10^4		

The values for the volumetric heat capacity were similar for each of the outer shell materials evaluated. However, the thermal conductivity varied between each. As expected, the more dense Nomex and PBI fabrics (7.5 oz/sq yd) had a higher thermal conductivity than the lighter variety (5.5 and 6.0 oz/sq yd). The thermal conductivity and the volumetric heat capacity of the Aralite Thermal Liner material are lower than the rest of the fabric materials. The thermal conductivity is very low, approximately 10% higher that of still air at nominally 75°C.[30] This material is made up of a fiber-fill layer stitched to a Nomex face cloth. The fiber-fill layer is much thicker than the outer shell materials and the moisture barrier. Much of this thickness is made up of air, which acts as an excellent insulator.

4.1.2 MOISTURE AFFECT

Most the testing to determine the time to 2nd degree burn described in this thesis utilized the dry fabric thermal properties. However, the effects of moisture on the material performance are critical, as the materials are frequently used damp, either from water spray or due to perspiration. The thermal properties of the damp materials were initially determined on a temperature dependent basis to determine if the change in temperature of the materials changes the heat transfer characteristics due to different rates of moisture transfer. Select materials were also

evaluated on a non-temperature dependent basis to provide a means of direct comparison with the dry thermal property values. A complete summary of the thermal property estimations for the materials with water added is included in Appendix B: Thermal Property Estimations.

The distilled water was added to the fabric materials to simulate the use of the materials in their actual intended environment. The addition of 0.25 grams of water per gram of fabric to the outer shell/stand alone materials did not drastically alter the appearance or feel of the material, whereas the addition of 1.0 grams of water was easily noticeable. However, adding one gram of water per gram of fabric to the Aralite thermal liner did not give the perception of a thoroughly soaked material like the outer shell fabrics. This level of moisture was attained by lightly spraying the Nomex face cloth stitched to the fiber fill layer of the thermal liner with water, until the entire surface was moist. The fiber-fill layer did not become noticeably damp at this moisture level. The appearance of the material at this moisture level was not dramatically different, although the blue face cloth material was a darker shade.

The heating stage of the TPTF evaluations of the wet materials lasted for nominally the same amount of time as the dry tests. The temperatures reached during these “wet” tests did not reach the same level as those achieved during the dry material evaluations. Although the temperatures of the heater in the wet thermal property evaluations were not as high as those attained during the dry tests, the heat flux produced was generally higher due to the higher amount of heat transferred away from the heater by the wet materials. These affects were magnified as additional water was added to the clothing. The following figures (Figure 28 –Figure 30) provide a comparison of the temperature rise of the heater and the Macor skin simulant surface, as well as the heat flux produced by the heater during evaluations of the Nomex 7.5 oz/sq yd material dry, and with different amounts of moisture added. These figures present the temperature and heat flux levels from only four tests, however the basic affect of the added moisture was similar for each clothing type, although the magnitude of the temperature and heat flux differences varies.

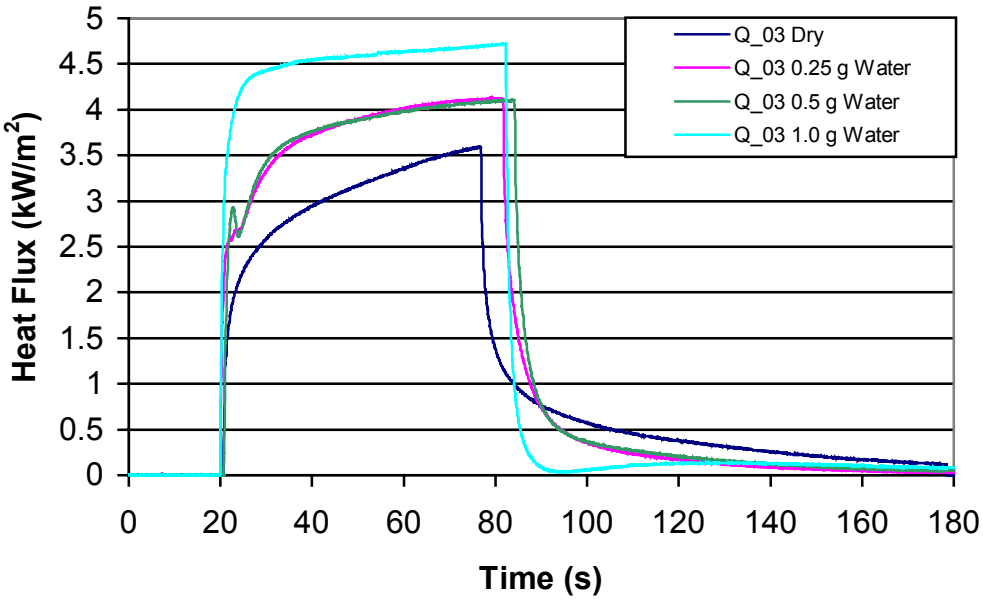

Figure 28: Thermal Properties Test Fixture – Sample Nomex 7.5 oz/sq yd Tests, 40 VDC Applied to Heater, Moisture Content Effects on Heat Flux at Q_03, Heater Top Thermopile Heat Flux Sensor. Moisture Added on a Gram of Water per Gram of Fabric Basis.

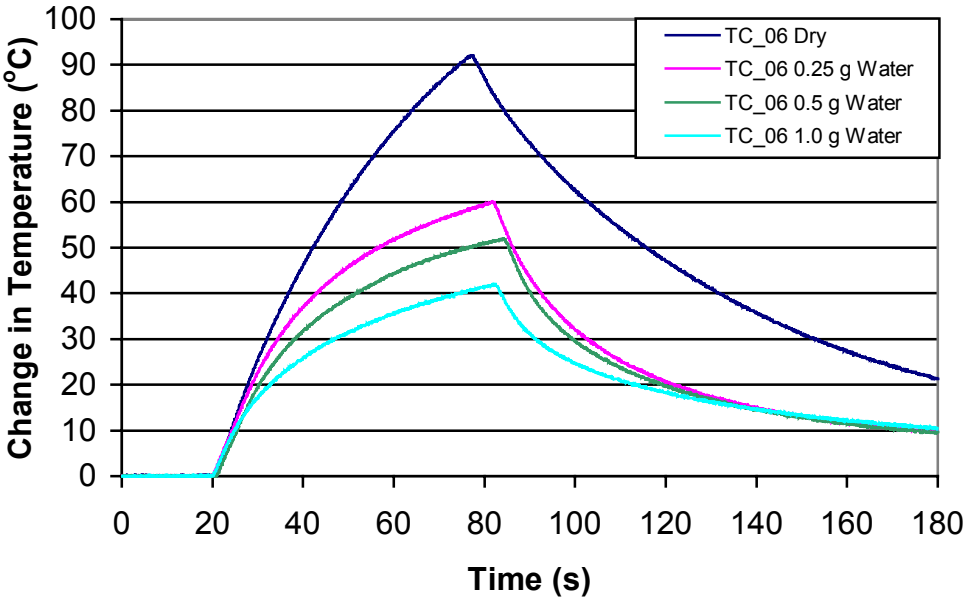

Figure 29: Thermal Properties Test Fixture – Sample Nomex 7.5 oz/sq yd Tests, 40 VDC Applied to Heater, Moisture Content Effects on Temperature Rise at TC_06, Heater Top Thermocouple. Moisture Added on a Gram of Water per Gram of Fabric Basis.

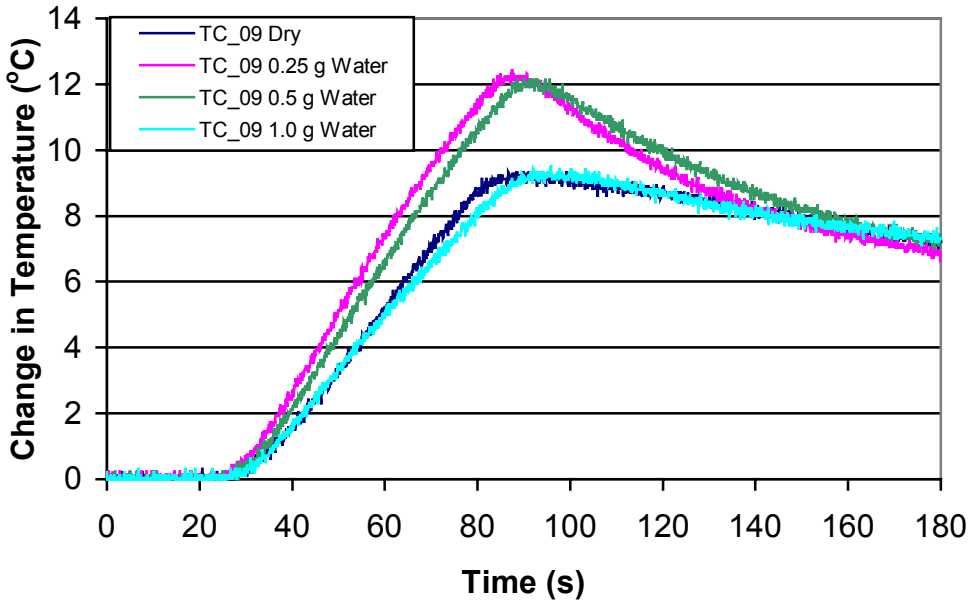

Figure 30: Thermal Properties Test Fixture – Sample Nomex 7.5 oz/sq yd Tests, 40 VDC Applied to Heater, Moisture Content Effects on Temperature Rise at TC_09, Macor Surface Thermocouple. Moisture Added on a Gram of Water per Gram of Fabric Basis.

The initial property estimates for each of the wet clothing evaluations were assumed temperature dependent. The Prop1D[6] program determines the temperature dependent thermal properties with a linear approximation between two temperatures reached during the testing. In order to provide a direct comparison to the dry thermal properties, the wet fabric results from one of the materials were analyzed on a non-temperature dependent basis. The results of this analysis are presented in Table 18.

Table 18: Moisture Content Effects on Navy 6.8 oz/sq yd Material.

Moisture Content	Value	Residuals	Thermal Conductivity (W/m-K)	Volumetric Heat Capacity (J/m^3-K)	Interfacial Conductance (W/m^2-K)
Dry	Average	1.93	0.044	1.62×10^6	410
	Standard Deviation		0.0001	1.54×10^4	
0.25 g water/g fabric	Average	1.84	0.13	1.46×10^6	1480
	Standard Deviation		0.0034	9.19×10^4	
0.5 g water/g fabric	Average	2.09	0.13	2.41×10^6	2000
	Standard Deviation		0.019	6.72×10^5	
1.0 g water/g fabric	Average	1.53	0.13	2.46×10^6	1080
	Standard Deviation		0.024	5.64×10^5	

The addition of the distilled water to the clothing dramatically affected the thermal conductivity of the clothing. At each level of moisture added, the thermal conductivity was approximately three times the thermal conductivity of the dry material. The effect of the added water on the thermal conductivity could not be calculated directly. For reference, the thermal conductivity of water in the temperature ranges experienced in this testing is approximately 0.6 – 0.68 W/m-K.[30] The volumetric heat capacity of the material when 0.25 grams of water per gram of fabric was added was nearly equivalent to the dry estimate. The estimates of the volumetric heat capacity for the fabric when 0.5 grams of water per gram of fabric and 1.0 grams of water per gram of fabric were added were approximately 1.5 times that of the dry estimate.

An estimation of the effects of the added water on the volumetric heat capacity can be developed by estimating the volumetric heat capacity of the water, and adding this to the value calculated for the dry material's volumetric heat capacity. To estimate the volumetric heat capacity of the water in the system, the specific heat of water (nominally 4.2×10^3 kJ/kg-K) can be multiplied by the mass of water added to the fabric. During the tests of the fabric with 0.5 grams of water added per gram of material, approximately 6 grams of water was added to each half of the test fixture. The product of the mass and the specific heat of water, can then be divided by the volume of the sample, determined by multiplying the surface area (0.017 m^2) by the approximate thickness of the three layers evaluated (0.015 m). This will approximate the volumetric heat capacity of the water added to the system. For the tests with 0.25, 0.5, and 1.0 grams of water per gram of fabric added to the material, the volumetric heat capacity of the water was calculated to be 4.9×10^5 J/m^3-K, 9.8×10^5 J/m^3-K, and 1.96×10^6 J/m^3-K, respectively. The estimated total volumetric heat capacity of the materials with 0.25, 0.5, and 1.0 grams of water per gram of fabric added is 2.11×10^6 J/m^3-K, 2.6×10^6 J/m^3-K, and 3.58×10^6 J/m^3-K, respectively. This method provided a reasonable estimate of the volumetric heat capacity when 0.5 grams of water per gram of material was added, but did not accurately estimate the volumetric heat capacity values with 0.25 and 1.0 grams of water per gram of fabric added. The inability to accurately estimate the affects of the moisture on the volumetric heat capacities may be due to the vaporization of the moisture

as the temperature of the clothing increases, or the effects of the moisture migration through the clothing, away from the heat source, on the clothing property estimations.

The effects of the added water on the thermal properties are presented in Figure 31 in the form of a multiplier factor of the dry estimate. For example, the value for the thermal conductivity with 0.25 grams water added per gram of fabric is 0.13/0.044 = 3.0.

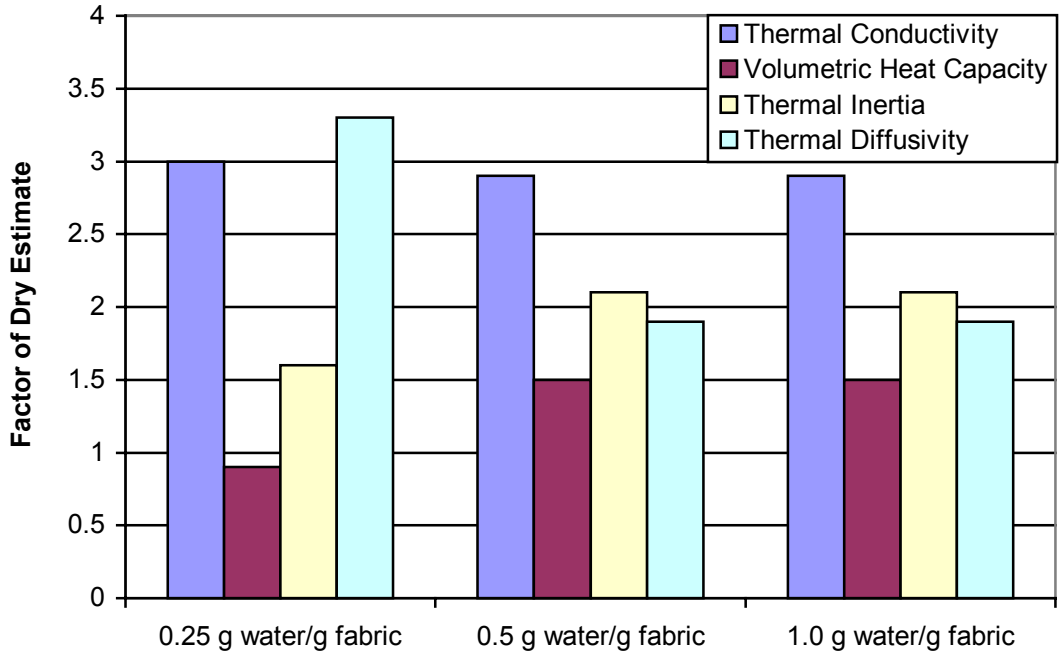

Figure 31: Navy 6.8 oz/sq yd – Wet Versus Dry Thermal Property Comparison. Thermal Conductivity – W/m-K, Volumetric Heat Capacity – J/m^3-K, Thermal Inertia W-s$^{1/2}$/m^2-K, Thermal Diffusivity m^2/s. Moisture Added on a Grams of Water per Gram of Fabric Basis

The remainder of the thermal property evaluations were completed with the properties estimated at 30^{o}C and 80^{o}C, which were typical values for the minimum and maximum temperatures attained during the testing of the wet fabric materials. Prop1D[6] determines the properties on a linear temperature dependent basis. The contact resistance for these tests was determined by manually changing the level for the thermal conductivity of the fictitious layer in the input file to produce the lowest residual RMS value. This manual adjustment was necessary because the program could only calculate four of the thermal property values at one time. Since the thermal

conductivity and the volumetric heat capacity values were being calculated for the fabric at two different temperatures, the program was unable to calculate the thermal conductivity of the fictitious layer. The value for the interfacial conductance, h_i, increased by a factor of 3 to 4 when water was added to the system.

The properties of the Navy 6.8 oz/sq yd material were estimated using both a temperature dependent assumption and a non-temperature dependent assumption. The evaluations with the temperature dependent assumption yielded property estimates producing slightly lower RMS values than the constant thermal property estimates, Table 19.

Table 19: Temperature Dependent Thermal Property RMS Comparison with Constant Thermal Property RMS for Navy 6.8 oz/sq yd Material.

Navy 6.8 oz/sq yd	Temp. Dependent Assumption Temperature RMS Residuals (K)	Non-Temp. Dependent Assumption Temperature RMS Residuals (K)
0.25 g water/ g fabric	1.81	1.84
0.5 g water/ g fabric	1.92	2.09
1.0 g water/ g fabric	1.52	1.53

The outer shell materials were evaluated with three layers of fabric on each side of the heater. Water was added to each piece of fabric separately, such that the measured weight was within 0.1 grams of the desired weight. After each test, the fabric samples were removed from the test fixture and allowed to cool. The materials were then re-weighed, and additional water was added if needed for the next test. Each of the individual fabric samples had a slightly different mass, so each required slightly different amounts of water to be added. In addition, the $\pm$0.1 gram tolerance led to slight variations in the amount of water added. This uncertainty, coupled with the variation between tests due to the removal and reinsertion of the samples before and after each test, produced results with more variation than the dry tests. The level of variation was determined by dividing the standard deviation of the test results used to calculate the average thermal properties by the average of each fabric's thermal properties at each moisture content. This value was expressed as the standard deviation percentage of the average. The variation

between tests typically escalated as more water was added to the fabrics, increasing from approximately 3.5% for the dry tests, to approximately 12% at 0.25 grams of water per gram fabric, 14% at 0.5 grams of water per gram fabric, to 24% at 1.0 grams of water per gram fabric.

Table 20 presents a complete summary of the material properties at each moisture content, with the exception of the Crosstech Moisture Barrier, which was tested dry only. The thermal conductivity at each level of water added increased above the dry estimates. The thermal conductivity of each fabric with 1.0 grams of water per gram of fabric added increased as the temperature increased. In many cases, the values for the thermal conductivity of the outer shell materials with 0.25 and 0.5 grams of water adder per gram of fabric were nominally equivalent over the temperature range investigated. This equivalency is based upon the overlap in 95% confidence region values that were added and subtracted from the predicted thermal conductivity values.

The volumetric heat capacity values for the outer shell materials decreased at higher temperatures when 0.5 and 1.0 grams of water were added per gram of material. The volumetric heat capacity of water decreases as the temperature is increased from 30^{o}C to 80^{o}C. The trend when 0.25 grams of water per gram of materials varied between fabrics, as in four of the cases the volumetric heat capacity was higher at the 80^{o}C, and in three cases it was lower at 80^{o}C. The computer program did not return 95% confidence regions for the volumetric heat capacity values. With the exception of the PBI materials, the values for the volumetric heat capacity in the cases where 0.25 grams of water per gram of fabric is added to the material are within 10-15% of each other, and may be within the confidence regions, and essentially equivalent.

The thermal conductivity of the Aralite thermal liner increases dramatically when water is added, Table 20. This is critical in the evaluation of turnout gear, as this layer acts as the primary thermal insulator in the ensemble, and is prone to becoming saturated with perspiration during fire fighting operations. In the temperature regions investigated, the thermal conductivity was

essential constant when 1.0 grams of water were per gram of material was added, and was approximately a factor of four higher than the dry thermal conductivity. When 1.5 grams of water per gram of material was added, the thermal conductivity was much more temperature dependent, and increased to nearly a factor of seven of the dry thermal conductivity at 80°C.

Table 20: Fabric Thermal Properties with Water Added.

Material (Weight - oz/sq yd)	Moisture Content g water/g fabric	k_1 (30°C) W/m K	k_2 (80°C) W/m K	ρC_{p1} (30°C) J/m^3 K	ρC_{p2} (80°C) J/m^3 K	95% Confidence Regions ±k1 (30°C) W/m K	95% Confidence Regions ±k2 (80°C) W/m K
Nomex 7.5	Dry	0.0528		1.56E+06		0.0017	
	0.25	0.1793	0.1290	1.68E+06	1.89E+06	0.0148	0.0112
	0.50	0.1824	0.2085	2.49E+06	1.88E+06	0.0128	0.0124
	1.00	0.1826	0.3033	3.88E+06	2.66E+06	0.0115	0.0178
Nomex 6.0	Dry	0.0430		1.56E+06		0.0010	
	0.25	0.1266	0.1288	1.51E+06	1.42E+06	0.0165	0.0105
	0.50	0.1256	0.1328	1.91E+06	1.40E+06	0.0139	0.0098
	1.00	0.0834	0.2395	3.55E+06	1.16E+06	0.0103	0.0146
Nomex 5.5	Dry	0.0433		1.53E+06		0.0009	
	0.25	0.1043	0.1137	1.24E+06	1.41E+06	0.0214	0.0144
	0.50	0.1143	0.0994	1.83E+06	1.77E+06	0.0149	0.0103
	1.00	0.1050	0.1281	2.27E+06	1.61E+06	0.0123	0.0111
PBI 7.5	Dry	0.0512		1.57E+06		0.0022	
	0.25	0.1050	0.1600	2.07E+06	1.42E+06	0.0072	0.0060
	0.50	0.0745	0.2048	2.43E+06	1.23E+06	0.0126	0.0098
	1.00	0.1199	0.2309	3.84E+06	1.67E+06	0.0106	0.0126
PBI 6.0	Dry	0.0450		1.58E+06		0.0008	
	0.25	0.1729	0.0949	1.60E+06	2.38E+06	0.0287	0.0173
	0.50	0.1349	0.1526	2.25E+06	1.29E+06	0.0154	0.0118
	1.00	0.0834	0.2395	3.55E+06	1.16E+06	0.0103	0.0146
Southern Mills 8.5	Dry	0.0442		1.63E+06		0.0017	
	0.25	0.1283	0.1531	1.54E+06	1.32E+06	0.0099	0.0069
	0.50	0.1310	0.1417	2.28E+06	1.42E+06	0.0121	0.0094
	1.00	0.1017	0.2819	3.51E+06	1.60E+06	0.0104	0.0157
Navy 6.8	Dry	0.0438		1.62E+06		0.0008	
	0.25	0.1503	0.1218	1.40E+06	1.52E+06	0.0250	0.0122
	0.50	0.1555	0.1201	2.16E+06	1.88E+06	0.0253	0.0197
	1.00	0.1070	0.1520	2.72E+06	1.89E+06	0.0111	0.0107
Aralite Thermal Liner	Dry	0.0320		7.75E+05		0.0010	
	1.00	0.1437	0.1290	9.88E+05	1.06E+06	0.0189	0.0126
	1.50	0.1057	0.2220	1.52E+06	6.27E+05	0.0122	0.0222

4.1.3 Ensemble Property Determination

In addition to the separate, individual, fabric layers evaluated using the TPTF, a series of Ensemble tests were conducted as well. There were three different ensemble configurations tested, each utilizing a different outer shell material, but the same type of moisture barrier and inner liner. In addition, one of the ensemble types was tested with 1.0 and 1.5 grams of water

added to the Aralite Thermal Liner to simulate the effects of perspiring skin on the material performance.

The overall thickness of the ensembles was similar regardless of the outer shell material, and was measured to be approximately 3.4 mm. This thickness is slightly greater than the sum of approximately 1.88 mm for the thermal liner, 0.7 mm for the Moisture Barrier, and 0.5 mm – 0.6 mm for the outer shell materials. The temperature residuals for the ensemble tests were greater than those for the individual fabric tests, even with the incorporation of the contact resistance. The average residual temperature for the dry ensemble tests was nominally 4.5^{o}C. Table 21 presents a summary of the thermal properties of the three ensembles evaluated without any water added to the thermal liner. A more detailed summary of the ensemble properties are included in Appendix B: Thermal Property Estimations.

Table 21: Dry Ensemble Thermal Properties. Standard Deviation Determined for Thermal Conductivity and Volumetric Heat Capacity Only.

Material	Value	k (W/m-K)	ρc_p (J/m^3-K)	95 % Confidence Region – $\pm$k (W/m-K)	h_i (W/m^2-K)
(Nomex 7.5 oz/sq yd Outer Shell)	Average	0.040	9.97E+05	0.016	123
	Standard Deviation	0.0036	6.20E+03		
(Nomex 6.0 oz/sq yd Outer Shell)	Average	0.036	9.66E+05	0.015	110
	Standard Deviation	0.0022	5.56E+04		
(PBI 7.5 oz/sq yd Outer Shell)	Average	0.041	9.68E+05	0.013	143
	Standard Deviation	0.003	5.79E+04		

The thermal conductivities of the dry ensembles are similar for each outer shell material. As expected, the ensemble with the Nomex 6.0 oz/sq yd outer shell had a slightly lower thermal conductivity, as this outer shell material has the lowest conductivity of the three outer shell materials. The 95% confidence intervals for these tests are approximately 30-40% of the thermal conductivity values, and are large enough where the thermal conductivity values for each ensemble could be considered essentially equal. The Prop1D[6] program did not return 95% confidence intervals for the volumetric heat capacity estimates, although these values are similar for each ensemble, and may be within the confidence intervals as well.

The thermal properties of the ensemble with Nomex 7.5 oz/sq yd as the outer shell material was evaluated with 1.0 and 1.5 grams of water per gram of Aralite added to the thermal liner material. These evaluations were done to simulate the dampening of the Aralite due to perspiration. These ensemble tests were analyzed with temperature dependent thermal properties, to determine if the properties varied with temperature. The properties were assessed at 30^{o}C and 100^{o}C, as these temperature levels were attained in each ensemble evaluation. The residuals for these ensemble evaluations were nominally 1.9^{o}C. The contact resistance was determined manually in these evaluations by varying the value for the thermal conductivity of the fictitious layer in the TPTF to obtain the smallest residual measurement, as was done in the wet outer shell material property determinations.

Table 22 presents the thermal property estimates for the ensemble with water added to the thermal liner. The thermal conductivity at each moisture content level decreased as the temperature increased. At 30^{o}C, the thermal conductivity of the ensembles with 1.0 grams of water per gram of Aralite was nominally a factor of 3.5 greater than the dry thermal conductivity; however at 100^{o}C, the value for the wet and dry test were nearly identical. When 1.5 grams of water per gram of Aralite was added to the thermal liner, the thermal conductivity at 30^{o}C was a factor of 3 higher than the dry value, with this value decreasing to a level approximately 25% greater than the dry thermal conductivity at 100^{o}C. The decrease in the thermal conductivity at higher temperatures for the wet ensembles may be due to the migration of the water away from the higher temperature of the surface. As the temperature of the heater increased, the water moved away from the heat source, towards the skin simulant sensor. At the beginning of the heating stages, this effect would increase the thermal conductivity, as the migrating water would be heated, and would contribute to the temperature rise of the Kapton sensor and the Macor skin simulant. However, as the heater temperature continued to rise, a buildup of water droplets formed on the Kapton sensor. This water condensation hindered the temperature rise of the

Kapton sensor and Macor skin simulant as the test continued, decreasing the thermal conductivity readings at higher temperatures.

While the thermal conductivity of the wet ensembles decreased with temperature, the volumetric heat capacity increased. The ensemble evaluation with 1.0 grams of water per gram of Aralite added had a volumetric heat capacity of approximately 57% of the dry ensemble at 30°C, with this value increasing to approximately double the dry volumetric heat capacity at 100°C. A similar pattern is followed by the ensemble with 1.5 grams of water per gram of Aralite, where the volumetric heat capacity at 30°C is approximately 63% of the dry ensemble volumetric heat capacity, while at 100°C the value increases to a factor of approximately 1.76 times that of the dry ensemble. The water migration effects presented in the previous paragraph may also be responsible for the changes in the volumetric heat capacity as well.

Table 22: Wet Ensemble Thermal Properties.

Ensemble – Nomex 7.5 oz/sq yd Outer Shell	Values	k_1 30°C (W/m-K)	k_2 100°C (W/m-K)	ρc_{p1} 30°C (J/m^3-K)	ρc_{p2} 100°C (J/m^3-K)
1.0 gram water per gram Aralite	Average	0.14	0.041	5.65E+05	1.96E+06
	Standard Deviation	0.0032	0.0042	9.65E+04	3.55E+05
1.5 gram water per gram Aralite	Average	0.12	0.050	6.28E+05	1.71E+06
	Standard Deviation	0.017	0.014	6.73E+04	5.02E+05

4.2 Radiant Protective Performance

The new test method described in this section is based upon the RPP test specified in NFPA 1977.[4] This test requires that the clothing be exposed to a radiant heat flux of nominally 21 kW/m^2, with the time to 2nd degree burn evaluated by a copper calorimeter. This exposure flux was used to evaluate a new test method and model to assess the time to 2nd degree burn using the Macor skin simulant sensor. The results from this new skin simulant sensor were compared to the burn predictions from the copper calorimeter tests. This model did not accurately predict the temperatures and the time to 2nd degree burn during the ensemble tests due to the complexity

of the ensemble, so a different approach utilizing the heat flux levels calculated using Diller's Algorithm (Equation 6) was developed.

4.2.1 COPPER CALORIMETER RESULTS

Outer Shell Materials

The initial copper calorimeter tests were completed with a 3 mm (1/8") air gap between the sensor and the clothing material. An air gap of this thickness was used in the Phase 1 portion of this project,[5] and results for fabric tests at this thickness have been included in the literature.[31] There are two similar tests for evaluating single layers of clothing specified in ASTM D 4108[16] and NFPA 1977.[4] The first requires the use of a 6.35 mm (¼") air gap, while the latter does not. While not specifically required, the NFPA test will have a slight air gap between the sensor and the back face of the clothing due to the 20 gage steel sample holder assembly required to hold the fabric and the sensor in place during the test.[4]

The initial RPP tests were completed using a quartz lamp as the heat source. A complete series of additional tests were completed using the heater from the cone calorimeter[24] as well. Both sets of tests were conducted at 21 kW/m^2, with the front face of the fabrics located 1" from the source. Additional RPP type tests were conducted using the cone heater with the fabric sample placed in immediate contact with the sensor to assess the impact of the 3 mm air gap. Table 23 presents a summary of the tests completed using the copper calorimeter for this thesis. The complete set of copper calorimeter RPP tests is attached in Appendix C: Radiant Protective Performance Test Data.

Table 23: Copper Calorimeter Test Summary.

Material Evaluated	Heat Source	Heat Flux Level (kW/m^2)
Nomex 7.5 oz/sq yd (with 3 mm air gap)	Quartz Lamp and Cone Heater	21
Nomex 6.0 oz/sq yd (with 3 mm air gap)	Quartz Lamp and Cone Heater	21
Nomex 5.5 oz/sq yd (with 3 mm air gap)	Quartz Lamp and Cone Heater	21
PBI 7.5 oz/sq yd (with 3 mm air gap)	Quartz Lamp and Cone Heater	21
PBI 6.0 oz/sq yd (with 3 mm air gap)	Quartz Lamp and Cone Heater	21
Southern Mills Green 8.5 oz/sq yd (with 3 mm air gap)	Quartz Lamp and Cone Heater	21
Navy 6.8 oz/sq yd (with 3 mm air gap)	Quartz Lamp and Cone Heater	21
Nomex 7.5 oz/sq yd (no air gap between fabric and copper cal.)	Cone Heater	21
PBI 7.5 oz/sq yd (no air gap between fabric and copper cal.)	Cone Heater	21
Ensemble with Nomex 7.5 oz/sq yd outer shell	Cone Heater	21
Ensemble with PBI 7.5 oz/sq yd outer shell	Cone Heater	21

Table 24 and Figure 32 present a summary of the time to 2nd degree burn for each of the outer shell fabric materials exposed to 21 kW/m^2 from the quartz lamp and the cone heater, measured using the copper calorimeter. A single layer of each fabric was evaluated during each test, although it is acknowledged that most protective clothing will consist of more than one layer.

Table 24: Copper Calorimeter Time to Second Degree Burn.

Material and Weight (oz/sq yd)	Time to Second Degree Burn	
	Quartz Lamp	Cone Heater
Nomex IIIA (7.5)	18.2	19.6
Nomex IIIA (6.0)	17.3	18.0
Nomex IIIA (5.5)	15.5	17.4
PBI (7.5)	20.0	19.2
PBI (6.0)	18.9	18.5
Southern Mills Green (8.5)	19.7	21.4
Navy Blue (6.8)	19.7	19.0

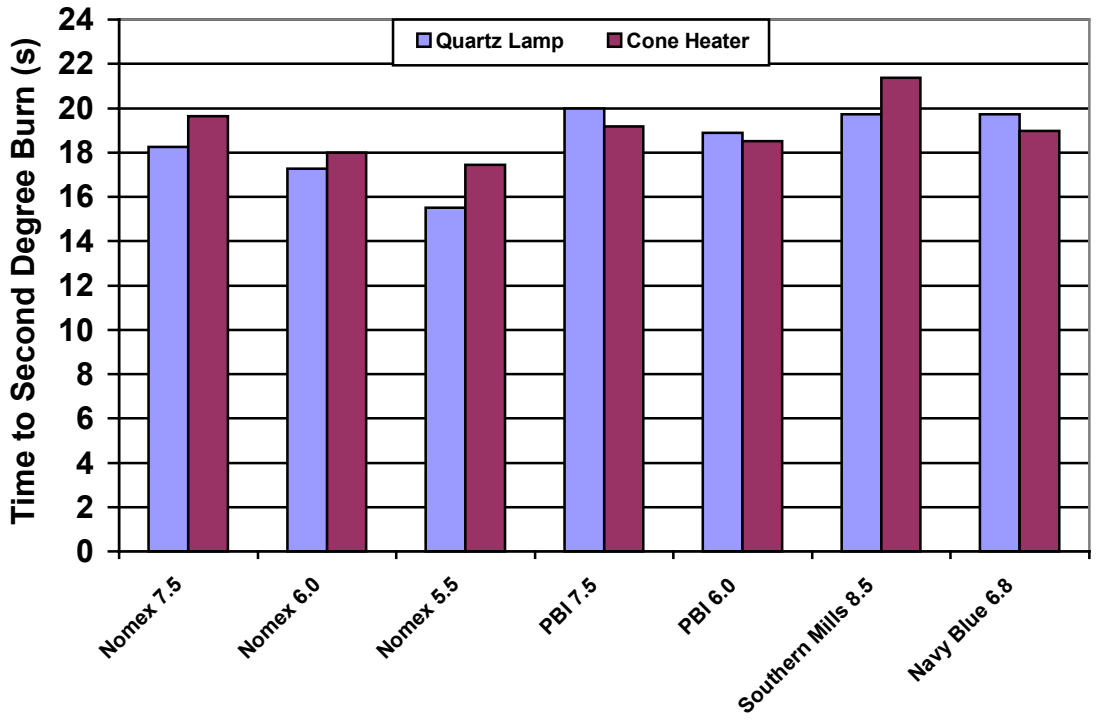

Figure 32: Copper Calorimeter – Time to Second Degree Burn, Exposure Nominally 21 kW/m^2 from Quartz Lamp and Cone Heater.

The time to 2nd degree burn for most of the materials was longer for the tests run with the cone heater, with the exception of the PBI materials and the Navy blue material. Regardless of the heat source, the time to 2nd degree burn is dependent on the weight of the fabric material, with the exception of the Southern Mills green material exposed with the quartz lamp. The Nomex and PBI fabrics provide excellent weight comparisons, as there are different weights for each material type. The PBI materials typically performed better than the Nomex materials of the same weight, and exhibited less damage after the test. Figure 33 and Figure 34 present a comparison of the change in temperature of the copper calorimeter for the Nomex 7.5 oz/sq yd and PBI 7.5 oz/sq yd fabric tests.

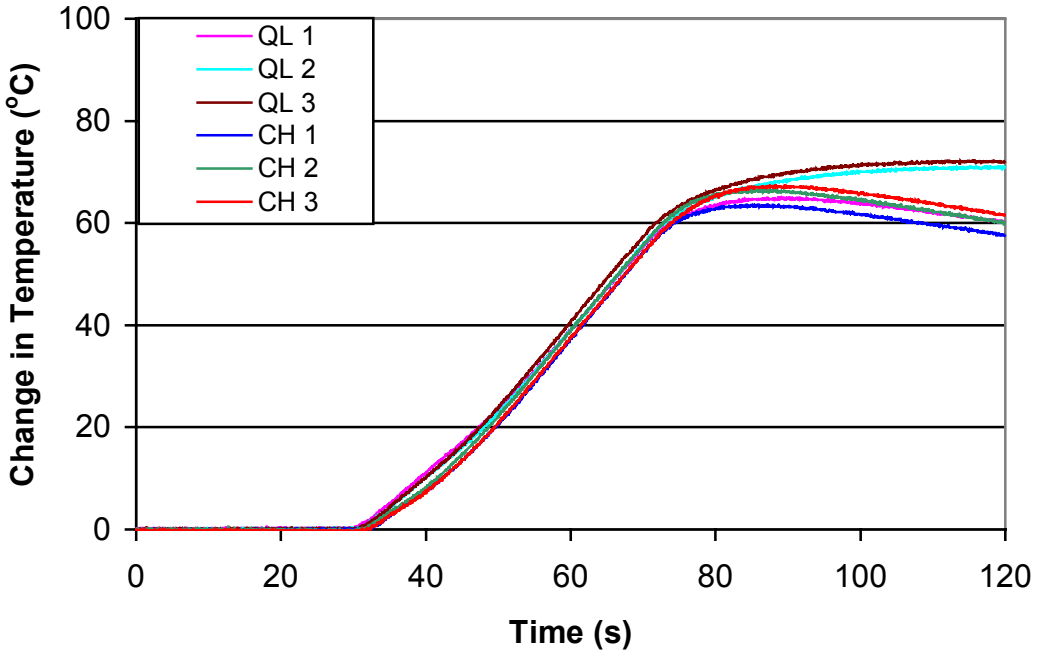

Figure 33: Copper RPP Exposure (21 kW/m^2), Nomex 7.5 oz/sq yd – Change in Temperature Comparison of Copper Calorimeter when Exposed with Quartz Lamp (QL) and Cone Heater (CH).

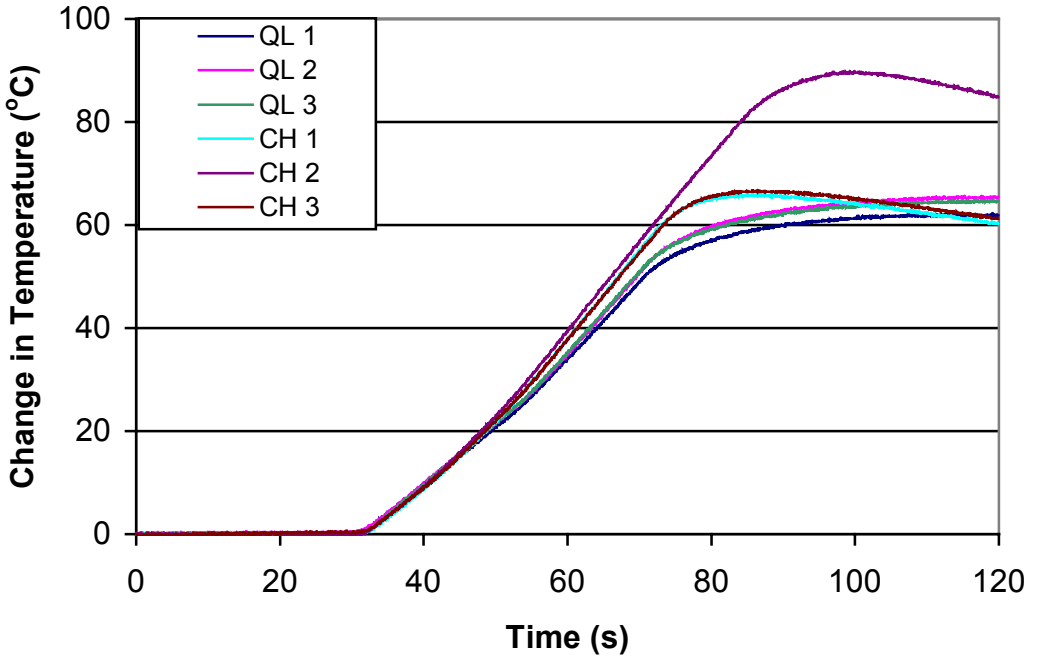

Figure 34: Copper RPP Exposure (21 kW/m^2), PBI 7.5 oz/sq yd – Change in Temperature Comparison of Copper Calorimeter when Exposed with Quartz Lamp (QL) and Cone Heater (CH).

The change in temperature in the Nomex tests are nearly identical for each heater type, while the change in temperature in the cone heater tests with the PBI material are greater than the quartz lamp tests. This difference in the sensor temperature response for the different fabrics may be due to the higher amount of charring and offgassing of the Nomex fabric when exposed to the cone heater. While each fabric produced some level of smoke during the radiant exposure, the Nomex materials exhibited a noticeable difference in damage when exposed to the cone heater as opposed to the quartz lamp, whereas the PBI materials did not show a noticeable change in the level of damage. Figure 35 demonstrates the differences in material damage to the Nomex 7.5 oz/sq yd and PBI 7.5 oz/sq yd fabrics exposed to the cone heater and the quartz lamp heater for nominally the same amount of time. The samples on the left were exposed with the quartz lamp, while those on the right were exposed with the cone heater.

The charring of the materials, which typically began approximately 8 to 10 seconds after exposure began, may increase the protective qualities of the materials by creating a better insulator. The difference in fabric response to the two different heater types may be due to the radiant characteristics of the quartz lamp and the cone heater. The quartz lamps operate at much higher temperatures than the cone heater when producing 21 kW/m^2, and this temperature difference produces radiant heat with different spectral characteristics. A more detailed presentation of the differences between the two heat sources is presented in the next section of this thesis.

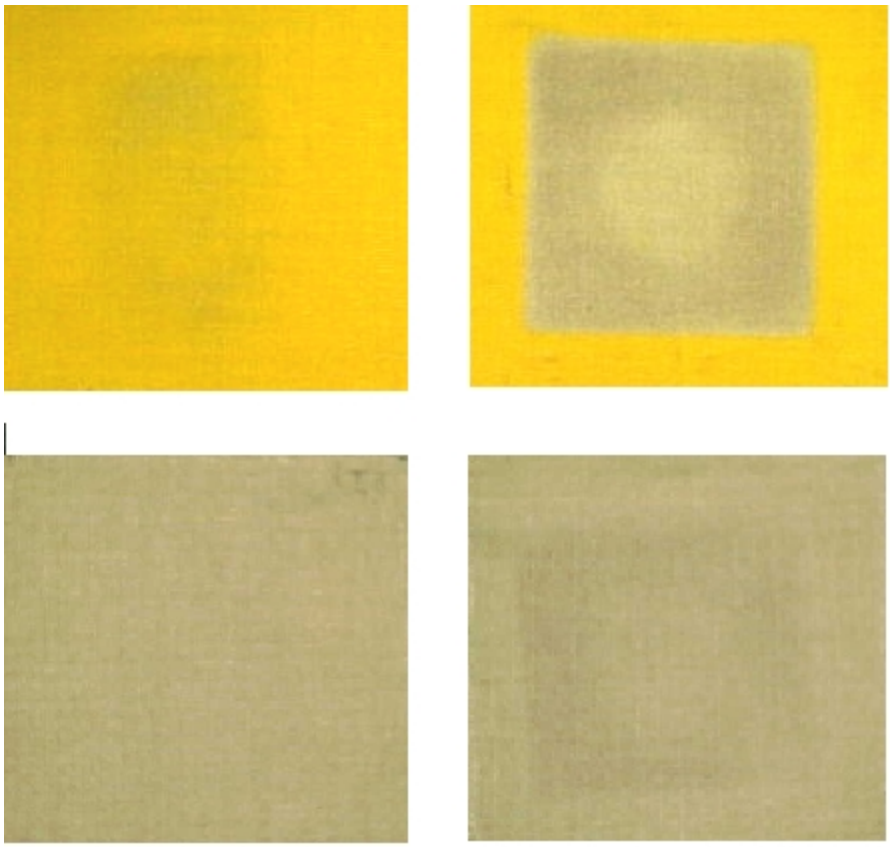

Figure 35: Material Damage Heater Dependence – Comparison of Post-Test Samples of Nomex 7.5 oz/sq yd (top) and PBI 7.5 oz/sq yd (bottom), Exposed to Nominally 21 kW/m^2 with Quartz Lamp (left side) and Cone Heater (right side).

Equation 4 was used to assess the transient heat flux at the surface of the copper calorimeter at each time step during the RPP tests. This method was used due to the fast response of the copper calorimeter.[26] Figure 36 presents the heat flux levels attained at the surface of the copper calorimeter during a representative RPP test on each of the three different weight Nomex fabrics. The amount of heat passing through the clothing materials to the copper calorimeter is dependent upon the weight of the test sample.

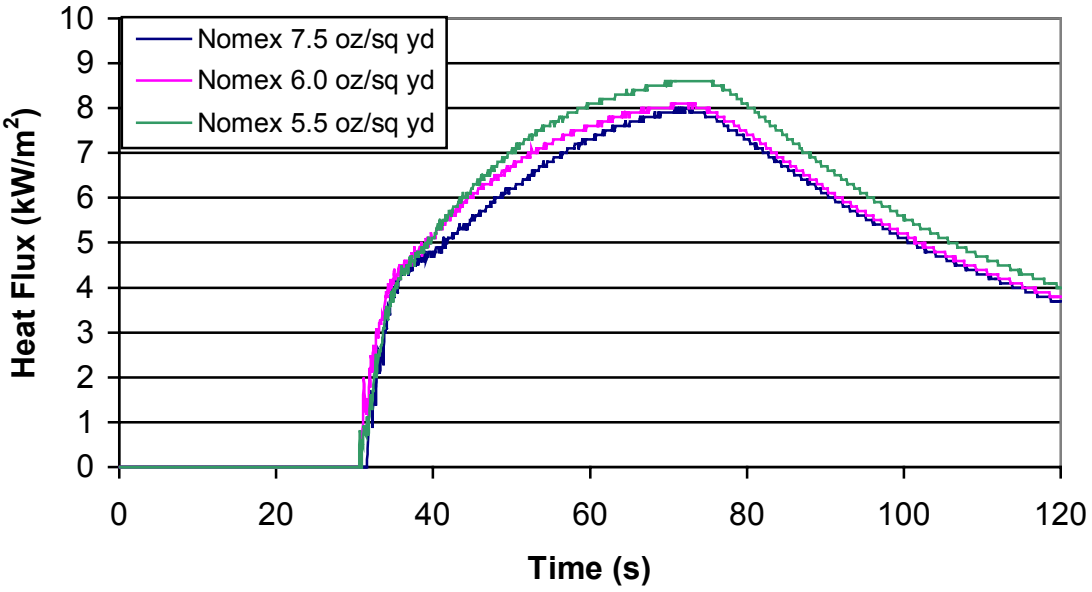

Figure 36: Copper Calorimeter RPP Exposure (21 kW/m^2 from Cone Heater) – Heat Flux at Copper Calorimeter Surface, Located Behind 1 Layer of Nomex Material. Comparison of Heat flux Level for Different Nomex Blends. Exposure Begins Nominally at 30 Seconds and Lasts for Approximately 40 Seconds.

The heat flux levels at the calorimeter surface, calculated nominally 30 seconds after the clothing/copper calorimeter system exposure began, are shown in Figure 37. These values relate well with the 2nd degree burn times presented in Figure 32, such that those fabric materials with lower heat levels at the copper calorimeter surface have higher values for 2nd degree burn times. The only discrepancy is with the Southern Mills Green fabric, where the heat flux levels at the copper surface were nearly identical for the two heat sources 30 seconds after the exposure began, but there was nearly a one second difference in the time to 2nd degree burn for the different heater types.

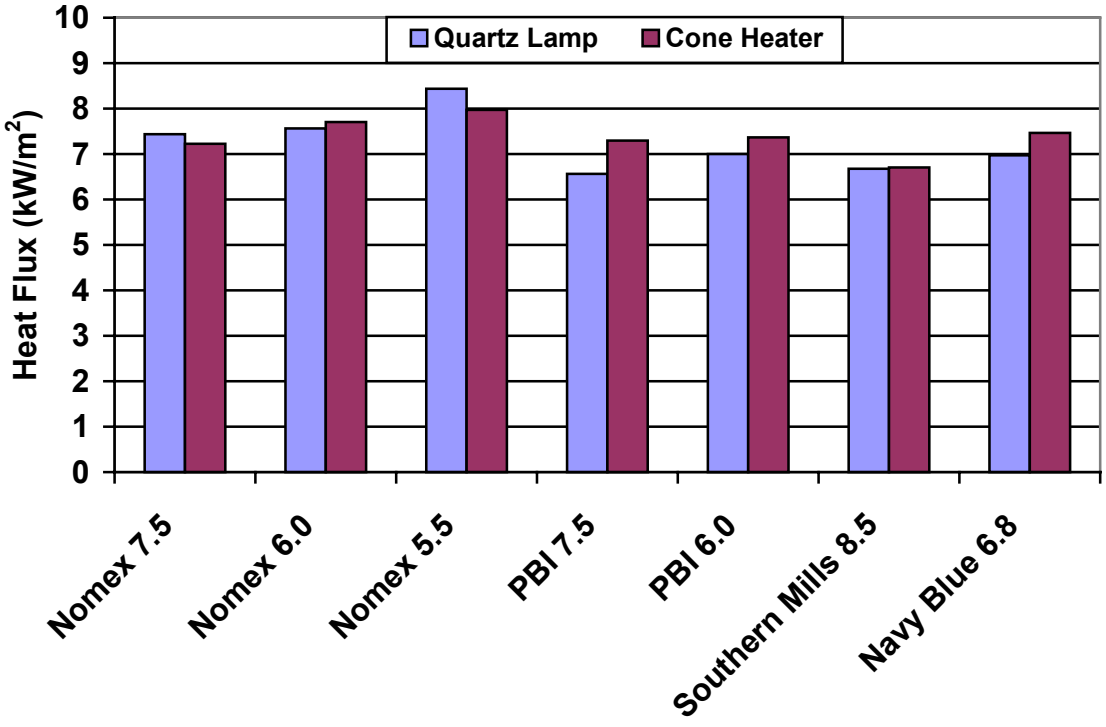

Figure 37: Heat Flux at Surface of Copper Calorimeter Approximately 30 Seconds after Exposure Began. Exposure Levels from Quartz Lamp and Cone Heater Nominally 21 kW/m^2.

To assess the impact of incorporating a 3 mm gap between the fabric and the sensor, two of the fabric materials were evaluated without this space using the cone heater, Table 25. The determination of the time to 2nd degree burn for these cases was shorter than the tests with the space, as expected. The 3 mm gap between the fabric layer and the copper calorimeter acts as an insulating layer.[15] This air gap is not required in the testing of ensembles and clothing with more than one layer in ASTM D 4108.[16] The heat flux at the sensor surface increased to approximately 10.5 kW/m^2 thirty seconds after the exposure began for both fabrics evaluated without a space between the fabric and the sensor. Figure 38 presents a comparison of the temperature rise of the copper calorimeter between a test with the 3 mm gap between the fabric and the sensor, and a test without this space. The temperature rise of the sensor was higher in those tests where no space was incorporated between the fabric and the layer.

Table 25: Impact of 3mm Space on Copper Calorimeter Burn Predictions.

Material and Weight (oz/sq yd)	Average Time to 2nd Degree Burn (Seconds)	
	With 3 mm Space	No Space (Fabric against Sensor)
Nomex (7.5)	19.6	12.8
PBI (7.5)	19.2	11.7

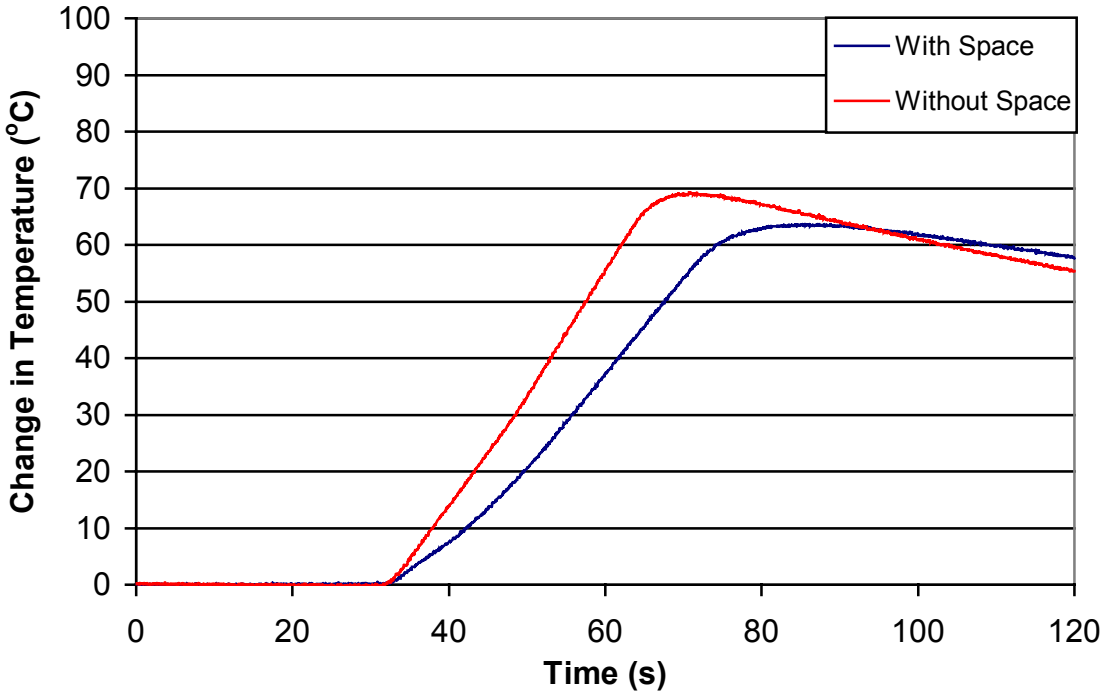

Figure 38: Copper Calorimeter RPP Exposure (21 kW/m^2) – Temperature Rise Comparison of Copper Calorimeter behind 1 Layer of Nomex 7.5 oz/sq yd when Evaluated with or without a 3 mm Air Gap Between the Fabric and Sensor.

Ensemble Evaluation

There were two ensembles evaluated using the copper calorimeter. These ensembles were exposed to a 21 kW/m^2 heat flux from the cone heater, with no space between the Aralite Thermal Liner and the copper calorimeter. Each of the ensembles used the same type of moisture barrier and thermal liner. The ensembles, which utilized the Nomex 7.5 oz/sq yd and PBI 7.5 oz/sq yd fabrics as the outer shell materials, were exposed for 60 seconds. Three tests were run with each ensemble type. Each layer of the ensemble exhibited signs of damage, and there was significant off gassing throughout the test exposure. Figure 39 presents a picture of

the three layers of an ensemble with Nomex 7.5 oz/sq yd as the outer shell material, exposed to 21 kW/m^2 from the cone heater for 60 seconds. A comparison of the time to 2nd degree burn for the two ensembles is presented in Table 26. The average heat flux level 30 seconds into the tests is approximately 1/5 that of the outer shell materials placed directly against the sensor, and less than 1/3 that of the outer shell materials when tested with the gap between the fabric and the sensor.

Table 26: Ensemble Copper Calorimeter Test Data.

Ensemble Outer Shell Material	Time to Second Degree Burn (s)	Heat Flux 30 Seconds After Exposure (kW/m^2)	Heat Flux 60 Seconds After Exposure (kW/m^2)
Nomex 7.5 oz/sq yd	50.8	2.1	3.3
PBI 7.5 oz/sq yd	51.7	2.0	3.3

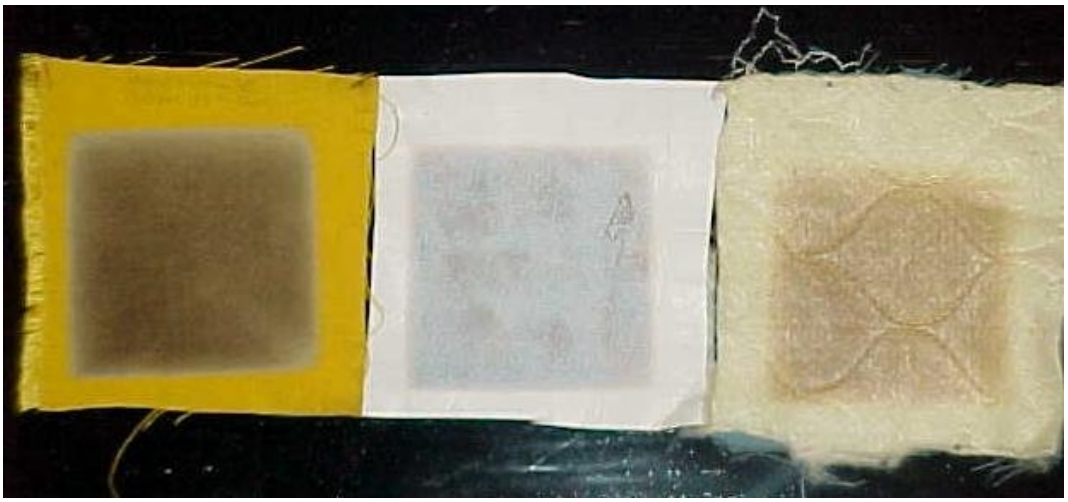

Figure 39: Damaged Ensemble with Nomex 7.5 oz/sq yd Outer Shell Material – Exposed to 21 kW/m^2 with Cone Heater for 60 Seconds. Damage Exhibited at Every Layer. Nomex Material on Left, Moisture Barrier in Middle, and Thermal Liner on Right.

4.2.2 SKIN SIMULANT PREDICTION

Outer Shell Materials

The characterization tests, and accompanying model evaluation, proved that the 1-D fabric/Macor finite difference model could accurately predict the Macor surface and subsurface temperatures during the fabric evaluations. There were three Macor RPP type tests run on each outer shell

material, with the cone heater and the quartz lamp. These tests were run without a space between the fabric and the sensor. The 1-D finite difference model procedure for the calculation of the time to 2nd degree burn outlined earlier in this thesis was applied to each of these tests. The individual test data and model predictions are attached in Appendix C: Radiant Protective Performance Test Data.

The method for predicting the time to 2nd degree burn for the Macor skin simulant is based upon using the fabric/Macor 1-D finite difference model to obtain surface and subsurface temperatures equivalent to those measured by the Macor skin simulant sensor during the RPP test. The input information for this model is then used in a 1-D finite difference model of the fabric/skin to predict the time to 2nd degree burn based upon the heating and cooling stages of the 1-D model exposure. This method is hereby referred to as the 1-D Model Method. There is a consistent difference between the 1-D Model Method predictions of the time to 2nd degree burn for the cone heater exposures and the quartz lamp exposures. The cone calorimeter tests consistently produced shorter times to 2nd degree burn for each fabric material evaluated. Table 27 and Figure 40 present the predicted values for the time to 2nd degree burn for the Macor RPP tests.

Table 27: Time to Second Degree Burn for Macor Skin Simulant RPP Tests (21 kW/m^2 Exposure)

Material and Weight (oz/sq yd)	Time to Second Degree Burn (s)	
	Quartz Lamp	Cone Heater
Nomex IIIA (7.5)	11.2	8.3
Nomex IIIA (6.0)	10.5	7.7
Nomex IIIA (5.5)	9.7	7.7
PBI (7.5)	12.8	8.8
PBI (6.0)	10.4	8.3
Southern Mills Green (8.5)	10.8	9.2
Navy Blue (6.8)	10.4	8.1

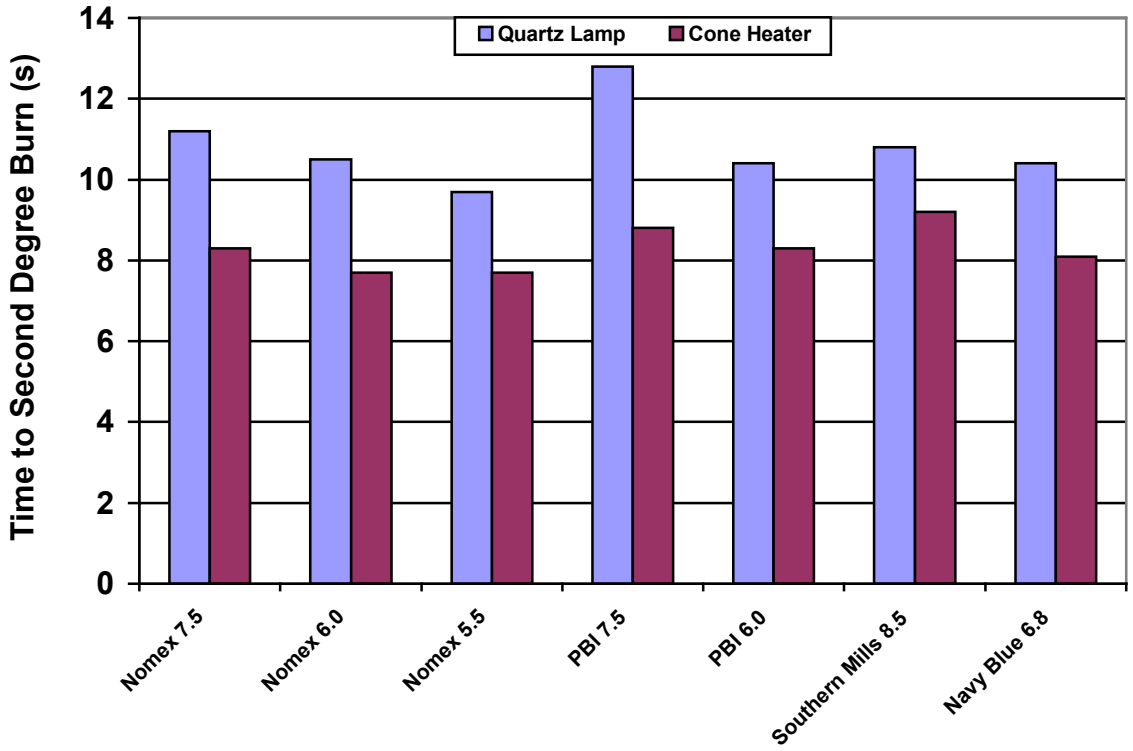

Figure 40: Macor RPP Exposure (21 kW/m^2) – Time to Second Degree Burn, Predicted Using 1-D Finite Difference Models of Fabric/Macor and Fabric/Skin, when Exposed with Quartz Lamp and Cone Heater. Labels are the Fabric Material and the Weight (oz/sq yd).

With few exceptions, the time to 2nd degree burn for the materials is dependent on the weight of the fabric. The Nomex materials provide a good comparison for the dependency of the time to 2nd degree burn on the weight of the protective clothing layer. The times are dependent upon the heat source, as the predictions for the tests in which the heat flux was supplied by the cone heater are consistently shorter than those when the heat flux was supplied by the quartz lamp. This topic is presented in greater detail later in this section.

The basic setup information for the 1-D models was assumed to be equivalent regardless of the heat source. This basic information included the convective heat transfer coefficient, which was assumed to be 5 W/m^2-K throughout. The emissivity of the clothing was assumed to be 0.9 for each fabric exposed to each heat source. This assumption is not an accurate assessment of the clothing properties, for reasons explained below. However, as information on the absorbtivity for

the fabrics involved in this evaluation could not be found, a uniform value was assumed. The differences in the absorbtivity of the radiant heat from the different heat sources contributed to the differences in the times to 2nd degree burn predicted for the different heat sources, although the level of contribution is not quantified in this thesis. As the emissivity was assumed equal throughout the analysis, the models lumped this information into the affects of the contact resistance between the fabrics and the Macor skin simulant, leading to consistently different values for the interfacial conductance, h_i for the two heat sources. Table 28 provides a list of the average interfacial conductance values for each fabric. Lower values, producing higher temperature drops at the interface, were required to obtain temperature predictions that accurately modeled those measured by the Macor skin simulant during the quartz lamp tests. If the emissivity of the clothing were the same for each heat source, then closer values for the interfacial conductance between the two heat sources would be expected. However, the lower interfacial conductance values for the quartz lamp suggests that less of the incident flux is being absorbed by the clothing. Instead of determining the actual amount of heat absorbed and using similar interfacial conductance values, these models assume a similar value for the clothing emissivity, and then use smaller interfacial conductance values to produce larger temperature drops to model the differences between the heat sources.

Table 28: Average Interfacial Conductance Values for Outer Shell Materials During Macor RPP Exposure (21 kW/m^2).

Material Weight – oz/sq yd)	Interfacial Conductance (hi – W/m^2-K)	
	Quartz Lamp	Cone Heater
Nomex IIIA 7.5	387	432
Nomex IIIA 6.0	368	415
Nomex IIIA 5.5	347	405
PBI 7.5	360	412
PBI 6.0	369	405
Navy Blue 6.8	363	403
Southern Mills Green 8.5	322	350

The values for the Interfacial Conductance, h_i, were varied in the 1-D finite difference model of the fabric/Macor to obtain temperature predictions which matched the temperatures measured by the skin simulant during the RPP exposure. More emphasis was placed on accurately predicting the Macor surface temperature than the temperature at the subsurface thermocouple, as there

was more uncertainty regarding the subsurface thermocouple measurement. This uncertainty included the actual depth of the thermocouple and the affect of the thermally conductive grease used to fill the hold into which the thermocouple is placed. Figure 41 provides a depiction of a typical temperature curve from the Macor RPP tests using the cone heater, along with the temperature predictions from the 1-D finite difference models of the fabric/Macor and the fabric/skin. The skin temperature decreases slowly after the removal of the heat source due to the elevated temperature of the clothing.

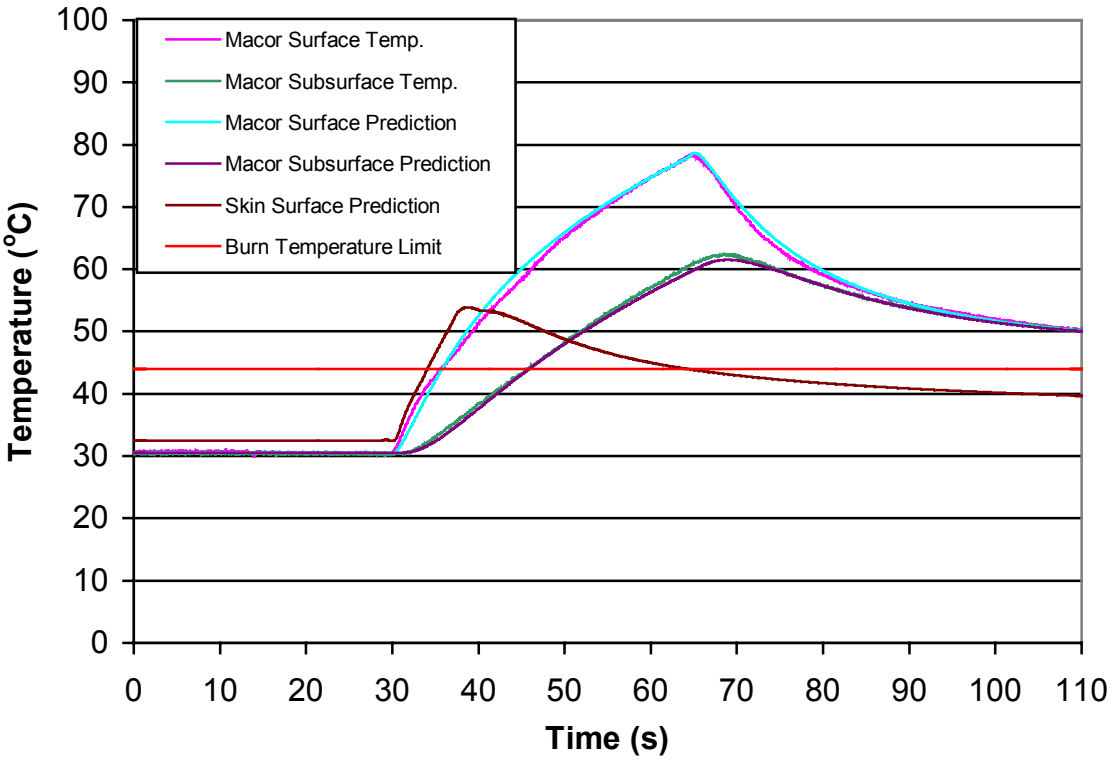

Figure 41: Macor RPP Exposure (21 kW/m^2) – Comparison of Measured Macor Surface and Subsurface Temperatures against Values Predicted with 1-D Finite Difference Fabric/Macor Model for Cone Heater Exposure of Navy 6.8 oz/sq yd fabric. Interfacial Conductance Value of 405 W/m^2-K in 1-D Model. Skin Surface Temperature from 1-D Finite Difference Fabric/Skin Model also included. Burn Damage will Occur for All Skin Temperatures Greater than 44°C, Presented as Burn Temperature Limit in Figure.

In addition to providing shorter predictions for the time to 2nd degree burn, the predicted temperatures for the cone heater tests were more accurate throughout the heating and cooling stages. The temperature data for the quartz lamp tests was not as smooth, particularly at the

beginning of the test. The temperature response of the Macor skin simulant during the quartz lamp tests typically started with a steep slope for the first five seconds of the exposure, before leveling out at a lower slope for the remainder of the heating. Figure 42 provides a depiction of a typical temperature curve from the Macor RPP tests using the quartz lamp heater.

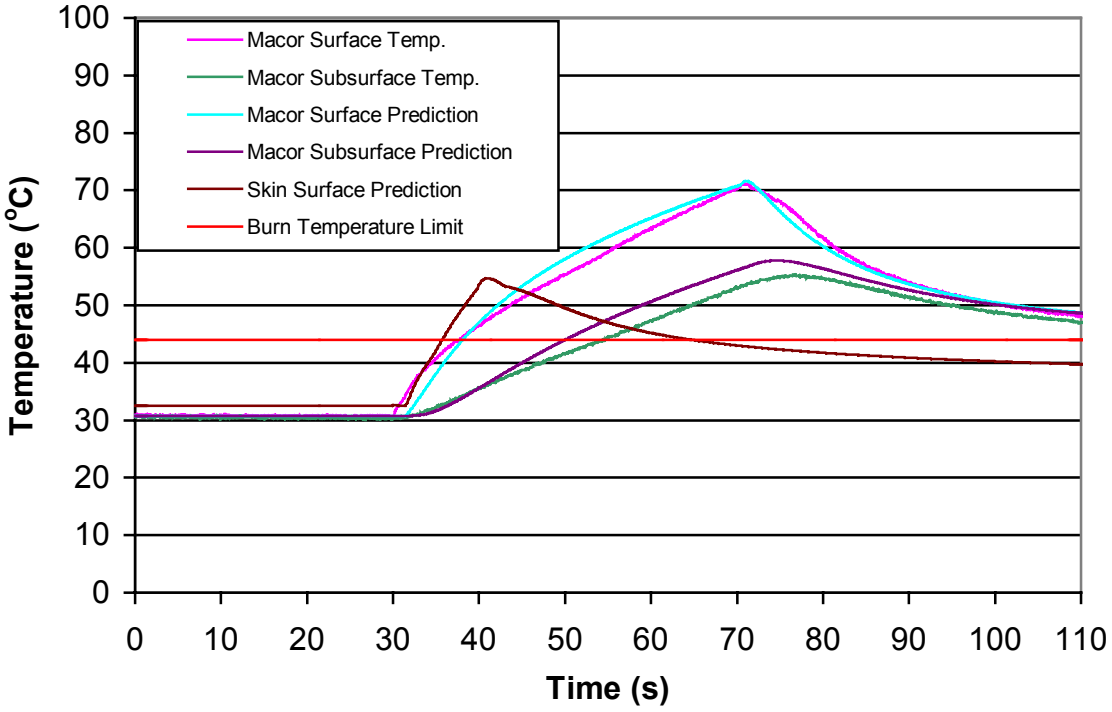

Figure 42: Macor RPP Exposure (21 kW/m^2) – Comparison of Measured Macor Surface and Subsurface Temperatures against Values Predicted with 1-D Finite Difference Fabric/Macor Model for Quartz Lamp Exposure of PBI 6.0 oz/sq yd fabric. Interfacial Conductance Value of 368 W/m^2-K in 1-D Model. Skin Surface Temperature from 1-D Finite Difference Fabric/Skin Model also included. Burn Damage will occur for all Skin Temperatures Greater than 44°C, Presented as Burn Temperature Limit in Figure.

The dependency of the time predictions on the heat flux source may be due to the radiant characteristics of the different sources. To produce a flux of 21 kW/m^2, the temperature of the quartz lamp filaments is approximately 1625 K. This temperature produces radiant heat mainly in the near to middle infrared region, with a spectral peak at approximately 1.8 μm. The quartz lamps absorb the energy produced by the heated element above approximately 4 μm.[5] To produce a flux of 21 kW/m^2, the cone heater operated at temperatures of approximately 870 K.

This temperature produces radiant heat mainly in the near to far infrared region, with 90% of the energy lying between 1 and 10.5 μm with a spectral peak of approximately 3.3 μm.

Data presented by Quintiere shows that fire fighting coat materials exhibit a strong absorption of infrared energy in a region centered around 3-μm, from about 2.8 to 3.2 μm.[32] Figure 43 provides a sample curve for the reflectance of the fire fighting coat materials, similar to those presented in Quintiere's paper, along with the calculated emissive power per unit wavelength distribution curves for the Quartz Lamp and the Cone Heater. The sample curve of the fabric reflectivity is provided to present the typical shape of the reflectance versus wavelength curve, and is not meant to be applicable to any particular material. At wavelengths lower than 3 μm the reflectivity increases significantly (decreasing the absorbtivity).

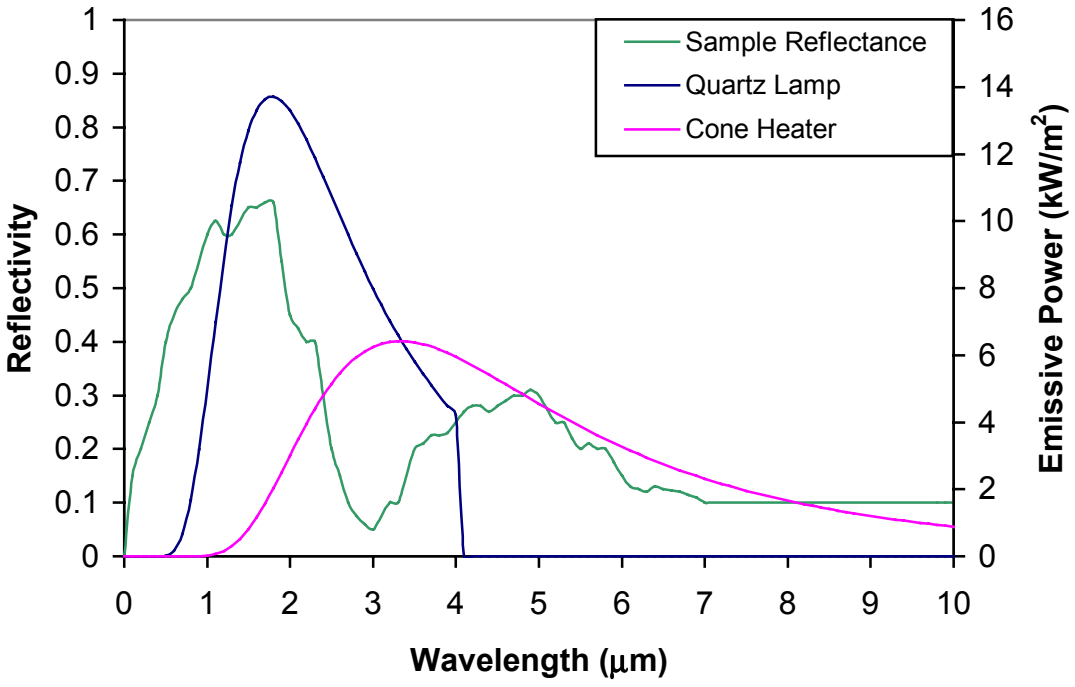

Figure 43: Emissive Power per Unit Wavelength of Quartz Lamp and Cone Heater in Relation to Characteristic Fire Fighting Coat Material Reflectivity.

Figure 43 presents the percentage of radiant energy lying in different wavelength bands for the quartz lamp and the cone heater. The Emissive Power, E_b, was determine at each wavelength between 0 and 10 μm, at increments of 0.1 μm using Equation 28.[33]. The emissive power per unit wavelength distribution curve for the Quartz Lamp has been scaled by approximately 90% to provide an equivalent area under the curve as the Cone Heater distribution so that both can be displayed on the same axis.

$$E_{b\lambda} = \frac{C_1 \lambda^{-5}}{e^{C_2/\lambda T} - 1} \qquad \text{Equation 28}$$

Where:
C1 = 3.743 x 10^8 W·μm^4/m^2
C2 = 1.4387 x 10^4 μm·K
λ = Wavelength (μm)

The emissivity of the quartz lamp was set to zero above four microns, as this is the approximate cutoff wavelength for quartz.[5] The spectral peak of the quartz lamp, at nominally 30% rated voltage, lies at approximately 1.8 μm, which is nearly equivalent to the peak of the characteristic reflectivity curve for the fire fighting coat material. The spectral peak of the Cone Heater at 870 K, is nearly equivalent to the downward peak of the characteristic reflectivity curve (point of maximum absorbtivity) for the sample fire fighting coat material. These differences in the emissivity per unit wavelength curves, when coupled with the sample reflectivity curve of fire fighting coat materials, suggests that differences in the actual absorbtivity of the clothing materials should be expected depending on the heat source.

These differences in the absorbtivity will lead to differences in the time to 2nd degree burn predictions for the two heat sources. An equivalent value for the emissivity of the clothing materials is used throughout the modeling and burn time predictions, regardless of the heat source. The difference between the heat sources is evaluated in the models by lumping this effect into the selection of the different values for the interfacial conductance. The interfacial conductance values used in the models for the quartz lamp tests are lower than those used in the models for the cone heater tests. Therefore, the temperature drop at the interface between the

clothing and the Macor, determined using Equation 10, will be higher. This higher temperature drop leads to lower temperatures in the Macor, and consequently the skin, leading to longer predictions for the time to 2nd degree burn, as shown in Table 27. If the actual wavelength dependent reflectivity of the clothing material was known, and the material had a higher reflectivity when exposed to the quartz lamp (as suggested by Figure 43), then the temperature of the Macor would be less than in the cone heater tests due to the decrease in absorbed energy. Unfortunately, this reflectivity information was not available, so the variation in the interfacial conductance was used. This method produced results consistent with the reflectivity information presented in Figure 43.

In addition to the standard Macor RPP tests, run at 21 kW/m^2, two sets of tests were run at 10 kW/m^2 to ensure that the model was accurate for more than one heat flux level. These additional tests utilized the cone heater, exposing the Macor skin simulant protected by the PBI 6.0 oz/sq yd and Navy Blue 6.8 oz/sq yd fabrics. Three tests were conducted with each fabric. The results of these tests are presented in Table 29. Figure 44 presents the temperature measurements and predicted values for one of the 10 kW/m^2 radiant exposure tests and accompanying model. The average values for the interfacial conductance for these exposures differ by approximately 10 W/m^2-K, differing by nominally 2% from the average interfacial conductance values for the 21 W/m^2 exposures (Table 28)

Table 29: Macor Radiant Exposure - 10 kW/m^2

Material (Weight – oz/sq yd)	Interfacial Conductance (h_i – W/m^2-K)	Time to Second Degree Burn (s)
PBI 6.0	413	18.2
Navy 6.8	414	17.1

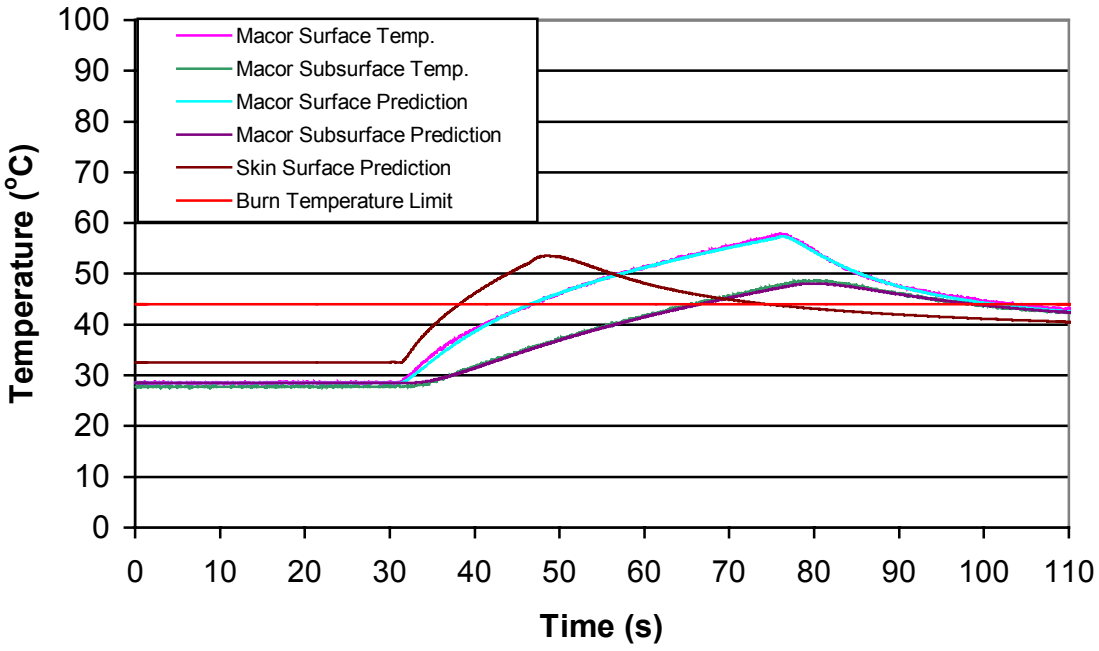

Figure 44: Macor Exposed to 10 kW/m^2 from Cone Heater– Comparison of Measured Macor Surface and Subsurface Temperatures against Values Predicted with 1-D Finite Difference Fabric/Macor Model. Test Conducted with Navy 6.8 oz/sq yd Material Protecting Macor. Interfacial Conductance Value of 412 W/m^2-K in 1-D Model. Skin Surface Temperature from 1-D Finite Difference Fabric/Skin Model also included. Burn Damage will occur for all Skin Temperatures Greater than 44°C, Presented as Burn Temperature Limit in Figure.

In addition to the tests that exposed the fabric/skin simulant sensor system to 10 kW/m^2, Macor RPP tests were conducted using the cone heater on fabrics with moisture added. The goal of these tests was to determine if the model could accurately predict the temperatures of the skin simulant from the wet material property information determined using the TPTF. The Southern Mills 8.5 oz/sq yd material was evaluated at 21 kWm^2 with 0.5 and 1.0 grams of water added per gram of fabric. The temperature dependent thermal properties for this material are presented in Table 20. The wet materials were exposed for a total of 30 seconds. The models of the Southern Mills material at both moisture contents assumed that the thermal properties of the clothing will remain equivalent to those presented in Table 20, predicted using the TPTF, and will not be altered by evaporation of the moisture during the test.

The temperature dependent thermal properties of the fabric with 1.0 grams of water added per gram of material were such that the Fourier number would become greater than 0.5 if the exposure time was greater than 20 seconds. This would lead to divergent results from the 1-D finite difference model of the fabric/Macor and the fabric/skin. The high temperatures at the exposed surface of the material caused this divergence. For this reason, the fabric/Macor model was set up with a maximum exposure time of 20 seconds. Figure 45 provides a comparison of the predicted temperatures versus the measured temperatures for the Southern Mills fabric with 1.0 grams of water per gram of fabric added.

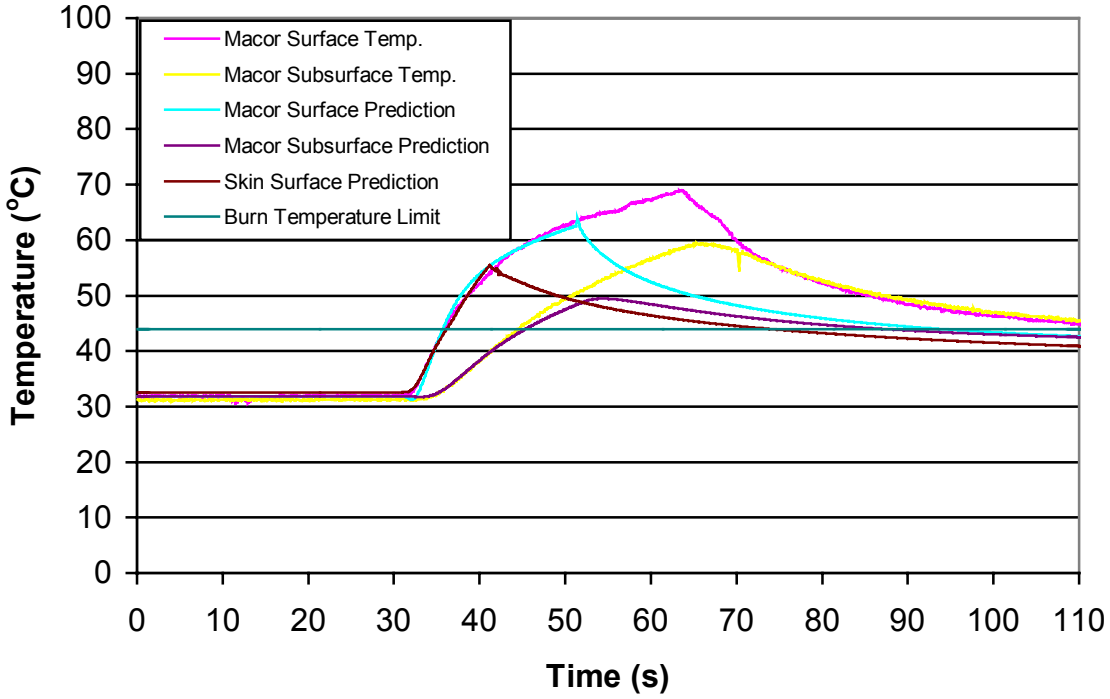

Figure 45: Macor RPP Exposure (21 kW/m^2) – Comparison of Measured Macor Surface and Subsurface Temperature against Values Predicted with 1-D Finite Difference Fabric/Macor Model for Cone Exposure of Southern Mills 8.5 oz/sq yd with 1.0 Grams of Water per Gram Fabric. Due to Temperature Dependent Thermal Properties of Wet Clothing and Restriction on the Fourier Number in this Analysis, the Model Only Provided Accurate Predictions for First 20 Seconds of Heating, After which the Results Began to Diverge due to High Temperatures of Clothing Surface. Skin Surface Temperature from 1-D Finite Difference Fabric/Skin Model also included. Burn Damage Will Occur for All Skin Temperatures Greater than 44°C, Presented as Burn Temperature Limit in Figure.

The slope and path of the temperature curves for the 1-D Macor model during the cooling stages of these tests are similar to the measured temperature data, suggesting a reasonably accurate temperature prediction. The linear thermal properties of the material with 0.5 grams of water decreased as the temperature increased (Table 20). As this property was extrapolated to higher temperatures, the value would eventually become negative. This problem was counteracted in the model by assuming a minimum value of 1.0 x 10^6 J/m^3-K for the volumetric heat capacity. This minimum level was chosen arbitrarily, as estimates of the actual minimum volumetric heat capacity were not available. Figure 46 provides a comparison of the predicted and measured temperatures from one of the Southern Mills 8.5 oz/sq yd tests where 0.5 grams of water per gram of fabric was added to the material.

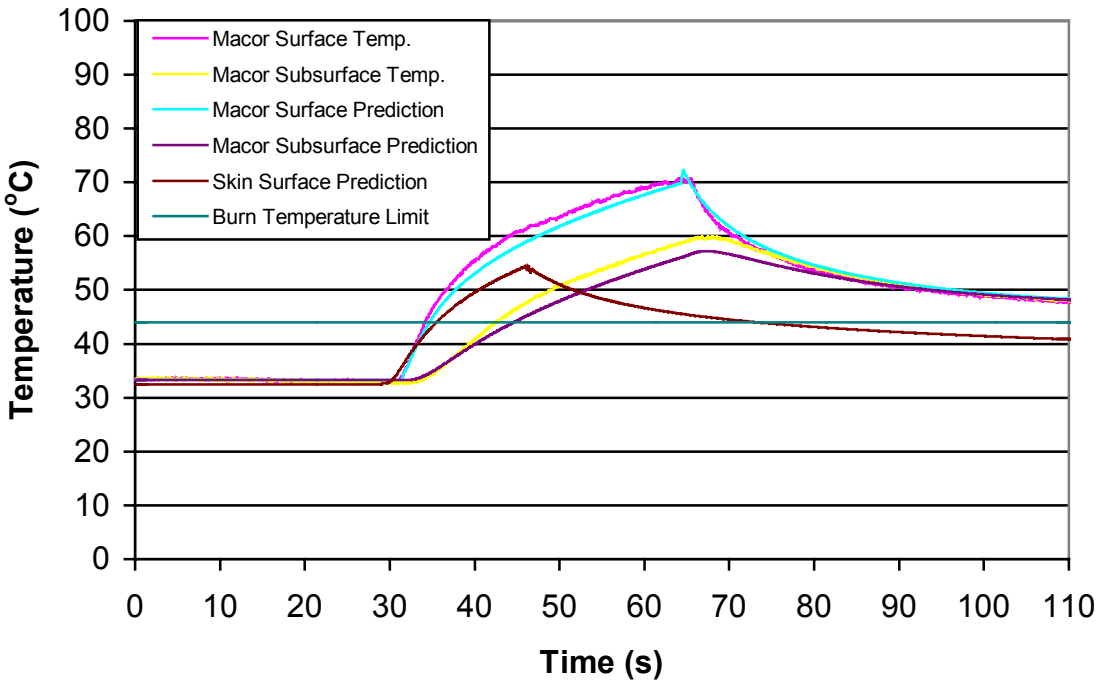

Figure 46: Macor RPP Exposure (21 kW/m^2) – Comparison of Measured Macor Surface and Subsurface Temperatures against Values Predicted with 1-D Finite Difference Fabric/Macor Model for Cone Exposure of Southern Mills 8.5 oz/sq yd with 0.5 Grams Water per Gram Fabric. Skin Surface Temperature from 1-D Finite Difference Fabric/Skin Model also included. Burn Damage Will Occur for All Skin Temperatures Greater than 44°C, Presented as Burn Temperature Limit in Figure.

As expected, the temperature predictions for the wet materials were not as accurate as those for the dry materials. Table 30 provides a summary of the model predictions for the Southern Mills 8.5 oz/sq yd material dry, and with 0.5 and 1.0 grams of water per gram of fabric added.

Table 30: Moisture Effect on Macor RPP Results. Residuals Not Available for Test with 1.0 Grams Water/Gram Fabric Added as Different Exposure Time Used in Test and 1-D Finite Difference Model of Clothing/Macor

Test Condition	Interfacial Conductance (h_i – W/m^2-K)	Time to Second Degree Burn (s)	Residuals (^{o}C)
Dry	403	9.1	0.032
0.5 grams water/gram fabric	392	7.0	0.078
1.0 grams water/gram fabric	707	10.2	Not Applicable

The addition of 0.5 grams of water per gram of fabric lessened the protective performance of the fabric, decreasing the time to second degree burn by nominally 23%. This difference in the time to 2nd degree burn may be due to the higher thermal conductivity of the wet material, which transmits more heat to the surface of the Macor, and consequently the skin. When an additional 0.5 grams of water per gram of material was added, the time predictions increased above those for dry fabrics. This change may be due to the evaporative cooling of the water at the fabric surface, which offsets the higher thermal conductivity of the wet material.

Ensemble Evaluations

In addition to the single layer clothing evaluations completed with the Macor skin simulant, a series of ensembles were evaluated. These tests were conducted using the cone calorimeter, set to provide an incident flux of 21 kW/m^2 to the ensembles. Each of the ensembles utilized the same type of moisture barrier and thermal liner. Ensembles utilizing the Nomex 7.5 oz/sq yd and the PBI 7.5 oz/sq yd were evaluated at this exposure level.

The 1-D finite difference models developed to predict the temperature of the Macor and skin when protected with a single layer of fabric was unable to accurately predict the temperature

response when protected by the full ensemble. The model would predict accurate values for the heating stage, but would not predict accurate values during the cooling stages.

To provide a calculation method for the Macor skin simulant sensor that could be used to predict the time to 2nd degree burn for the ensemble evaluations, an alternative method, originally presented in Section 3.2.2, utilizing the heat flux calculation results from Diller's Algorithm (Equation 6) was re-evaluated. This method, hereafter referred to as the Macor Heat Flux Method, assumes that the heat flux calculated by Diller's Algorithm during the cooling stage of the test can be approximated linearly, and that the slope of this curve will be identical no matter when the heat source was removed. Therefore, if the test was run for 30 seconds, one could use Equation 6 to calculate the heat flux curve. Using this curve, a linear approximation is made for the heat flux during the cooling stage of the test. The slope of this curve is then used to simulate the heat flux after the heat source is removed in a modeled exposure. Therefore, if the heat source in the model is removed 10 seconds into the exposure, the heat flux to the surface of the Macor after this point is approximated using the heat flux slope from the cooling stage of the test data.

This method requires accurate knowledge regarding the time when the heat source is removed during the actual test in order to assess the time between when the incident flux stops and when the skin simulant actually begins to cool. The development of this method also assumes that this delay time will be equivalent regardless of when the heat source is removed. As the 1-D finite difference fabric/Macor model can accurately predict the temperature response for the stand alone fabrics, this time delay can be determined directly from the model. However, this delay time must be estimated based upon the exposure time and the measured temperatures during the ensemble evaluations.

This method was applied to the Nomex 7.5 oz/sq yd, Macor RPP tests conducted with the cone heater to provide a comparison of the results with those from the 1-D Model Method. Instead of

modeling the heat flow through the clothing, and the interaction of the clothing and the Macor or skin, this method determines the heat flux at the Macor surface and directly inputs this information into the finite difference model of the Macor or the skin. Figure 47 compares the temperature predictions from a 1-D finite difference model of the Macor using the heat flux calculated by Diller's Algorithm as the net flux to the Macor surface, to those measured during a test of the Nomex 7.5 oz/sq yd of material. The 1-D finite difference Macor model provided reasonably accurate predictions of the temperatures measured with the Macor surface and subsurface thermocouples. The predicted values were slightly lower than the measured temperatures. The temperature residuals for both thermocouples, calculated using Equation 27, were 0.031°C, 0.018°C, and 0.021°C for the three Nomex 7.5 oz/sq yd tests.

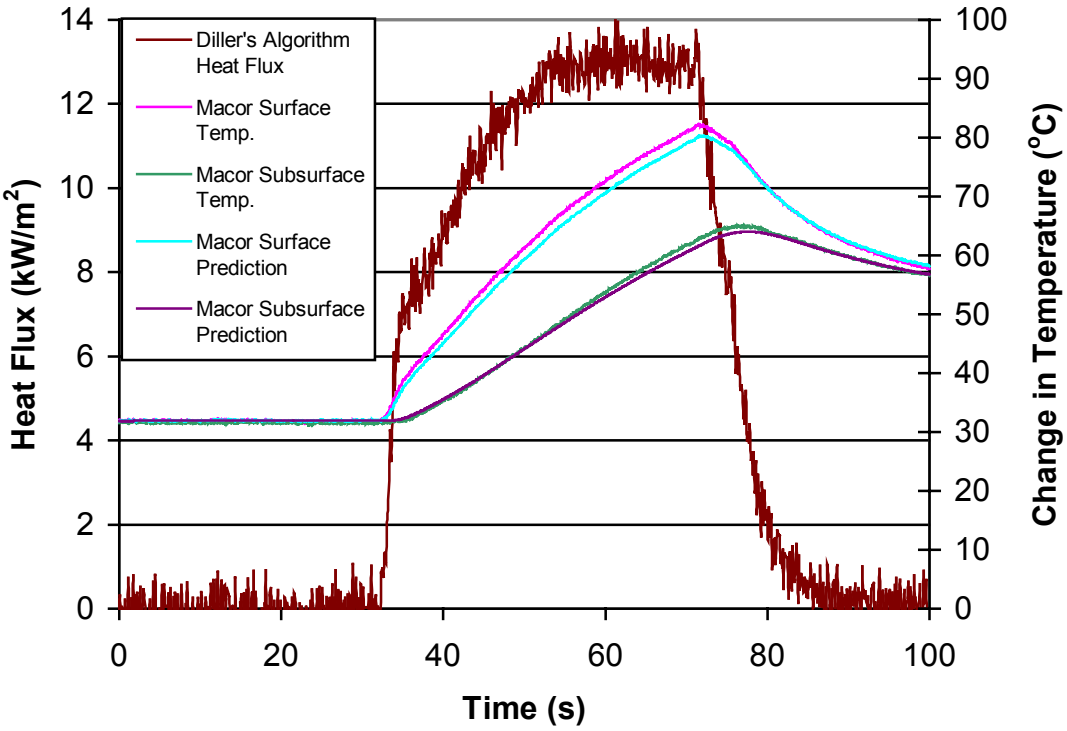

Figure 47: Macor RPP Exposure (21 kW/m^2) – Comparison of Measured Temperatures against Values Calculated Using 1-D Finite Difference Model of Macor with Heat Flux Calculated from Diller's Algorithm used as Input for Evaluation of Nomex 7.5 oz/sq yd.

The average time between when the exposure from the cone heater stopped, and when the system began to cool was 1.1 seconds for the three tests on the Nomex 7.5 oz/sq yd. This delay

time was assessed using the fabric/Macor 1-D finite difference model. The average slope of the cooling portion of the three heat flux curves, was –1.3 kW/m^2. This slope was determined over a five second span nominally one second after the system began to cool (after approximately 70 seconds in Figure 47). This information was used to construct a new heat flux curve to be used as input in the 1-D finite difference Macor model. The actual heat flux curve during the cooling stage is predominantly linear; however, it levels out at the end and slowly tapers down to zero. In addition, when the temperature of the clothing directly against the skin drops below the temperature of the skin, the net heat flux at the skin surface would actually become a negative value. These affects were ignored in the this burn time calculation method, and the heat flux was assumed to decrease linearly to zero, staying at this level for the remainder of the model duration.

Diller's Algorithm was used to calculate the heat flux before the system began to cool. When the system began to cool, nominally 1.1 seconds after the heat source was removed, the heat flux was decreased linearly with a slope of –1.3 kW/m^2, until it reached zero, where it was held constant. The heat flux determined by the 1-D Finite Difference fabric/Macor model for the Nomex 7.5 oz/sq yd tests during the cooling portion actually became a negative value approximately 40 second after the removal of the incident flux. However this negative heat flux value was low (on the order of –0.1 kW/m^2) and this effect was ignored in this analysis.

The adjusted heat flux curve was input into the 1-D finite difference model of the Macor skin simulant. The temperature residuals at the Macor surface, calculated using Equation 27, were determined to be 0.03^oC, 0.018^oC, and 0.21^oC for the three Nomex 7.5 oz/sq yd tests. These values are nearly identical to the temperature residuals determined from the models using the Diller Algorithm heat flux values throughout. Figure 48 presents the revised temperature predictions, developed using the assumptions regarding the heat flux levels following the removal of the exposure source. These predictions are based upon the same test data as Figure 47.

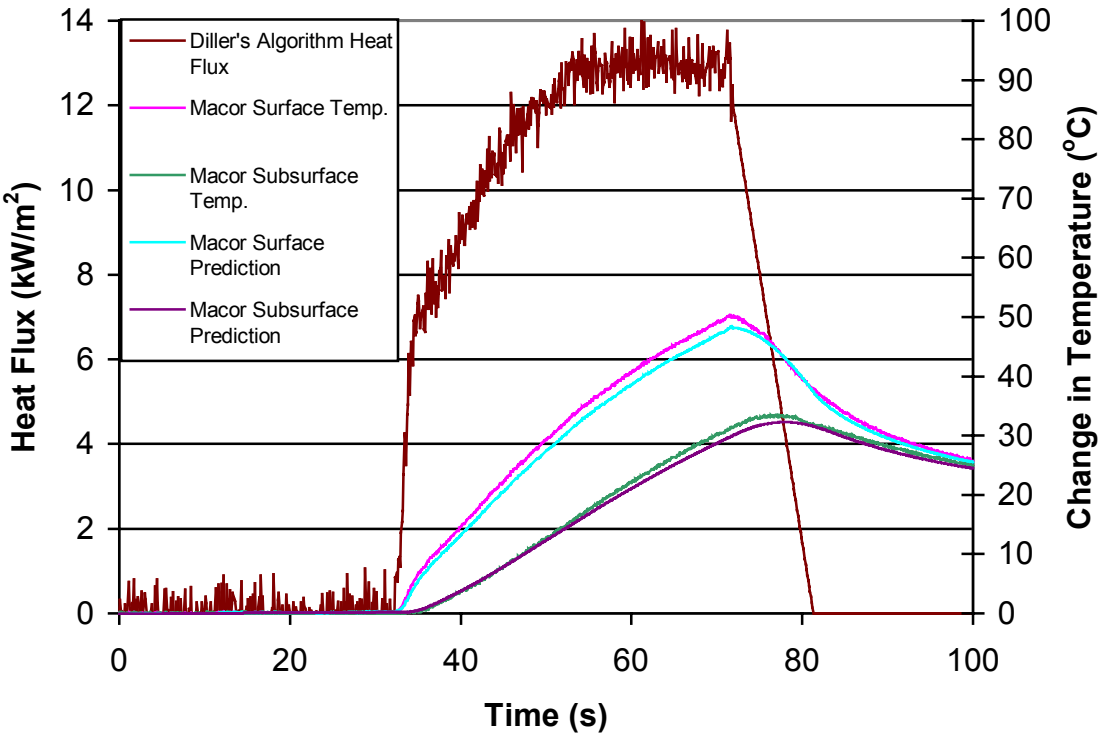

Figure 48: Macor RPP Exposure (21 kW/m^2) – Comparison of Measured Temperatures against Values Calculated Using 1-D Model of Macor with Heat Flux from Diller's Algorithm used at Input during Macor Heater and Assumed Linear Decrease in Heat Flux to 0 kW/m^2 used during Macor Cooling for Evaluation of Nomex 7.5 oz/sq yd.

The temperature predictions for the two figures presented above are nearly identical. This calculation technique was used to estimate the time to second degree burn using similar assumptions and a 1-D finite difference model of skin to predict the time to 2nd degree burn. If the skin were exposed to the same flux levels as those in Figure 48, the temperature rise would be slightly higher than that of the Macor, due to the differences in the thermal properties between the two. Figure 49 presents the differences in the temperature rise for the two materials. To predict the time to 2nd degree burn using this method, the exposure duration was decreased for the 1-D finite difference model of the skin until Henriques Integral damage function, Ω, increased above 1.0.

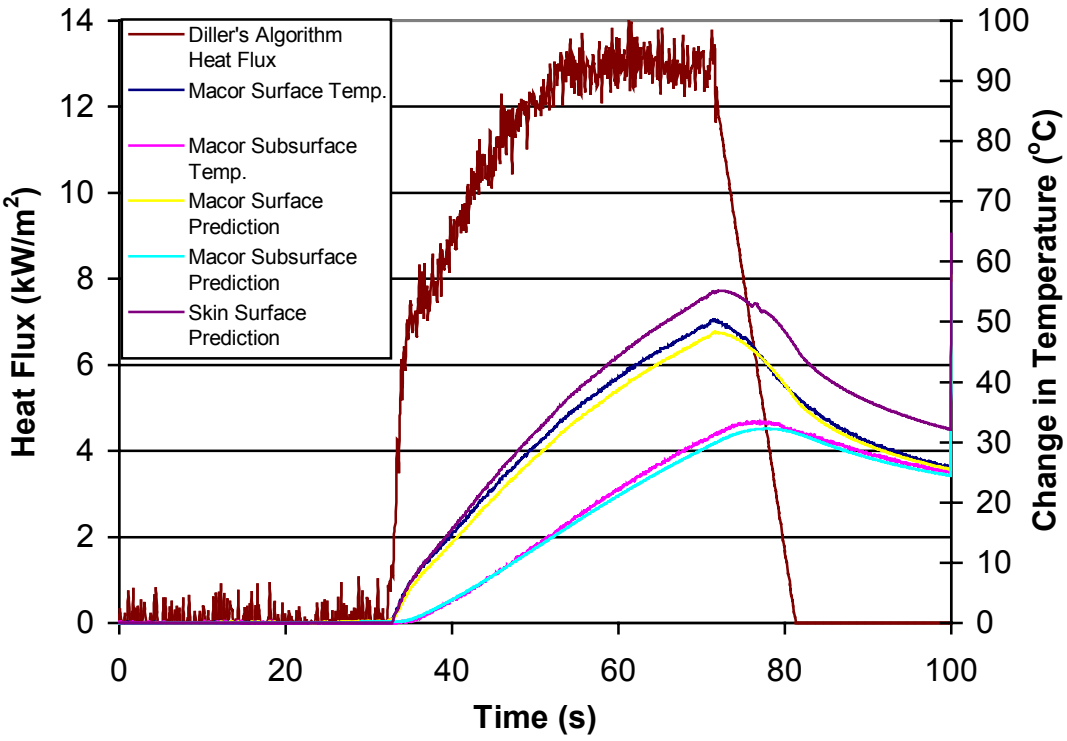

Figure 49: Macor RPP Exposure (21 kW/m^2) – Comparison of Predicted Skin Temperature Rise against Macor Temperature Rise with Heat Flux from Diller's Algorithm used at Input during Macor Heater and Assumed Linear Decrease in Heat Flux to a Value of 0 kW/m^2 used during Macor Cooling in 1-D models During Evaluation of Nomex 7.5 oz/sq yd.

The time to second degree burn for the two Macor calculation methods are presented in Table 31. The average values for the two calculation methods for the Nomex 7.5 oz/sq yd fabric tests differ by nominally 1 second. This difference is most likely due to the increased level of uncertainty in the Macor Heat Flux Methods regarding the delay time and the heat flux curve assumptions.

Table 31: Macor Calculation Method – Burn Prediction Time Comparison. 1-D Model Method Models the Heat Transfer Through the Clothing Using 1-D Finite Difference Models of Fabric/Macor and Fabric/Skin. The Macor Heat Flux Method Calculates the Heat Flux at the Macor Surface, and Inputs This Information Directly Into a 1-D Finite Difference Skin Model.

Material	Prediction Method	Test 1 (s)	Test 2 (s)	Test 3 (s)	Average (s)
Nomex 7.5 oz/sq yd	1-D Model Method	8.4	8.4	8.2	8.3
	Macor Heat Flux Method	9.8	9.5	8.6	9.3
PBI 7.5 oz/sq yd	1-D Model Method	8.7	8.9	8.7	8.8
	Macor Heat Flux Method	9.9	11	9.8	10.2

The Macor Heat Flux Method relies upon the heat flux predictions at the surface of the skin simulant to predict the time to 2nd degree burn. It can be used with any test setup and material, including those with a space between the fabric and the sensor or those evaluating ensembles. This method was also applied to the PBI 7.5 oz/sq yd RPP test data to confirm it predictive capabilities. This material also had a delay time of 1.1 seconds between the time when the heat source was removed and when the Macor began to cool. This delay time was assessed using the fabric/Macor 1-D finite difference model. The slope of the heat flux curve during the cooling stage was estimated to be –1.4 kW/m^2. The burn prediction information for this fabric is also included in Table 31. The predictions using this method differed from those of the 1-D Model Method for the PBI 7.5 oz/sq yd material by slightly more than the predictions for the Nomex 7.5 oz/sq yd fabric.

The main drawback for this method is that the time between when the heat source is removed and when the skin simulant actually begins to cool must be assumed or accurately assessed in order to obtain accurate burn time predictions. The 1-D finite difference fabric/Macor models of the single fabric layers were used to assess the magnitude of the delay time in these tests. For the Nomex and PBI materials discussed above, this time was 1.1 seconds. Differences in the delay time can be expected if a space is incorporated between the fabric and the sensor. A larger period of time is anticipated when ensembles are evaluated, due to the thicker overall material.

There were a series of ensemble tests completed using the Macor skin simulant sensor. The 1-D modeling method described earlier in this section was developed to determine the time to 2nd degree burn when evaluating outer shell or stand-alone fabric materials, and did not accurately predict the temperature history of the Macor skin simulant during these tests. The complexity of the ensembles, which consisted of three separate layers of different types of clothing, prevented the use of the finite difference models to predict the heat transfer through the garment. The Macor Heat Flux Method was applied to these tests to determine the time to second degree burn.

The exposure for each ensemble test utilizing the Nomex 7.5 oz/sq yd material as the outer shell material began 30 seconds into the data collection. The temperature at the Macor surface began to rise approximately 6 seconds later. The exposure varied for each test; 30 second exposure in Test 1, 60 second exposure in Test 2, and 45 Second Exposure in Test 3. The average period of time between when the heat flux source was removed and when the heat flux calculated at the Macor surface began to decrease was estimated to be 8 seconds. This value was used in both the Macor and the skin models. The average slope of the heat flux curve during the cooling stage of the test was approximated as –0.12 kW/m^2. This information was incorporated into a model similar to that used to assess the Nomex and PBI fabrics, described above. Figure 50 presents the measured temperatures and calculated heat flux at the Macor skin simulant surface during a 45 second exposure of the Nomex 7.5 oz/sq yd ensemble. The temperature rise and heat flux levels are much lower than those achieved during the testing of the outer shell materials.

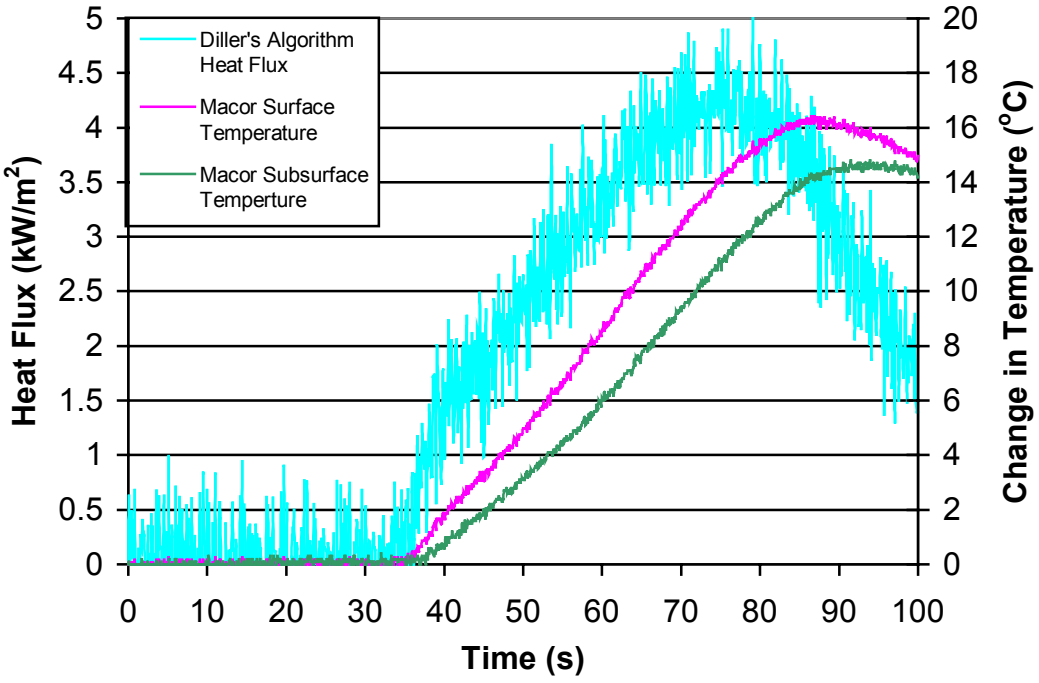

Figure 50: Macor RPP Exposure (21 kW/m^2) – Temperature Rise and Heat Flux During Exposure of Nomex 7.5 oz/sq yd Outer Shell, Crosstech Moisture Barrier, and Aralite Thermal Liner Ensemble to Cone Heater for 45 Seconds. Exposure Begins at 30 Seconds.

Figure 51 presents a comparison between the measured temperatures and those predicted using the Macor Heat Flux Method. The predicted temperatures closely track the Macor surface temperature, but underestimate the subsurface temperatures by up to 3°C. This method was used to predict the time to 2nd degree burn for the ensembles evaluated using the Macor skin simulant. The results of these evaluations are presented in Table 32.

The ensemble tests in which the PBI 7.5 oz/sq yd fabric was the outer shell material were all exposed to the cone heater for over one minute. To determine the delay time and the slope of the heat flux curve during cooling, the Macor surface temperatures were input into Diller's Algorithm starting at 30 seconds into the test, before the exposure began. The time period between when the heat flux source was removed, and when the Macor began to cool was approximately 10 seconds for these tests, which is 2 seconds longer than the delay time for the

Nomex 7.5 oz/sq yd ensembles. The average slope of the heat flux curve during the cooling portion of the PBI 7.5 oz/sq yd ensemble evaluations was nominally –0.13 kW/m^2.

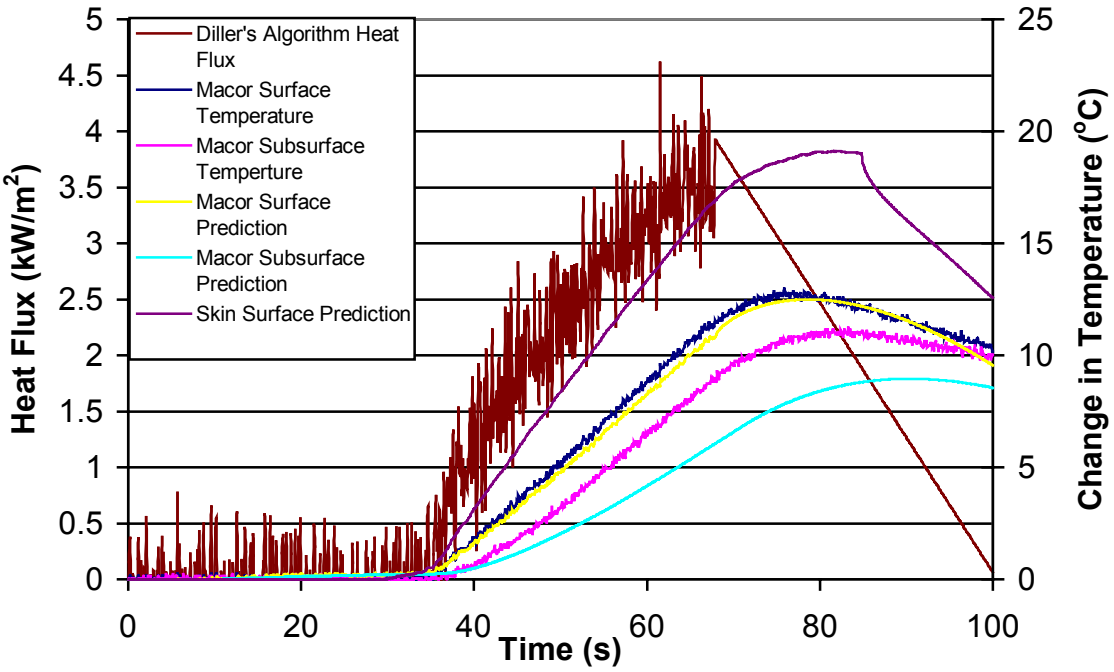

Figure 51: Macor RPP Exposure (21 kW/m^2) – Comparison of Measured Temperature Rise and Temperatures Predicted for Macor Surface and Subsurface Thermocouples During Evaluation of Nomex 7.5 oz/sq yd Outer Shell, Crosstech Moisture Barrier, and Aralite Thermal Liner Ensemble Exposed to Cone Heater for 30 Seconds. Exposure Begins at 30 Seconds. Prediction of Skin Surface and Macor Temperature Rise Using Heat Flux Method. Heat Flux During Heating Calculated Using Diller's Algorithm. Linear Decrease in Heat Flux During Cooling Assumed, with Eight Second Delay Between Removal of Heat Source and Beginning of Heat Flux Decrease.

Table 32: Macor Heat Flux Method – Time to 2nd Degree Burn Predictions for Dry Ensembles Exposed to 21 kW/m^2 from Cone Heater.

Ensemble Setup	Test 1 (s)	Test 2 (s)	Test 3 (s)	Average
Nomex 7.5 oz/sq yd Outer Shell Material	30.4	28.9	30.6	30
PBI 7.5 oz/sq yd Outer Shell Material	28.1	31.5	31.3	30.3

The time to 2nd degree burn predictions for the two ensembles are nearly identical, given the uncertainty involved in this analysis. This uncertainty includes the actual time delay between the removal of the heat source and the onset of cooling of the Macor, the actual slope of the cooling portion of the heat flux curve, and the assumption that this information will be the same

regardless of when the heat flux source is removed. Each of the Nomex ensembles was exposed for a different duration. The delay time and the slope of the cooling portion of the heat flux curve determined for this analysis were similar for each exposure. The heat flux curves, calculated using Diller's Algorithm (Equation 6) are presented in Figure 52. The slope of the heat flux curve during the cooling portion of the test, as well as the delay time is similar for each exposure duration.

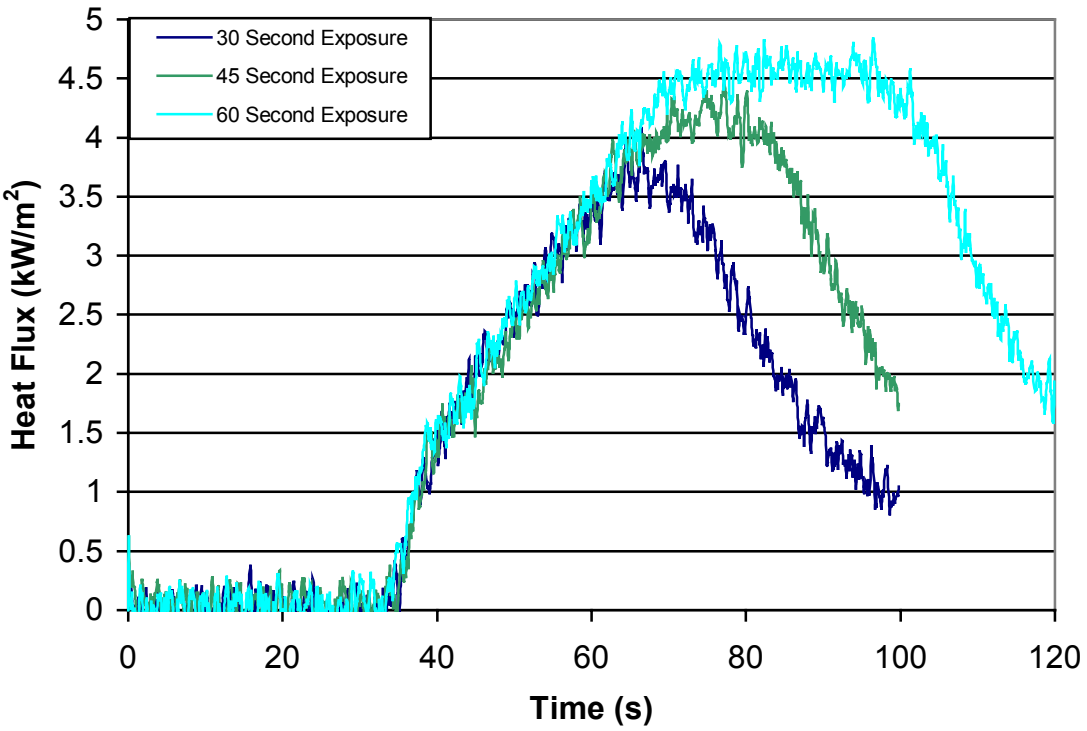

Figure 52: Macor RPP Exposure (21 kW/m^2) – Comparison of the Heat Flux at the Macor Skin Simulant Surface, Calculated Using Diller's Algorithm (Equation 6), for Three Exposure Durations of Nomex 7.5 oz/sq yd Outer Shell, Crosstech Moisture Barrier, and Aralite Thermal Liner Ensemble Exposed with Cone Heater.

In addition to the dry evaluations, the ensembles with the Nomex 7.5 oz/sq yd fabric as the outer shell material were also evaluated with 1.0 grams of water per gram of Aralite added to the thermal liner. The water was added to the thermal liner to simulate the effects of perspiration from the fire fighter during the actual use of the ensemble. The temperature and heat flux data were analyzed in a manner similar to the dry ensembles to predict the time to 2nd degree burn. The temperature and heat flux levels at the surface of the Macor increased above the

temperatures and heat flux levels from the dry ensemble evaluations. Figure 53 presents a comparison of the heat flux and temperature rise for two longer duration ensemble evaluations, where one of the ensembles had a thermal liner with 1.0 grams of water per gram of Aralite added, while the other was evaluated with no water added to the thermal liner.

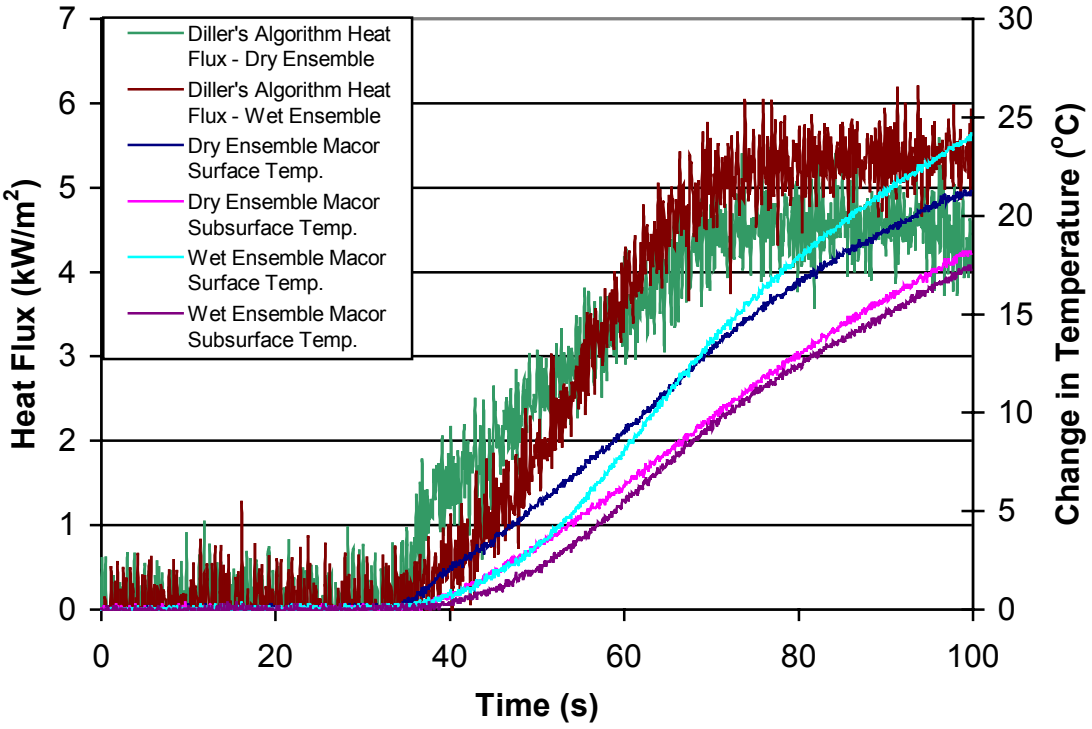

Figure 53: Macor RPP Exposure (21 kW/m^2) – Comparison of Temperature Rise and Heat Flux Levels at the Surface of the Macor Skin Simulant During Exposure of Nomex 7.5 oz/sq yd Outer Shell, Crosstech Moisture Barrier, and Aralite Thermal Liner Ensembles, with 1.0 Grams of Water Per Gram of Aralite Added to the Thermal Liner of One of the Ensembles. Ensembles Exposed to 21 kW/m^2 from Cone Heater for More than 60 Seconds.

The temperature and heat flux curves for the two ensembles presented in Figure 53 are similar in magnitude, but they differ slightly in shape. The initial response of the Macor skin simulant in the ensemble test where 1.0 grams of water per gram of Aralite was added to the thermal liner was slower than the case with the dry ensemble. This slow response was most likely caused by water condensing on the surface of the Macor skin simulant at the beginning of the exposure. However, as the exposure continued, the higher thermal conductivity of the wet ensemble

increased the heat flow to the skin, overcoming this effect and eventually increasing the Macor surface temperature and heat flux above the levels attained during the dry ensemble evaluation.

The time delay between the removal of the heat source and the onset of cooling of the Macor skin simulant, and the value for the negative slope of the heat flux curve during the cooling stage, were determine through the use of Diller's Algorithm (Equation 6). Due to the long duration tests, this algorithm was applied after the initial 25 seconds of the test, before the ensemble was exposed to the heat source. The actual exposure begins 30 seconds into the test, with the Macor surface temperature responding nominally eight seconds later. The wire connection for Macor surface thermocouple disconnected from the connection terminal during Test 1 of the wet ensemble. Additionally, during Test 3, the temperature measurements for the Macor surface and subsurface thermocouples began to fluctuate and diverge as the skin simulant sensor was removed from the heat source, providing unusable results for the cooling stage of the test. Test 2, however, produced results similar in magnitude to the dry ensemble evaluations, and was used to determine the slope of the heat flux curve during the cooling stage of the test and the delay time between the removal of the heat source and the onset of cooling of the Macor skin simulant. The measured temperature rise and the calculated heat flux rise for this test are presented in Figure 54.

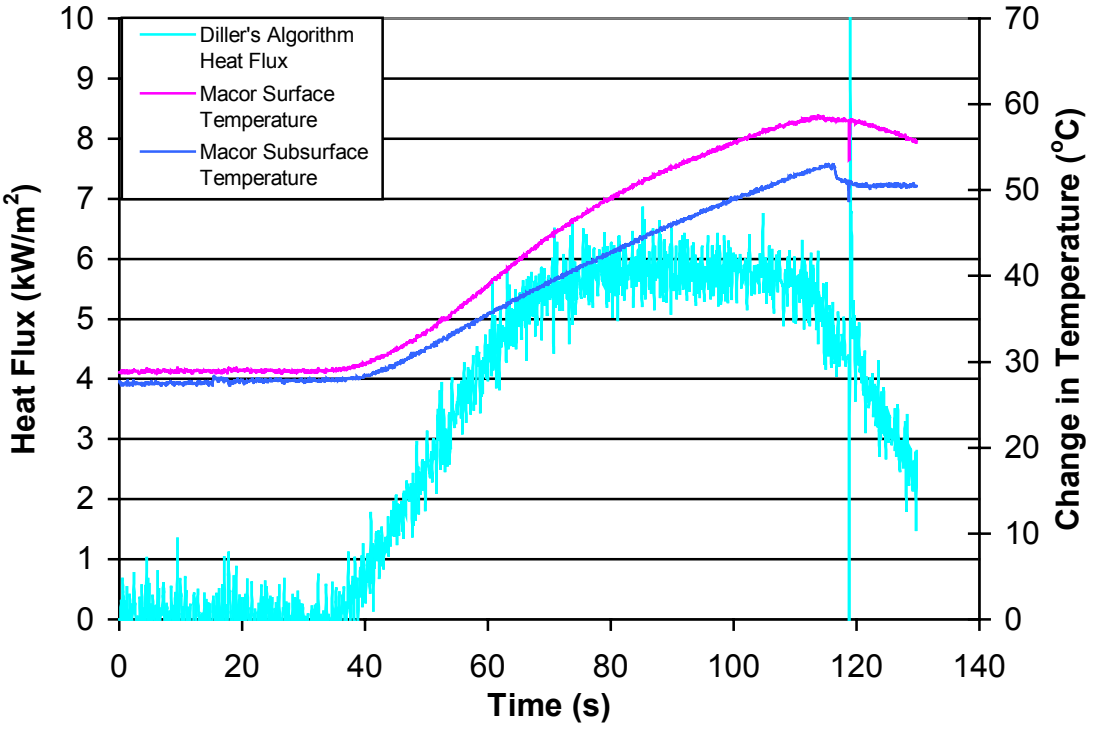

Figure 54: Macor RPP Exposure (21 kW/m^2) – Temperature Rise and Heat Flux During Exposure of Nomex 7.5 oz/sq yd Outer Shell, Crosstech Moisture Barrier, and Aralite Thermal Liner Ensembles, with 1.0 Grams of Water per Gram of Aralite Added to Thermal Liner. Ensemble Exposed to 21 kW/m^2 from Cone Heater for 75 Seconds.

The ensemble was exposed for a total of 75 seconds, with a 30 second pre-exposure time The temperature and heat flux levels in this wet ensemble evaluation do not begin to decrease for an additional 10 seconds. The slope of the heat flux curve during cooling was essentially linear, with the exception of one large fluctuation in the data around 119 seconds (Figure 54). The slope of this curve during this cooling stage is approximately –0.15 kW/m^2. This slope and delay time were incorporated into the Macor Heat Flux Method calculations for the time to 2nd degree burn for the three wet ensemble tests. Figure 55 presents a comparison between the measured temperatures during a wet ensemble exposure and those predicted using the Macor Heat Flux Method with the 10 second delay time and heat flux cooling slope of –0.15 kW/m^2.

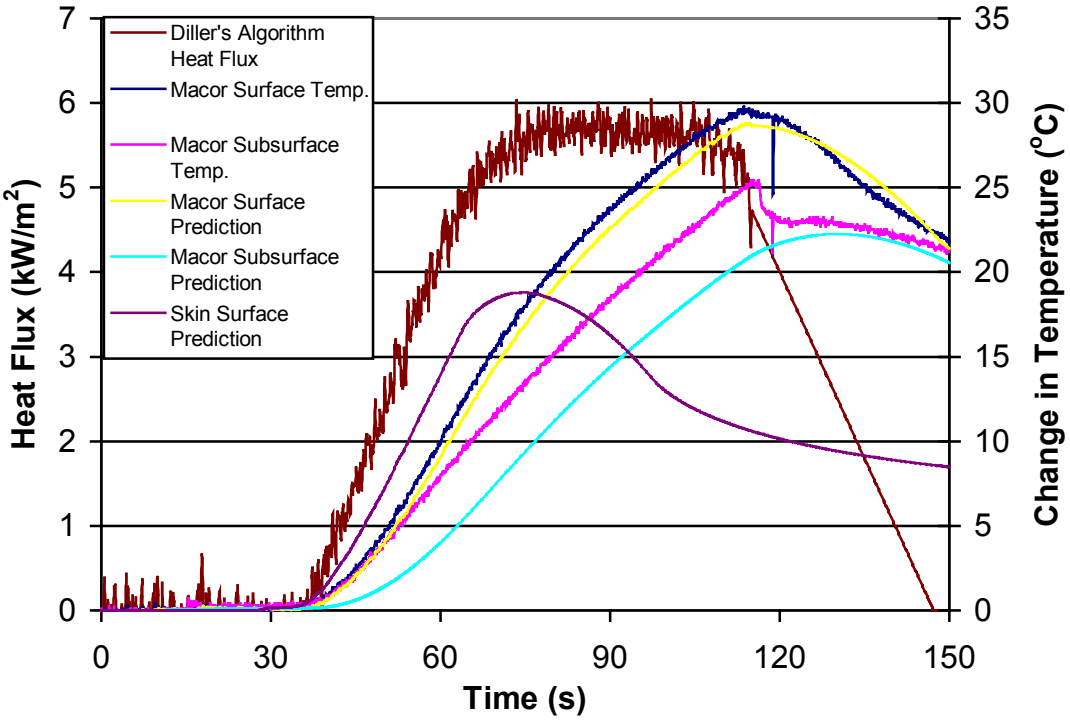

Figure 55: Macor RPP Exposure (21 kW/m^2) – Comparison of Macor Surface and Subsurface Temperature Rise During Exposure of Nomex 7.5 oz/sq yd Outer Shell, Crosstech Moisture Barrier, and Aralite Thermal Liner Ensemble with 1 Gram of Water per Gram of Aralite Added to Thermal Liner Using Macor Heat Flux Method. Heat Flux During Heating Calculated Using Diller's Algorithm (Equation 6). Linear Decrease in Heat Flux with Slope of –0.15 kW/m^2 Assumed During Cooling Period. Ten Second Delay Between Removal of Heat Source and Beginning of Heat Flux Decrease. Macor Temperature Predictions Based upon 75 Second Exposure. Skin Temperature Predictions Based on 26 Second Exposure.

As was the case with the dry ensembles, the Macor Heat Flux Method under-predicts the temperature rise at the Macor subsurface thermocouple, while providing very accurate predictions for the Macor surface temperature. After confirming that this method could accurately predict the surface temperature of the Macor skin simulant throughout the 150 second exposure and cooling period, this method was applied to the other wet ensemble tests to determine the time to 2nd degree burn. The time to 2nd degree burn predictions for the wet and dry ensembles is presented in Table 33.

Table 33: Macor Heat Flux Method – Burn Prediction Comparison for Wet and Dry Ensembles Utilizing Same Outer Shell Material. Wet Ensemble Evaluated with 1.0 Grams of Water per Gram of Aralite Added to Thermal Liner.

Nomex 7.5 oz/sq yd Ensemble Tests	Test 1 (s)	Test 2 (s)	Test 3 (s)	Average (s)
Dry Thermal Liner	30.4	28.7	30.6	29.9
Wet Thermal Liner	No Heat Flux Data Available due to Failed Macor Surface Thermocouple Connection	24.2	27.6	25.9

Due to the failed connection for the surface thermocouple in Test 1 of the wet ensembles, there was no heat flux information available to calculate the time to 2nd degree burn. The times predicted for the other two tests with water added to the thermal liner are shorter than those for the dry ensembles. Much of this difference is due to the longer delay time between the removal of the heat source and the point where the heat flux curve begins to decrease. In addition to the longer delay time, the heat flux rise at the Macor surface during the wet ensemble test was higher than during the dry ensemble tests. So despite having a larger magnitude for the negative slope of the heat flux during the cooling stage (-0.12 kW/m^2 for the dry ensembles, -0.15 kW/m^2 for the wet ensembles), the burn time in the wet ensemble evaluations was less than during the dry evaluations.

Burn Damage Assessment

In the determination of the time to 2nd degree burn, both of the Macor calculation methods determine the value for Henriques Burn Integral at each time step. This solution method allows for the determination of the percentage of damage caused during different phases of the test. For example, the amount of damage caused during the heating stage can be determined, and compared against the amount of damage caused during cooling. For bare skin, as much as 10% of the damage can occur during skin cooling at low exposure levels. For higher exposure levels, as much as 35% of the damage may be caused during skin cooling.[7]

In theory, when a layer of clothing is protecting the skin, the amount of damage occurring after the removal of the heat source should be greater than that of bare skin. The clothing layer will protect the skin during the heating stage, preventing much of the heat flux from reaching the skin

surface. The temperatures of the protective clothing will increase much higher than the temperature of the skin. This effect is presented in Figure 24, where a thermocouple was mounted on the exposed surface of the clothing during one of the Macor RPP tests. The temperature rise of the clothing in comparison to the skin would be similar to that of the clothing in comparison with the Macor. When the heat source is removed, the clothing begins to cool. However, it is still conducting heat to the skin as it remains at a higher temperature than the skin.

The 1-D finite difference models for the fabric/Macor and the fabric/skin are set up to allow the time delay between the removal of the heat source and the beginning of skin cooling to be determined. This information is critical when using the Macor Heat Flux Method to determine the time to 2nd degree burn. The time delay between when the heat flux source was removed and when the surface temperature of the skin began to decrease in the 1-D finite difference fabric/skin models for the outer shell material, exposed to 21 kW/m^2 for between 8 and 9 seconds, was nominally 2 seconds. This value is nearly 25% of the overall exposure time. During this delay time, the temperature of the skin continues to increase, as the energy stored in the clothing is conducted to the skin.

When the skin does finally begin to cool, some period of time following the removal of the heat source, it does not cool at the same rate as it would if left exposed in open air. The clothing layer, which is still at an elevated temperature, restricts the flow of heat away from the skin, slowing the cooling process. This affect will increase the level of damage caused to the skin during the cooling period.

The Henriques Burn Integral data for Nomex 7.5 oz/sq yd and PBI 7.5 oz/sq yd fabric materials was analyzed to determine the amount of damage caused before and after the heat flux source was removed. Figure 56 presents a curve of the basal layer temperature for one of the PBI 7.5 oz/sq yd exposures. Several points of interest are marked on the chart, including the beginning

of the exposure, the end of the exposure, when the skin begins to cool, and when the thermal damage to the skin actual stops.

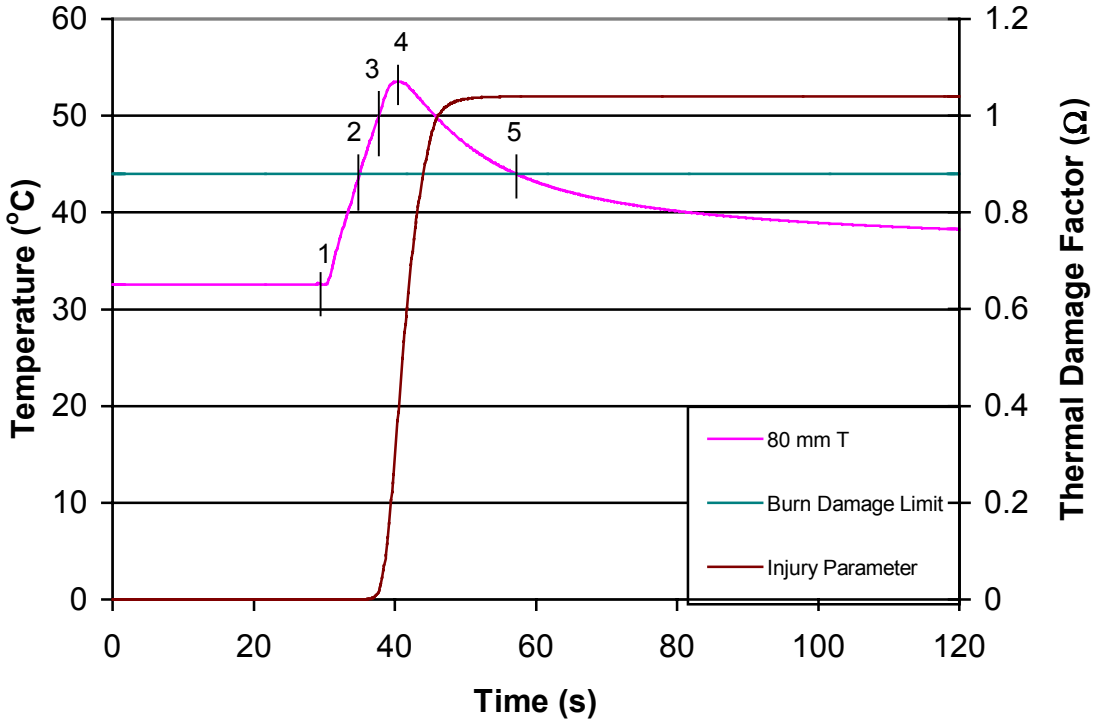

Figure 56: Basal Layer Temperature and Henriques Damage Integral Function During Evaluation of PBI 7.5 oz/sq yd, Points of Interest on Curve in Order from Left to Right

1 – Exposure Begins (29 Seconds)
2 – Basal Layer Temperature Rises Above 44°C (35.1 Seconds)
3 – Exposure Source Removed (37.7 Seconds)
4 – Skin Begins to Cool (40.3 Seconds)
5 – End of Damage to Skin (57.2 Seconds)

Figure 56 shows that very little of the damage actually occurs before the heat source is removed. The Henriques Damage Integral is a rate function equation, such that damage occurs at a higher rate the higher the basal temperature. The damage to the skin begins after its basal layer temperature increases above 44°C, nominally 35.1 seconds in Figure 56. The heat source is removed 2.6 seconds later. The basal layer temperature continues to rise for an additional 2.6 seconds, before cooling to temperatures below 44°C over a 16.9 second period. A breakdown for the amount of damage caused during the heating and post heating stages of the Macor RPP tests is presented in Table 34. Essentially all of the damage occurs after the removal of the heat

source. The Henriques burn integral can also be used to assess the time to pain. Pain will be felt when Ω equals 0.53.[7,11] This value for Ω will not be reached until after the heat source is removed, and the skin begins to cool. Consequently, by the time the wearer begins to feel pain, a 2nd degree burn is imminent unless the wearer can remove the clothing and immediately cool the skin. The time between when the wearer feels pain and when a 2nd degree burn will occur is between 5 and 10 seconds for the two outer shell materials analyzed.

Table 34: Values for Henriques Integral Damage Function, Ω, Through Each Stage of Heating and Cooling in Macor RPP Exposure of Nomex 7.5 oz/sq yd and PBI 7.5 oz/sq yd (2nd Degree Burn Occurs When Ω = 1)

Material and Test Number	Heating	Post Heating	
		Delay Between End of Heating and Start of Cooling	Cooling
Nomex 7.5 oz/sq yd – Test 1	0.016	0.35	1.01
Nomex 7.5 oz/sq yd – Test 2	0.016	0.34	1.01
Nomex 7.5 oz/sq yd – Test 3	0.015	0.35	1.02
PBI 7.5 oz/sq yd – Test 1	0.016	0.34	1.04
PBI 7.5 oz/sq yd – Test 2	0.017	0.34	1.00
PBI 7.5 oz/sq yd – Test 3	0016	0.34	1.04

This type of analysis was completed on the ensembles as well, using the Henriques Burn Damage Integral information from the Macor Heat Flux Method. Even more of the damage was caused during the post heating stage of the ensemble evaluations, as more energy was stored within the clothing during the exposure. For each of the ensembles evaluated with the Macor skin simulant, less than 1% of the thermal damage was caused during the actual heating stage, which lasted approximately 30 seconds for each ensemble.

4.2.3 SENSOR COMPARISON

The predictions for the times to 2nd degree burn from the Macor skin simulant are lower for each material evaluated than the predictions from the copper calorimeter. The Macor skin simulant has properties similar to those of skin, and the temperature rise during the RPP exposure is closer to that of skin than the copper calorimeter. Two different methods were used to calculate the 2nd degree burn time for the Macor skin simulant. The first utilized 1-D finite difference models of the fabric/Macor and the fabric/skin to model the heat transfer through the clothing

layer and into the Macor or the skin. The other calculated the heat flux at the Macor surface using Diller's Algorithm (Equation 6), and input this information directly into the 1-D finite difference model of the skin to predict the time to 2nd degree burn.

To provide direct comparison between the two sensors, two materials, Nomex 7.5 oz/sq yd and PBI 7.5 oz/sq yd, were evaluated with no space between the fabric and the copper calorimeter. This test configuration was the same as that used during the Macor skin simulant RPP evaluations.

Figure 57 compares the Macor skin simulant temperature rise to that of the copper calorimeter during tests of Nomex 7.5 oz/sq yd, exposed to 21 kW/m^2 with the cone heater with no space between the fabric and the sensors. The data from test 1 with both sensors are not included in this figure, as they either didn't begin at the same time as the other tests or exhibited slightly different temperature curves.

For the tests included, the initial temperature rise of the Macor is greater than that of copper calorimeter. However, after approximately 20 seconds, the curves cross and the copper calorimeter temperature rise become greater than that of the Macor. The heat flux at the surface of the Macor skin simulant, calculated using Diller's Algorithm (Equation 6) is also greater than the heat flux calculated at the surface of the copper calorimeter, (Equation 4). The heat flux at the sensor surface, calculated using the temperature rise data in Figure 57, is presented in Figure 58.

The primary difference in the heat flux curves takes place during the first 20 seconds of the exposure, when the temperature rise of the Macor is higher than that of the copper. This difference between the Macor skin simulant and the copper calorimeter temperature measurements may be caused by the semi-infinite behavior of the Macor, which will result in higher surface temperatures as the thermally thick slab is heated by conduction. This is different

than the thermally thin copper sensor, which acts as a slug calorimeter.[26] The temperature rise of the Macor skin simulant is measured at the surface, while the copper calorimeter is a volumetric temperature measurement.

The thermal properties of the Macor skin simulant are such that the temperature of actual skin would rise at a faster rate than the Macor, and consequently much faster than the copper calorimeter at the beginning of the test.

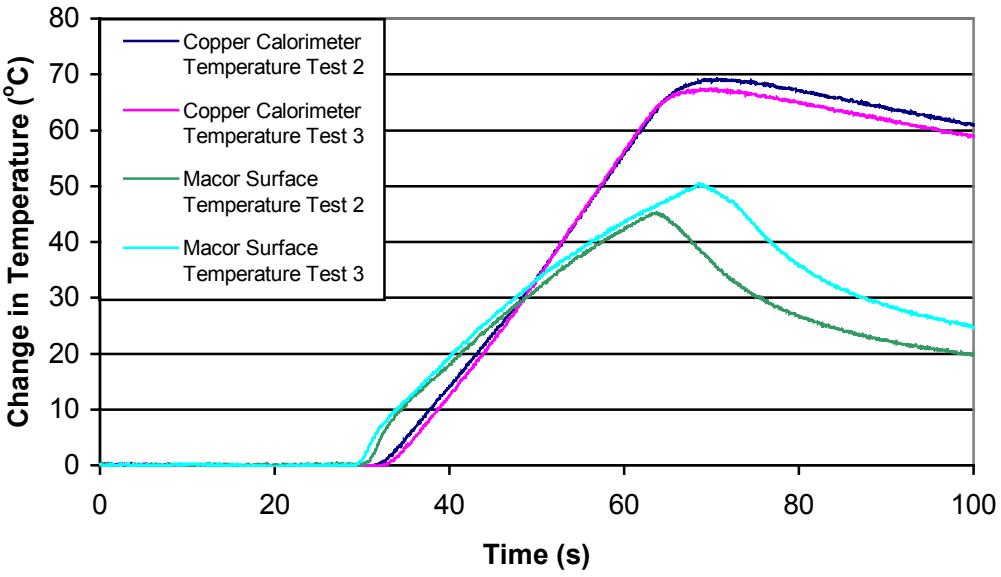

Figure 57: RPP Exposure (21 kW/m^2) – Comparison of the Temperature Rise at the Surface of the Copper Calorimeter and Macor Skin Simulant during Cone Heater Evaluations of Nomex 7.5 oz/sq yd.

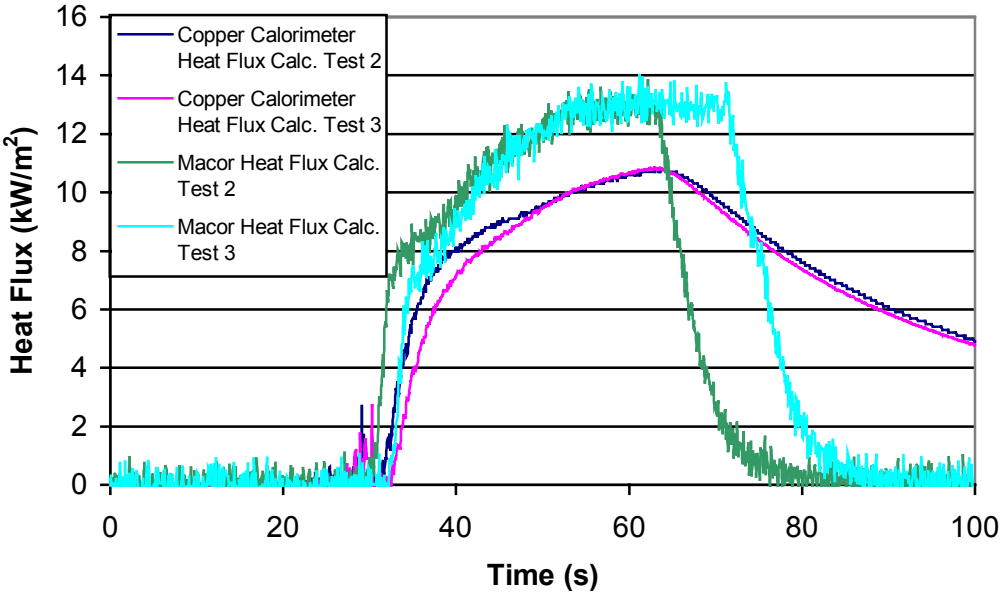

Figure 58: RPP Exposure (21 kW/m^2) – Comparison of the Heat Flux at the Surface of the Copper Calorimeter and Macor Skin Simulant during Cone Heater Evaluations of Nomex 7.5 oz/sq yd.

The initial method used to determine the time to 2nd degree burn for the Macor skin simulant utilized 1-D finite difference models of the fabric/Macor and the fabric/skin. This method is referred to as the 1-D Model Method in this thesis. The fabric/Macor model was used to calculate the interfacial conductance that would provide accurate heat flux and temperature rise predictions for the Macor skin simulant sensor. This interfacial conductance value was then used in a separate 1-D model of the fabric/skin to calculate the time to 2nd degree burn. The calculation of the time to 2nd degree burn was based upon manually specified exposure times, which were varied within the Microsoft Excel calculation sheets until the value for the damage function, Ω, was greater than 1.0. The benefits of the 1-D Model Method was that it used the physical and thermal properties of the clothing as input, allowing the user to assess the importance of the various clothing properties, such as the thickness, emissivity, thermal conductivity, and volumetric heat capacity. These are each separate input values in the model, and can be varied to assess the impact of each.

The second calculation method for the Macor skin simulant sensor, referred to as the Macor Heat Flux Method, used Diller's Algorithm (Equation 6) to calculate the heat flux at the surface of the Macor. This heat flux was then used to assess the time delay between the removal of the heat source and when the system began to cool, as well as to determine a characteristic curve for the heat flux during the cooling stage of the test. This information was assumed constant, regardless of when the heat flux source was removed. This time delay and cooling heat flux information was then used to determine the heat flux curve after the heat source was removed, and this information was applied to a 1-D finite difference model of the skin to determine the time to second degree burn. The benefits of this method is that is can be applied to a variety of test configurations, including ensemble evaluations, tests with an air gap between the fabric and the sensor, or tests on materials with unknown properties, because the heat transfer through the clothing is not being determined. The heat flux impinging on the sensor surface is used directly in the skin model to predict the time to 2nd degree burn.

Each calculation method for the Macor provided time to 2nd degree burn estimates lower than those determine by the copper calorimeter for the outer shell materials. Table 35 provides a comparison of the time predictions from the various calculation methods. The time predictions of the copper calorimeter with and without the 3 mm air gap are included.

Table 35: Copper Calorimeter Versus Macor Skin Simulant Time to 2nd Degree Burn Prediction Comparison – Single Layer Outer Shell Materials Exposed to 21 kW/m^2 with Cone Heater.

Material	Copper Calorimeter (3 mm air gap)	Copper Calorimeter (Fabric against Sensor)	Macor 1-D Model	Macor Heat Flux Method
Nomex 7.5 oz/sq yd	19.6	12.5	8.3	9.3
PBI 7.5 oz/sq yd	19.2	12.5	8.8	10.2

As expected, the copper calorimeter tests with an air gap between the fabric and the sensor produce the highest time to 2nd degree burn estimates. The copper calorimeter tests with this air gap removed provide time estimates much closer to those predicted by the two Macor calculation methods. The time to 2nd degree burn predictions for the Macor skin simulant by the 1-D Model Method were lower than those predicted by the Macor Heat Flux Method by approximately 12% – 15%. The copper calorimeter predictions for the time to 2nd degree burn, when the materials are evaluated with no air gap between the fabric and the sensor, were nominally 40% to 50% higher than the predictions by the 1-D Model Method, and between 23% and 34% higher than the predictions from the Macor Heat Flux Method. The problems associated with predicting the time to 2nd degree burn using the copper calorimeter and the thermal endpoint information from Table 5 are presented in Section 2.3. These problems include the use of test data for the time to 2nd degree burn from constant heat pulse levels to assess transient heat flux problems. In addition, the copper calorimeter burn calculation method does not consider the effects of the heated clothing material on the cooling of the skin, and the impact this hot layer will have on the thermal damage.

The 1-D Model Method is the most complicated of the methods employed in this study, however it should also be the most accurate. This method, which actually consists of two finite difference models linked in a Microsoft Excel spreadsheet, utilizes the Henriques Burn Integral to calculate the time to 2nd degree burn for a layer of skin covered by the fabric in question. This fabric/skin model takes into consideration the flux passing through the clothing during the heating stages, as well as the prevention of cooling due to the hot fabric layer covering the skin after the heat source is removed.

In addition to testing single clothing layers, full ensembles were evaluated, utilizing the two fabric types presented earlier in this section as the outer shell materials. The ensembles were evaluated without a space between the fabric and the copper calorimeter. The 1-D Model Method did not accurately predict the heat flux reaching the Macor surface, nor did it accurately predict the temperatures of the Macor during the heating and cooling stages of the ensemble evaluations, due to the complexity of the ensembles. This lead to the use of the Macor Heat Flux Method to predict the time to 2nd degree burn for the ensembles tested with the Macor skin simulant. Table 36 provides a comparison of the time to 2nd degree burn for the ensemble tests, evaluated with the copper calorimeter and the Macor skin simulant.

Table 36: Copper Calorimeter Versus Macor Skin Simulant Time to 2nd Degree Burn Prediction Comparison – Ensembles Consisting of Outer Shell Material, Moisture Barrier, and Thermal Liner Exposed to 21 kW/m^2 with Cone Heater.

Ensemble Outer Shell Material	Copper Calorimeter (s)	Macor Heat Flux Method (s)
Nomex 7.5 oz/sq yd	50.8	29.9
PBI 7.5 oz/sq yd	51.7	32.0

The time to 2nd degree burn predictions for the Macor skin simulant evaluations were much lower than the predictions from the copper calorimeter. The time to 2nd degree burn predictions for the copper calorimeter were between 60% and 70% higher than the predicted values from the Macor skin simulant. The magnitude of the difference in the ensemble evaluations is greater than the difference in the evaluations of the single fabric layers due to the larger amount of damage done to the skin after the heat flux is removed. In the ensembles evaluated with the Macor skin

simulant, there is an 8 to 10 second time delay between the removal of the heat source and the onset of cooling at the Macor surface. This time delay is caused by the energy stored in the ensemble, which continues to conduct heat to the skin after the removal of the heat source. In addition, the heated ensemble prevents the skin from cooling as it would in normal air. The copper calorimeter method for determining the time to 2nd degree burn based upon the time to reach a thermal endpoint on the Stoll and Chianta Curve[8] does not consider these affects.

5.0 CONCLUSION

This thesis addressed several potential problems with the current test methods for fire fighting clothing.[2,4] Examples of these potential problems include the validity of using a copper calorimeter to evaluate the clothing based upon the time to reach a thermal endpoint, and the use of a quartz lamp to determine the time to 2nd degree burn. In addition to addressing these issues, this thesis determined the thermal properties of several materials used in fire fighting clothing to determine if this information could be incorporated into the assessment of the clothing performance as well.

While the determination of the property data for the fire fighting clothing may not be necessary in the test standards, it does provide a useful tool to evaluate the clothing performance. The 1-D Model Method, used to evaluate the outer shell materials during the Macor skin simulant RPP exposure tests, utilized the property data to model the performance of the clothing. This model could be used to assess the performance of the clothing under a variety of heat flux conditions. Due to the complexity of the clothing ensembles, the finite difference model was unable to accurately predict the temperature response of the Macor during the evaluation of these clothing layers. More complicated models to assess the performance of fire fighting ensembles are in development[29,34], and will require accurate thermal property information to properly predict the performance of the clothing materials.

5.1 Summary

5.1.1 THERMAL PROPERTIES TEST FIXTURE – MATERIAL PROPERTY SUMMARY

The Thermal Properties Test Fixture (TPTF), developed by Ktech Corporation, provides a small scale test apparatus that could be used to calculate the thermal properties of fire fighting clothing materials at low heat flux exposure levels. This apparatus was designed to evaluate the clothing

materials with relatively no compression loads, while allowing for the evaluation of wet materials. The results from this test apparatus were used as input for the computer program Prop1D[6], which determined the thermal properties based upon the heat flux and temperature rise of the different layers in the test fixture.

The TPTF was used to evaluate several types of outer shell materials, as well as one moisture barrier, and one thermal liner. These materials, with the exception of the moisture barrier, were evaluated with different levels of water added to evaluate the effects of the moisture on the clothing performance. Select outer shell materials were then tested in combination with the moisture barrier and thermal liner materials, to calculate the thermal properties of different ensembles. These ensembles were then evaluated with water added to simulate their end use environment, where perspiration may wet the thermal liner material and change the heat transfer characteristics of the material.

The results obtained from the TPTF were consistent with the results obtained in Phase 1 of this testing[5], as well as results found in the literature.[35] The ensemble results were obtained as a lumped sum of the thermal properties of the entire ensemble, and were not analyzed to determine the contribution from each layer.

The addition of water to the fabric materials significantly changed the thermal properties. The thermal properties of the wet materials were evaluated on a temperature dependent basis. Although the properties of the Navy 6.8 oz/sq yd material were also evaluated on a non-temperate dependent basis, allowing direct comparison with the dry property estimates. The thermal conductivity for each of the moisture contents evaluated increased by a factor of approximately 3 over the dry thermal conductivity. The volumetric heat capacity at the higher moisture contents (0.5 and 1.0 grams of water per gram of material) increased by a factor of nominally 1.5. These changes in the thermal properties increased the thermal inertia and the thermal diffusivity by factors of approximately 2 for the materials with 0.5 and 1.0 grams of water

per gram of material evaluated. The increases in these parameters will increase the flow of heat through the clothing and into the skin during an exposure.

The determination of the thermal properties of fire fighting clothing materials, as outlined in this thesis, will allow for the development of more accurate, detailed models and tests. These models and tests will be able to better evaluate the clothing's performance when exposed to conditions and thermal environments representative of the clothing's intended use environment in the future.

5.1.2 RPP Evaluations - 2nd Degree Burn Prediction

The current test methods used to evaluate the ability of fire fighting clothing to prevent 2nd degree burns when exposed to constant, specified heat flux levels were investigated.[2,4] These test methods rely upon exposing the clothing materials to radiant heat from a quartz lamp, with the time to 2nd degree burn determined using a copper calorimeter.

These tests provide a relatively easy method to compare the fabric performance through the use of the RPP and TPP ratings. However, these test methods do not accurately correlate to the time to 2nd degree burn for a variety of reasons. The copper calorimeter does not accurately predict this time for the transient heat flux exposures to which it is subjected to when protected by a layer of clothing. The copper calorimeter predictions are based upon the time to reach a thermal endpoint, determined using 2nd degree burn test data for skin exposed to constant heat pulse levels. The use of this flux-time product data developed from constant heat pulse levels for transient exposures will not accurately predict the time to 2nd degree burn. One example case was provided in Section 2.3, where the copper calorimeter was exposed to a high heat pulse level for one second at different points during a 30 second exposure to a low heat pulse level. If the copper calorimeter is exposed to this high heat pulse limit at the beginning of the exposure, a 2nd degree burn is said to occur. However, if the copper calorimeter is exposed to a low pulse limit for ten seconds, and then exposed to the same high heat pulse level that produced a burn in the

previous case, no burn is said to occur until well after the high heat pulse. This simple example calls into the question the use of the constant heat pulse data for the transient exposures occurring during the clothing testing.

An additional problem associated with the copper calorimeter and it's use of the constant heat pulse test data to predict the time to 2nd degree burn, is that these test data were collected on bare skin. If the skin is exposed to a heat flux level without a protective clothing layer, it will cool at a different rate than if exposed to this same heat flux while covered with a layer of protective clothing. During the exposure of the fire fighting clothing materials, the exposed side of the fabric increases to temperatures much higher than the underlying protected skin. However, as the exposure continues, the skin will eventually begin to heat up. If the exposure stops, the clothing will continue to conduct heat to the underlying skin, as it remains at higher temperatures. As the temperature of the clothing decreases, the skin will soon begin to cool. However, this cooling rate will not be as fast as the cooling rate of bare skin, because the warm clothing layer, which is designed to minimize the flow of heat, will prevent the skin from dissipating the excess heat. Since damage to the skin is dependent upon all times when the basal layer temperature is greater than 44^{o}C, this effect will increase the percentage of damage caused during skin cooling. This effect is ignored during the copper calorimeter burn calculations for the fire fighting clothing.

The time to 2nd degree burn predictions for the skin simulant tests were shorter than those from the copper calorimeter. The comparative RPP tests on the single layers and the ensembles were completed using the cone heater with similar test configurations for each sensor. The differences between the time predictions from the two sensor types for the outer shell materials is between 40% and 50%, while the difference between the ensemble predictions for the two sensors is between 60% and 70%. These differences are due to the topics presented in the previous paragraphs.

The quartz lamp used to provide the heat flux in the RPP test, and the radiative portion of the heat flux in the TPP test, operates at temperatures much higher than those experienced during typical fire fighting operations. This difference in the source temperature creates a difference in the spectral distribution of the radiant energy. The fire fighting jacket materials were found to have reflectivity and absorbtivity curves dependent upon the wavelength of the radiant energy.[32] A typical curve of the reflectivity of the fire fighting coat materials was compared against the spectral distribution curve for the emissivity of the quartz lamp and a cone heater (Figure 43). The cone heater was used as an alternative to the quartz lamp, as it operates at temperatures more representative of actual fires. These spectral distribution and reflectivity curves show that the representative reflectivity curve for the fire fighting coat materials reaches it peak at the spectral peak of the quartz lamp emissivity curve (maximum reflectivity), while reaching it's downward peak at the spectral peak of the cone heater curve (maximum absorbtivity). This difference in the absorbtivity of the clothing materials may produce differences in the time to 2nd degree burn for the outer shell materials.

The Macor skin simulant burn predictions showed a distinct difference in the time to 2nd degree burn predictions for the two heat flux sources. The time to 2nd degree burn for the quartz lamp exposures was consistently longer than the time to 2nd degree burn for the cone heater exposures. This disparity is caused by the difference in the absorbtivity of the radiant energy produced by the two heat sources by the clothing materials. The average time to 2nd degree burn for the outer shell material evaluations conducted with the quartz lamp is nominally 30% longer than the average time to 2nd degree burn for the outer shell material evaluations conducted with the cone heater.

5.2 Future Research

In addition to supplying the Thermal Properties Test Fixture used to evaluate the clothing materials for this thesis, Ktech Corporation designed and donated a Thermal Properties Compression Fixture (TPCF) as well. This test apparatus is instrumented in a manner similar to

the TPTF, and can be used to evaluate the clothing materials in a similar manner. In addition to the uncompressed clothing evaluations, this test apparatus also allows the clothing samples to be tested under various compression loads, controlled by the user. The TPCF was also designed and built to allow destructive and non-destructive testing, involving sudden contact with a heated surface, of protective clothing materials. The non-destructive testing can be done to track the thermal properties of in-service fire fighting coats and jackets. This information can then be used to determine if the clothing samples should remain in service based upon actual performance criteria. This test apparatus is described in greater detail in Appendix D: Compression Test Fixture. Sample test data for some of the materials evaluated in this thesis is also included in this Appendix.

In addition to the continued testing of different clothing materials under different levels of compressive loading and at different moisture contents, work continues in the development of accurate models for fire fighting clothing.[29,34] The model developed for this thesis provided accurate temperature predictions for the Macor skin simulant when protected by the outer shell materials. However, it was unable to predict the temperature rise and fall of the Macor skin simulant when protected by a full ensemble. The development of these models should allow accurate predictions of the clothing performance based upon the thermal properties of the materials involved.

APPENDIX A: THERMAL PROPERTY TEST FIXTURE DATA

The test data from the Thermal Properties Test Fixture evaluations is presented on the attached compact disc labeled Appendix A. This test data is presented in a series of zip files. Each zip file presents the TPTF test data for one of the fabric materials. Included in each zip file are the tests completed on that fabric material, when evaluated dry and with moisture added. In addition to the individual clothing materials, there is a file for the ensembles evaluated with the TPTF. Each of the ensemble evaluations completed in the TPTF is presented in this zip file. The file names included in the zip files indicate the type of fabric evaluated in that particular test, as well as the moisture content, and the test number. The CD labeled Appendix A includes a readme file available in Microsoft Word or text format. This readme file presents a brief description of the TPTF data files, including the information presented in each file.

APPENDIX B: THERMAL PROPERTY ESTIMATIONS

The output data from Prop1D[6] is included on the attached compact disc labeled Appendices B, C, and D. This output data is presented in the directory labeled, Appendix B Thermal Property Estimations. The property estimation files are presented in 10 folders, separated by fabric type, in a similar manner as the test data for Appendix A. The material property estimate files can be opened using Microsoft Word. The actual material property estimates are included on the last page of the word document. The folder names for each fabric type are listed in the table below, along with a description of the files included in each folder. The property estimation file names include the fabric type and weight, the moisture content, and test number. The test numbers correspond to the test numbers for the files presented in Appendix A

Folder Name	Files Included (File Description)
Aralite	Aralite_dry_t1_contact – Aralite thermal liner evaluated Dry, test 1, with contact resistance. Aralite_1_t1_contact – Aralite Thermal Liner Evaluated with 1.0 grams water per gram of Aralite, test 1, with contact resistance. Aralite_15_t1_contact – Aralite Thermal Liner Evaluated with 1.5 grams water per gram of Aralite, test 1, with contact resistance.
Crosstech	CrosstechMB_dry_t1_contact – Crosstech moisture barrier evaluated dry, test 1, with contact resistance.
Ensemble	Ens_nom6_0_dry_t1_contact – Ensemble with Nomex 6.0 oz/sq yd outer shell evaluated dry, test 1, with contact resistance Ens_nom7_5_15_t1_35_100_contact – Ensemble with Nomex 7.5 oz/sq yd outer shell evaluated with 1.5 grams of water per gram of Aralite, temperature dependent properties determined at 35°C and 100°C.
Navycontact	Navy6_8_dry_t1_contact – Navy 6.8 oz/sq yd evaluated dry, test 1, with contact resistance. Navy6_8_25_t1_contact – Navy 6.8 oz/sq yd evaluated with 0.25 grams water per gram fabric, test 1, with contact resistance. Navy6_8_5_t1_contact – Navy 6.8 oz/sq yd evaluated 0.5 grams water per gram fabric, test 1, with contact resistance. Navy6_8_1_t1_contact – Navy 6.8 oz/sq yd evaluated 1.0 gram water per gram fabric, test 1, with contact resistance.
Nomex5.5contact	Similar to Navy File
Nomex6contact	Similar to Navy File
Nomex7.5contact	Similar to Navy File Nom7_5dry_30V_t1_contact – Nomex 7.5 oz/sq yd evaluated dry, test 1, DC power supply set at 30 Volts, with contact resistance.
PBI6.0contact	Similar to Navy File
PBI7.5contact	Similar to Navy File
Southernmillscontact	Similar to Navy File

APPENDIX C: RADIANT PROTECTIVE PERFORMANCE TEST DATA

The test data and accompanying models for the Radiant Protective Performance (RPP) Evaluations are included on the attached compact disc labeled Appendices B, C, and D. This output data is presented in the directory labeled Appendix C Radiant Protective Performance Test Data. This data is separated into folders for the Macor skin simulant and the Copper Calorimeter. Additionally, each of these folders contains separate folders for the RPP evaluations conducted with the quartz lamp and the cone heater. There were typically three tests completed on each fabric using each heat source. The test file names include the type of fabric evaluated and the test number. RPP test files are included for each outer shell material. In addition, there is a separate folder included in the cone heater folder for each sensor type labeled ensembles, which contains the test data and calculations for each ensemble evaluated. In addition to the ensemble folder, the cone heater folder for the Macor skin simulant contains folders labeled 10 kW_m2 Exposure and Wet Materials. These folders contain the test data and accompanying calculation information for the materials exposed to 10 kW/m^2 from the cone heater and the wet material RPP evaluations.

APPENDIX D: COMPRESSION TEST FIXTURE

A brief overview of the Compression Test Fixture is included on the attached compact disc labeled Appendices B, C, and D. This overview is presented in the directory labeled Appendix D Compression Test Fixture. The overview includes setup information for the tests that can be conducted with the Compression Test Fixture, as well as some sample evaluations. The sample evaluations were similar to those conducted with the Thermal Properties Test Fixture, and the data are presented in a similar manner. In addition to the excel files, the property estimation files are included. This information is presented in the folders Compression Test Fixture Tests and Compression Property Estimations, included as subdirectories to the Appendix D Compression Test Fixture folder.

REFERENCES

[1] Veghte, James H., "Design Criteria for Fire Fighter's Protective Clothing, 2nd Edition" Janesville Apparel, Dayton, Ohio, 1986.

[2] NFPA 1971, *Protective Clothing Ensemble for Structural Fire Fighting*, 1997 Edition, National Fire Protection Association, Quincy, MA, 1996.

[3] Karter, M.J., Leblanc, P.R., "U.S. Firefighter Injuries 1995", NFPA Journal, Volume 90, No. 6, November/December 1996, pp. 103-110.

[4] NFPA 1977, *Protective Clothing and Equipment for Wildland Fire Fighting*, 1993 Edition, National Fire Protection Association, Quincy, MA, 1996.

[5] Keltner, N.R. et al, "New Methods for Evaluating Thermal Performance of Protective Clothing for Fire Fighters," Ktech Document TR 98-01, Ktech Corporation, Albuquerque, NM. Submitted to United States Department of Commerce, Small Business Innovative Research Program, Phase I – Contract Number 50-DKNB-7-90134, 1998.

[6] Beck, James V., and McMasters, Robert L., *Users Manual for Prop1D – Program for Estimating Thermal Properties from Transient Temperature and Heat Flux Measurements,* Version 7.0, Beck Engineering Consultants Company, Okemos, MI 48864.

[7] SFPE Task Group on Engineering Practices, "Predicting 1st and 2nd Degree Skin Burns from Thermal Radiation," Society of Fire Protection Engineers, Bethesda, MD, 2000.

[8] Stoll, A.M. and Chianta, M.A., "Method and Rating System for Evaluation of Thermal Protection," Aerospace Medicine, Vol. 40, pp. 1232-1238, 1968.

[9] Stoll, A.M. and Greene L.C., "Relationship Between Pain and Tissue Damage Due to Thermal Radiation," Journal of Applied Physiology, Vol. 14, p 373-382, 1959.

[10] Stoll, A.M. and Chianta, M.K., "Heat Transfer through Fabrics as Related to Thermal Injury," Transactions-New York Academy of Sciences, 33:7, pp. 649-670, 1971.

[11] Henriques, F.C., Jr., “Studies of Thermal Injury V. The Predictability and the Significance of Thermally Induced Rate Processes Leading to Irreversible Epidermal Injury,” Archives of Pathology, Vol. 43, pp. 489-502, 1947.

[12] Weaver, J.A. and Stoll, A.M., “Mathematical Model of Skin Exposed to Thermal Radiation,” Aerospace Medicine, Vol. 40, pp. 24-30, 1969.

[13] Dale, J.D. and Torvi, D.A.,”A Finite Element Model of Skin Subjected to a Flash Fire,” Journal of Biomechanical Engineering, Vol. 116, pp. 250-255, 1994.

[14] Lawson, J. R., “Fire Fighter’s Protective Clothing and Thermal Environments of Structural Fire Fighting,” U.S. Department of Commerce, NISTIR 96-5804, Building and Fire Research Laboratory, National Institute of Standards and Technology, Gaithersburg, MD, 1996.

[15] Veghte, J.H., “Functional Integration of Fire Fighters Protective Clothing,” *Performance of Protective Clothing, ASTM STP 900,* R.L. Barker and G.C. Coletta, Eds., American Society for Testing and Materials, Philadelphia, 1986, pp. 487-496.

[16] ASTM D 4108, *Standard Test Method for Thermal Protective Performance of Materials for Clothing by Open flame Method*, 1987 Edition, American Society for Testing and Materials, Philadelphia, PA (Last Printed in 1996).

[17] Keltner, N.R., B.L. Bainbridge, and J.V. Beck, “Rectangular Heat Source on a Semi-Infinite Solid – an Analysis for a Thin Film Heat Flux Gage Calibration,” Journal of Heat Transfer, Vol. 110, pp 42-48, 1988.

[18] Drysdale, Dougal, “An Introduction to Fire Dynamics,” John Wiley and Sons, New York, NY 1996.

[19] *The Temperature Handbook*, Omega Engineering, Inc. Stamford, CT, 1999.

[20] Beck, James V., Users Manual for IHCP1-D – *Program for Calculating Surface Heat flux levels from Transient Temperatures Inside Solids*, Version 7.0, Beck Engineering Consultants Company, Okemos, MI 48864.

[21] Granier, B., Delaunay, D., and Beck, J.V., "Estimation of Thermal Properties of Composite Materials without Instrumentation Inside the Samples," International Journal of Thermophysics, Vol. 6, November 1992.

[22] Croft, D., and Lilley, D., "Heat Transfer Calculations Using Finite Difference Equations," Applied Science Publishers, Ltd., London, England, 1977.

[23] Mills, A.F., *Heat and Mass Transfer*, Richard D. Irwin, Inc. Chicago, IL, 1995.

[24] ASTM E 1354 *Standard Test Method for Heat and Visible Smoke Release Rates for Materials and Products Using the Oxygen Consumption Calorimeter*, 1992 Edition, American Society for Testing and Materials, Philadelphia, PA.

[25] Diller, T.E., "Methods of Determining Heat Flux from Temperature Measurement", Proceedings of the 42nd International Instrumentation Symposium, Aerospace Industries Division and Test Measurement Division of ISA, 1996.

[26] ASTM E 457, *Standard Test Method for Measuring Heat-Transfer Rate Using a Thermal Capacitance (Slug) Calorimeter*, 1996 Edition, American Society for Testing and Materials, Philadelphia, PA.

[27] Carslaw, H.S. and Jaeger, J.C., *Conduction of Heat in Solids*, Oxford Press University, Oxford, UK, 1959, Chapter 2, Equation 9.

[28] Griffith, M.V. and Horton, G.K., "The Transient Flow of Heat Through a Two-Layer Wall," Process Physical Society, Vol. 58, pp. 481-487, 1946.

[29] Torvi, D.A. and Dale, J.D., "Numerical Models for Use in the Design of Protective Clothing for Firefighters," Proceedings from the International Conference on Fire Research and Engineering 3, Society of Fire Protection Engineers, Bethesda, MD, 1999.

[30] DiNenno, P.J., "Appendix B: Thermophysical Property Data" in the *SFPE Handbook of Fire Protection Engineering,* 2nd Edition, National Fire Protection Association, Quincy, MA, 1995.

[31] Hoschke, B.N., Holcombe, B.V., and Plante, A.M., "A Critical Appraisal of Test Methods for Thermal Protective Clothing Fabrics," *Performance of Protective Clothing, ASTM STP 900,*

R.L. Barker and G.C. Coletta, Eds., American Society for Testing and Materials, Philadelphia, 1986, pp. 311-326.

[32] Quintiere, James, “Radiative Characteristics of fire Fighter’s Coat Fabrics,” Fire Technology, Vol. 10, No.2, pp153-161, May, 1974.

[33] Holman, J.P., *Heat Transfer*, Fifth Edition, McGraw-Hill International, Tokyo, Japan, 1981, Chapter 8.

[34] Mell, W.E. and Lawson, J. R., “A Heat Transfer Model for Fire Fighter’s Protective Clothing,” U.S. Department of Commerce, NISTIR 99-6299, August 1999.

[35] Torvi, D.A. and Dale, J.D., “Heat Transfer in Protective Fabrics Under Flash Fire Conditions,” Proceedings of the Second International Conference on Fire Research and Engineering, Society of fire Protection Engineers, Bethesda, MD, 1997.